# APPLYING COLLISION-INDUCED UNFOLDING TO STUDY GAS PHASE STABILITY OF PARTIALLY METALATED METALLOTHIONEIN-2A

A Dissertation

by

SHIYU DONG

Submitted to the Office of Graduate and Professional Studies of
Texas A&M University
in partial fulfillment of the requirements for the degree of

DOCTOR OF PHILOSOPHY

| | |
|---|---|
| Chair of Committee, | David H. Russell |
| Committee Members, | Tadhg P. Begley |
| | Pingwei Li |
| | Simon W. North |
| Head of Department, | Simon W. North |

May 2020

Major Subject: Chemistry

## ABSTRACT

Metallothioneins (MTs) constitute a family of cysteine-rich proteins that have the ability to bind a wide range of metal ions including $Cd^{2+}$, $Zn^{2+}$ and $Ag^{+}$. MTs are important in metal homeostasis and detoxification. Even through apo- and partially metalated MTs are physiologically predominant, limited structural information is known about those species. Nanoelectrospray ion mobility mass spectrometry (nESI-IM-MS) provides another possibility to study apo- and partially metalated-MT.

We presented here for the first report to apply collision-induced unfolding (CIU) to study the gas-phase stabilities of MTs after partially metalated by $Cd^{2+}$, $Zn^{2+}$ and $Ag^{+}$. $Cd_4$-MT, $Zn_4$-MT, $Ag_4$-MT and $Ag_6$-MT differ dramatically in their gas-phase stabilities. A static mixing tee with variable lengths of capillary was chosen to probe abundance change of partially metalated species of MT binding with $Cd^{2+}$ and $Zn^{2+}$ during short reaction time. The mixing tee system also allows CIU study of intermediates under pre-equilibrium conditions. The sequential addition of each $Cd^{2+}$ and $Zn^{2+}$ ion to MT results in the incremental stabilization of unique unfolding intermediates.

We further focused on $Ag^{+}$ metalated MT and combined multiple MS strategies, including mixed metalation, CIU, chemical labeling, top-down and bottom-up MS, and 2D MS-CID-IM-MS, to unambiguously identify the binding sites of $Ag_4$-MT. Both $Cd^{2+}$ and $Ag^{+}$ bind to MT cooperatively, however, $Cd_4$-MT prefers binding to α domain while $Ag_4$-MT binds to β domain.

Furthermore, some attempts including kinetic study with mixing tee during $Cd^{2+}$ metalation, $Cu^{+}$ binding to MT and studies related to possible solution phase structures of different charge states of MT are summarized. We hope those attempts can inspire future study.

## ACKNOWLEDGEMENTS

I would like to thank my advisor Dr. David H. Russell for his consistent support throughout my Ph.D study. I have been impacted by his scientific attitude, critical thinking and enthusiasm for science. I appreciate the training in problem solving and independent research capabilities I have received from Dr. Russell, which will influence and benefit my future career.

I would like to thank my committee members, Dr. Tadhg P. Begley, Dr. Pingwei Li and Dr. Simon W. North, for their support and guidance on this research. Thanks also go to all the members in Russell research group. A special thanks to Dr. Shu-hua Chen for her assistance to starting this project, as well as Dr. Nicole Wagner for being a good friend and providing advices for my research and Ph.D life. I am also grateful to all the department faculty and staff for making my time at Texas A&M University a great experience.

I would also like to thank Dr. Danke Xu, Dr. Aidong Zhou, Dr. Jing Zhao and Dr. Gui Yin in Nanjing University. They encouraged me to pursue an advanced education in United States and kindly provided recommendations.

Finally, thanks to my mother and father. As an only child, I always feel guilty not be able to take care of them by their sides. I would like to thank my parents for their encouragement, supporting and understanding, and my cousins helping to take care of my parents in China.

## CONTRIBUTORS AND FUNDING SOURCES

### Contributors

This work was supervised by a thesis dissertation committee consisting of Dr. David H. Russell, Dr. Tadhg P. Begley and Dr. Simon W. North of the Department of Chemistry and Dr. Pingwei Li of the Department of Biochemistry and Biophysics.

All work conducted for the dissertation was completed by the student independently.

### Funding Sources

This work was supported in part by the National Institutes of Health under Grant Number [R01GM121751-01A1, R01GM121751 and P41GM128577], the National Science Foundation [CHE-1707675] and endowment funds provided by the MDS Sciex Professorship.

Its contents are solely the responsibility of the authors and do not necessarily represent the official views of the National Institutes of Health and National Science Foundation.

## NOMENCLATURE

| | |
|---|---|
| CE | Collision energy |
| CID | Collision-induced dissociate |
| CIU | Collision-induced unfolding |
| DTPA | Diethylenetriaminepentaacetic acid |
| ESI | Electrospray ionization |
| IM | Ion mobility |
| MT | Metallothioneins |
| MS | Mass spectrometry |
| NEM | N-ethymaleimide |
| TCEP | Tris(2-carboxyethyl)phosphine |

## TABLE OF CONTENTS

Page

## LIST OF FIGURES

Page

FIGURE

## LIST OF TABLES

Page

# CHAPTER I

# INTRODUCTION

Metallothioneins (MTs) constitute a group of metalloproteins characterized by their small size (0.5-14 kDa), extremely high thiolate sulfur and metal content (both in the order of 10 %, w/w), and a lack of tertiary structure in their apo form.[1-2] Based on their sequence similarities and phylogenetic relationship, mammal MTs can be divided into subgroups: MT1 and MT2 are highly expressed in almost all organs such as liver and kidney; MT3 is expressed mainly in brain while MT4 can only be found in certain stratified tissues.[3-5] Those subgroups of MTs differ in amino acid residues other than the conserved cysteines.[1]

Since the discovery of mammalian MTs in 1957, it has received tense attention and research.[6] However, the biological properties of MTs haven't been fully understood yet, as further properties are still discovered continually. The main difficulty in understanding MT's biological properties comes from the fact that MTs have been implied in tens of biological process, and the functions vary from one type of organisms to another, or even vary from isoforms in a single organism.[2, 7] For the most widely expressed isoforms in mammals, MT1 and MT2, the properties are related to their high thiolate sulfur content. These involve basic metal homeostasis,[8-9] heavy metal detoxification,[10] defense against oxidative stress and scavenging reactive oxygen species.[11] MT3 is thought to be a neuronal growth inhibitory factor.[12] It plays important roles in homeostasis of the essential metal ions Cu(I) and Zn(II) in mammal brains, and may be involved in preventing the formation of neurotoxic β-amyloid plaques in

Alzheimer's disease.[13-16] MT4 is reported to have higher affinity towards Cu(I) than Zn(II) or Cd(II);[17] its biological functions are related to the Cu-thioneine formation and tissue-specific expression.[18-19] It is also reported that MT induction occurs in response to tissue injury, inflection and inflammation.[20] Aberrant expression of MTs is even disclosed as a prognostic factor for tumor progression or as a cause of resistance in cancer treatment.[21-22]

In order to understand the biological function of MTs, it is necessary to study the structure change of MTs during metalation and demetalation process. MTs are considered as natively unfolded proteins or intrinsically disordered proteins (IDP). Following their names, natively unfolded proteins show complete or almost complete loss of any ordered structure under physiological conditions *in vitro* and have the properties like low overall hydrophobicity and high net charge; the absence of a tightly packed core and high conformational flexibility.[23] The structures of IDPs are governed by binding of their targets.[23] For MTs, the structure properties are based on the formation of metal-thiolate clusters in a single domain (yeast), or in two such domains (mammals).[2, 24-25] MTs have different affinity order of metal ions for the thiolate ligands: Zn(II) < Cd(II) < Cu(I) < Ag(I).[26] Mammal MT1 and MT2 adopt similar structures binding with metal ions.[27] **Figure 1.1** shows the two types of metal-thiolate clusters that have been reported for MT2 binding with divalent metal ions like Zn(II) and Cd(II).[28] An $M_3Cys_9$ cluster is formed in the N terminal β domain of mammal MTs with three metal ions and three bridging cysteine sulfurs forming a six-membered ring. The $M_4Cys_{11}$ cluster found in the C terminal α domain contains two distorted six-membered

rings. Two bonds are shared between those two rings. Limited information for monovalent ions metalated mammal MT has been reported. At least twelve monovalent metals ions are required to form fully metalated MT.[29] Both trigonal planar and line/diagonal coordination geometry can be involved in the cluster structure.[1]

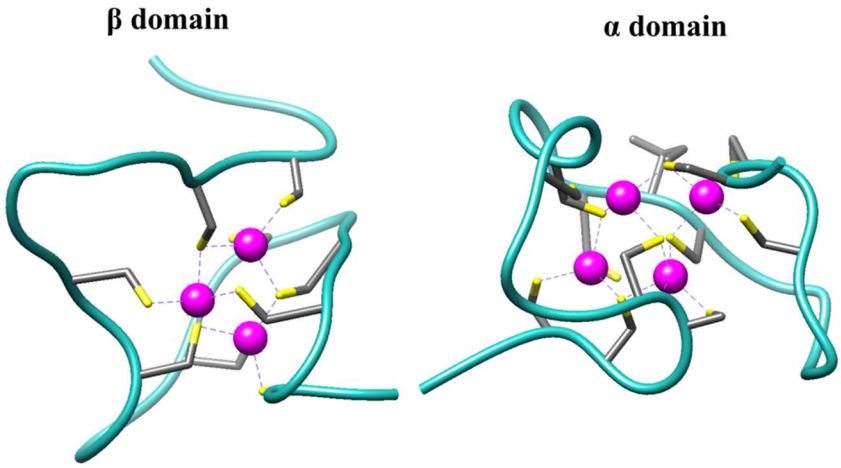


**Figure 1.1.** NMR structure of rabbit liver $Cd_7$-metallothionein 2A. Cadmium atoms are shown as magenta spheres, thiolate bonds as yellow sticks. The amino acid sequence for rabbit MT2A is MDPNCSCAAA GDSCTCANSC TCKACKCTSC KKSCCSCCPP GCAKCAQGCI CKGASDKCSC CA.[28] (β domain: 1MRB; α domain: 2MRB)

Types of analytical techniques have been applied to elucidate the chemical properties and structures of MTs. MTs lack aromatic amino acids, instead, they show ligand-to-metal-charge-transfer (LMCT) absorption bands detectable in the ultraviolet–visible (UV-vis) region.[30-32] The LMCT bands fall around 220-240 nm for Zn(II) and 240-250 nm for Cd(II).[32] Circular dichroism (CD) spectroscopy is one of the most classic methods to study the structure changes of MTs during metalation. [31, 33-35] Infrared (IR) and Raman spectroscopy are also applied to MT studies. [36-37] The drawback of those

optical spectroscopy methods is the bands are usually broad and lack of details, since the products are usually mixtures of multiple metalated species. Due to band overlapping of the complex systems and lack of absorption information of each pure partially metalated species, optical spectroscopy can only provide an overall picture during the metalation process.[1]

Structure determination for MTs is also challenging. The two most commonly used methods in structure study, X-ray crystallography and nuclear magnetic resonance (NMR) spectroscopy, all meet difficulties obtaining the 3-dimentional structures of MTs.[1] MTs are hard to crystalize due to the relatively high flexibility of their backbone. For example, since the discovery of yeast copper thionein in 1975, crystallization attempts started.[38] It was only until 2005 that Weser and co-workers succeeded to obtain a conclusive structure.[39] Only 2 out of the 33 solved entries for MTs in the Protein Data Bank (PDB) are X-ray structures up to now. Even though solving most of the known structures, NMR meets challenges as well, such as very little information for glycine groups, difficulty to locate the positions of cysteine groups with conventional protein NMR spectroscopy.[1] A replacement of the native metal ion by an NMR-active nucleus is always required, for example, Zn(II) is replaced by $^{111}$Cd(II) or $^{113}$Cd(II).[28, 40-41] It cannot be guaranteed if the replacement is isostructural.[1, 42] Finally, all the structures in PDB are for fully metalated MTs. In fact, apo form and the partially metalated species are more likely to be physiological predominant.[43-45] Due to the unfolded property and flexible backbone, the structure of partially metalated species are unlikely to be obtained by either X-ray crystallography or NMR spectroscopy.[1]

One of the most popular methods in MTs study nowadays is mass spectrometry, especially electrospray ionization mass spectrometry (ESI-MS). ESI-MS is a soft ionization technique.[46-47] It can generate tiny droplets with solution and target protein molecules. When solution molecules are evaporated during ESI process, the target protein can maintain a native-like structure without breaking covalence bonds.[48-50] Non-covalence bonds can be maintained by careful experimental design.[51-53] The structure and folding of MTs are governed by the metal-thiolate bonds, which are thought to be covalence bonds.[2, 54] Fenselau's group is the first to introduce ESI-MS to MTs study.[55] With optimized experiment conditions such as neutral pH, volatile buffer, instrumental parameters, MTs are especially suitable for analysis by ESI-MS. In fact, ESI-MS is the only method allows the directly observation of individual partially metalated species of MTs during metal uptake and release.[1, 56-59]

ESI-MS can not only provide classical mass-to-charge ratio (m/z), but also combined with other separation methods to provide structural related information. Ion-mobility (IM) spectroscopy is one of those methods. IM is a gas-phase post ionization separation method which can provide an additional dimension to separate ions based on chemical classes or conformational classes.[60-62] IM obtains the rotationally averaged collision cross-section (CCS) of gas-phase ions and nuclei acids along with m/z value.[63-64] ESI-IM-MS can thus act as a tool to separate complex mixtures, to resolve ions that may be difficult to distinguish by mass spectrometry only, to obtain structural information, or to study conformational dynamics like protein flexibility and folding/unfolding mechanisms.[65-68] Even though ESI-IM-MS cannot provide atomic

resolution compared with NMR or X-ray crystallography, it has been applied successfully to examine protein dynamics and shows great potential for getting the structure characterization of IDP like MTs. [48, 56, 69-71]

Our group have focused on researches of MTs using ESI-IM-MS for years and made progress in understanding partially metalated species and the related structure-function relationships. Molecular dynamics (MD) simulations data was integrated with IM-MS to provide a global view that shows stepwise metal-induced conformational transition: apo-MT and partially metalated MTs converge toward ordered, compact conformations as the number of bound $Cd^{2+}$ ions increase.[70] Bottom-up and top-down IM-MS was combined with chemical labels by N-ethylmaleimide (NEM) to unambiguously identify four Cd-binding sites of human $Cd_4$-MT.[56] Similar method was applied for kinetic study in the reaction of human $Cd_7$-MT and NEM, and Cys33 was found to play special role in the metal displacement process.[71] MTs are also used as examples to comparing conformations sampled by ESI-IM-MS to solution phase structures.[48]

Most recently, we introduced collision-induced unfolding (CIU) to MT studies. CIU is a collisional activation method in which the CCSs of a protein complex under different activation energy are monitored.[72] During a typical CIU experiment, the isolated ions are activated by collisions with a background gas (e.g. Argon). The internal energy of the ions is increased, leading to conformational change or unfolding. The increased internal energy is not sufficient to cause significant dissociation of covalent bonds.[73-74] CIU describes the unfolding process of the protein complex, which reflects

gas-phase stability.[75] CIU has been applied to distinguish subtle differences between biomarkers, study the structures of gas-phase biomolecules as well as protein-ligand interactions.[76-82] Ruotolo and coworkers have developed software to simplify the data analysis process of CIU.[83-84]

In CAPTURE II, the conformational preferences for partial metalated rabbit metallothionein-2A (MT) by $Cd^{2+}$, $Zn^{2+}$, and $Ag^{+}$ is studied using nESI-IM-MS. We employ CIU to probe differences in the gas-phase stabilities of these partially metalated MTs. Our results show that despite their similarity in IM profiles under cool instrumental conditions, $Cd_4$-MT, $Zn_4$-MT, $Ag_4$-MT and $Ag_6$-MT differ dramatically in their gas-phase stabilities. Furthermore, the sequential addition of each $Cd^{2+}$ and $Zn^{2+}$ ion result in the incremental stabilization of unique unfolding intermediates.

Among all the partially metalated MTs we studied ($Zn_i$-MT, $Cd_i$-MT and $Ag_i$-MT), $Ag_i$-MT is extremely interesting. MT can bind more $Ag^{+}$ ions than $Cd^{2+}$ and $Zn^{2+}$ ions; meanwhile, $Ag_4$-MT behave as a cooperative products. Further research was performed to get better understanding of silver metalated MTs. In CAPTURE III, direct metalation and CIU are used to obtain cooperative binding pattern of MT towards $Ag^{+}$ and track structural changes of multiple partially metalated-MT. The result proves that $Ag_4$-MT is a cooperative product. Mixed metalation experiment, top-down and bottom-up mass spectrometry is combined with NEM labeling to identify that all four $Ag^{+}$ ions in $Ag_4$-MT are bound to β domain, which is significantly different from $Cd^{2+}$ or $Zn^{2+}$. These differences might be important to MTs' physiologically function in metal homeostasis and detoxification as well as diseases development.

In CAPTURE V, we provided a comprehensive investigation of other MT related projects, which included real-time MS based kinetic study, Cu(I) metalation and CIU of Cu(I) metalated MT, as well as the relationship between solution-phase structures and gas-phase structures sampled by ESI-MS. We hope those results can inspire future research of MT.

# CHAPTER II

# COLLISION-INDUCED UNFOLDING OF PARTIALLY METALATED METALLOTHIONEIN-2A: TRACKING UNFOLDING REACTIONS OF GAS-PHASE IONS*

## Introduction

Metallothioneins (MTs) constitute a group of metalloproteins characterized by their small size (0.5-14 kDa) and the high abundance of cysteines which serve as metal ion coordination sites. The apo forms of MT exhibit a diverse array of disordered tertiary structures, but metal binding to the cysteine residues (thiolate groups) serve as strong determinants of MT structural properties.[1-2, 24] It has been suggested that the apo- and partially-metalated MT species are more likely to be physiologically predominant species,[85-86] but due to their conformational diversity and low *in vitro* abundances, the structures of partially metalated species are difficult to study using X-ray crystallography or NMR spectroscopy.[1]

Fenselau et al. pioneered the use of electrospray ionization mass spectrometry (ESI-MS) for studies of metallothioneins,[55] and Stillman et al. have championed ESI for studies of ion reactivity and kinetics of metalation reactions.[31, 87-91] More recently, we have made extensive use of nano-electrospray ionization mass spectrometry in

---

* Reprinted with permission from Dong, S.; Wagner, N. D. and Russell, D. H.. COLLISION-INDUCED UNFOLDING OF PARTIALLY METALATED METALLOTHIONEIN-2A: TRACKINF UNFOLDING REACTIONS OF GAS-PHASE IONS. *Anal. Chem.* **2018,** *90* (20), 11856-11862. 

combination with ion mobility (IM) spectrometry (nESI-IM-MS) for determination of the conformational preferences of both partially and fully metalated MTs.[48, 56, 70-71] IM-MS has been applied to protein structure study, and can be used to probe protein dynamics and shows great potential for structural characterization of natively unfolded MTs, specifically conformational changes upon binding metal ions or other folding effectors.[60, 63, 65, 69, 92-96] As examples, Chen *et al*. combined bottom-up and top-down nESI-IM-MS proteomic approaches with chemical labeling to unambiguously show that metalation involves sequential addition of $Cd^{2+}$ to the α-domain resulting in preferential formation of an intermediate, $Cd_4$-MT2, but at higher metal ion concentrations the excess $Cd^{2+}$ ions add to the β-domain to yield the fully metalated $Cd_7$-MT2.[56] Likewise, demetalation (by EDTA) occurs in the reverse order.[56] A similar approach was used to examine the reaction of human $Cd_7$-MT2 and N-Ethylmaleimide (NEM) to show that Cys33 played an important role in the metal displacement process.[71] Another study used molecular dynamics (MD) simulations to identify candidate structures for the partially and fully metalated MTs.[70] The simulation results were integrated with IM-MS to provide a global view of stepwise metal-induced conformational transitions; apo-MT2 and partially metalated ions converge toward ordered, compact conformations as the number of bound $Cd^{2+}$ ions increases.[70-48]

Here, we employ collision-induced unfolding (CIU) experiments to investigate how the rotationally-averaged collision cross section (CCS) of the partially metalated MT ions change as the ion's internal energy is increased upon collisional activation. This approach is used to compare the conformational preference of partially metalated ions

and the differences in their gas-phase stabilities.[77] CIU is analogous to protein melting experiments,[97] but instead of thermal heating of a solution containing the protein of interest, the ions are heated by energetic collisions with a bath gas.[79] The unfolding that occurs as a result of collisional activation (CA) can be related to the relative stabilities of noncovalent (secondary/tertiary structure) intramolecular interactions of the gas-phase protein ions. Although the mass spectral data for the partially metalated MT species reveal some similarities, the CIU plots for these ions are quite different and reveal substantial differences in gas-phase stability. In some cases, however, the abundances for the partially metalated ions, viz., $(metal)_i$-MT, where $i$ = 1-3, are quite low; consequently, a mixing tee apparatus was developed in an effort to kinetically trap the low abundance ions.

**Experimental Section**

Recombinant rabbit metal-free MT2A (denoted as apo-MT) was obtained from Bestenbalt LLC (Tallinn, Estonia). Bradykinin and bradykinin mutant peptide, cadmium acetate, zinc acetate, silver acetate, ammonium acetate, formic acid (FA) and tris (2-carboxyethyl) phosphine hydrochloride (TCEP) were purchased from Sigma-Aldrich (St. Louis, MO). Deionized water (18.2 MΩ) was obtained from a Milli-Q water apparatus (Millipore, Billerica, MA).

Rabbit apo-MT powder was reconstituted in 1% FA and 0.6 mM TCEP, divided into 10 μL aliquots, flash frozen in liquid nitrogen, and lyophilized. These apo-MT samples were stored at -20 °C until use. 17.5 μM apo-MT was reconstituted in 50 mM

ammonium acetate (pH = 6.8), 10 % methanol and 1 mM TCEP. 70 μM (four equivalents) cadmium acetate, zinc acetate, and silver acetate, or 105 μM (six equivalents) silver acetate were added for partially metalated studies. The solution was incubated for 1 h at room temperature and then analyzed by nESI-IM-MS.

All experiments were performed on a Waters Synapt-G2 HDMS instrument (Manchester, UK). nESI-IM-MS experiments were carried out using instrument conditions that minimize collisional heating as previously described.[48] nESI-CIU-MS experiments were carried out as described previously.[98] Identical collisional heat minimizing conditions were used prior to collisional activation. The ion of interest was mass-selected by the quadrupole mass analyzer and then collisionally activated (CA) prior to IM analysis. Different collision energies were applied by changing the voltage (increments of 5 V) drop between the exit of the quadrupole and the entrance to the TWIG-trap region filled with the collision gas argon. The activation energy was reported as lab-frame collision energy which was calculated as the product of ion charge and acceleration voltage. CA data were compiled into CIU heat maps, i.e. 2-dimensional plots of CCS vs. lab-frame collision energies using CIUSuite as described by Ruotolo *et al*.[83]

The CIU heat maps for the partially metalated species obtained using titration experiments are of poor quality owing to the low abundances of the $Cd_i$-MT ($i$ = 1-3) product ions during the titration experiments. This problem was circumvented by using a micro-mixing tee (IDEX Heath & Science LLC, Oak Harbor, WA) apparatus that allows for better control of the reaction time, i.e. kinetic trapping of the partially metalated

product ions (see **Figure 2.1**). The length of capillary between the mixing tee and the ESI source is variable, which allows for better control of the reaction time. For these experiments one channel of the micro-mixing tee contained 35 μM apo-MT (1 mM TCEP, 10 % MeOH and 50 mM ammonium acetate) and the other channel contained four equivalents of cadmium acetate or zinc acetate in 10 % MeOH and 50 mM ammonium acetate. The two channels were mixed in the mixing tee and allowed to react in a capillary prior to nESI; the reaction time was then selected by varying the length of the capillary. CIU for apo-, $Cd_1$-, $Cd_2$-, $Cd_3$-MT and $Cd_4$-MT was obtained using a capillary with a length of 60 cm and an internal diameter of 75 μm. The CIU for $Zn_1$-, $Zn_2$-, $Zn_3$-MT and $Zn_4$-MT was obtained using a capillary with a length of 10 cm and an internal diameter of 75 μm.

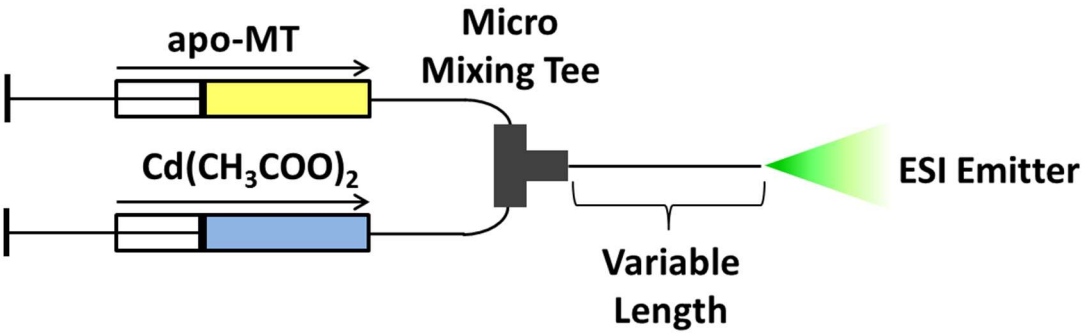


**Figure 2.1.** Schematic diagram of the micro-mixing tee assembly used to kinetically trap partially metalated $Cd_i$-MT ($i$=1-3). Reprinted with permission from [123].

## Results and Discussion

**Figure 2.2** contains nESI mass spectra for apo- and partially metalated MT ions ($Cd^{2+}$, $Zn^{2+}$, and $Ag^{+}$) acquired from equilibrated solutions. Specifically, apo-MT ions react with $Cd^{2+}$, $Zn^{2+}$, and $Ag^{+}$ to yield product ions of 5+ charge states ($Cd_4$-MT, m/z 1314.6; $Zn_4$-MT, m/z 1276.4; and $Ag_4$-MT, m/z 1311.4), and 4+ product ions ($Cd_4$-MT, m/z 1642.7; $Zn_4$-MT, m/z 1595.5; and $Ag_4$-MT, m/z 1639.2). Signals corresponding to $Zn_1$-MT, $Zn_2$-MT and $Zn_3$-MT are also detected, as well as low abundance $Ag_5$-MT and $Ag_6$-MT, whereas in the case of $Cd^{2+}$ only metalated product ions corresponding to $Cd_4$-MT product ions are observed.

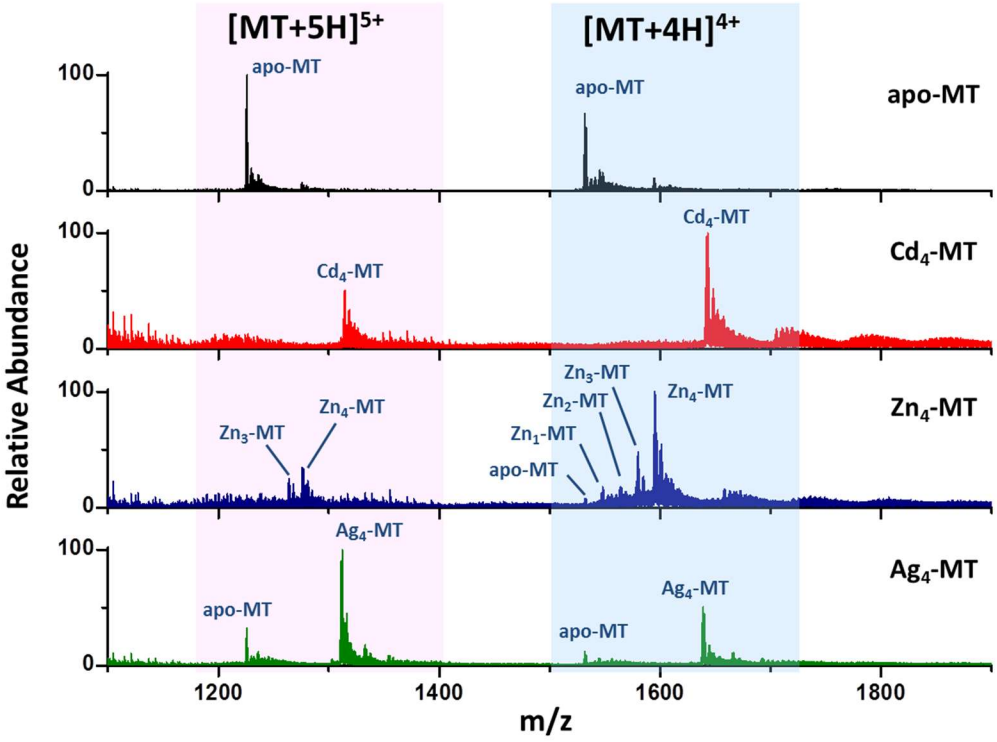


**Figure 2.2.** ESI-MS spectra acquired from equilibrated solutions containing MT and either no metal ion (apo-MT) or four equivalents of $Cd^{2+}$, $Zn^{2+}$, or $Ag^{+}$ ($Cd_4$-MT, $Zn_4$-MT, and $Ag_4$-MT). The solution was incubated for 1 h at room temperature and then analyzed by nESI-MS. Reprinted with permission from [123].

It is interesting to note the changes in the charge state distribution that occur upon metal ion binding. Previous studies showed that charge state distributions of the metalated ions are dependent on the numbers of metal ions bound to MT,[70] and here it is shown to also be dependent on the identity of the metal species. For example, the 5+ ion is the most abundant charge state for apo-MT; however, after binding four equivalents of $Cd^{2+}$ or $Zn^{2+}$, the 4+ ion is the most abundant charge state, but this behavior is not observed upon binding of $Ag^{+}$ ions. This observation suggests that the solvent accessible surface area (SASA) for the 5+ and 4+ charge states are quite different---indirect evidence that these ions have very different conformations. That is, binding of $Cd^{2+}$ or $Zn^{2+}$ ions results in formation of conformers that are very different from that for apo-MT, and these differences in conformation alters the exposure of hydrophilic regions of the protein. As reported previously,[70] $Cd_4$-MT is a relatively stable product wherein the first four $Cd^{2+}$ ions bind preferentially to the α-domain, resulting in more compact conformations of this domain; a similar structure for $Zn_4$-MT has been proposed by Messerle.[99] This increase in order in the α-domain would likely result in an overall decrease in the SASA of the protein, which is consistent with the observed lower charge state. $Ag_4$-MT, on the other hand, shows a preference for 5+ ions---very much like that observed for apo-MT, thus it appears that the SASA of $Ag_4$-MT is similar to that of apo-MT, as opposed to the other partially metalated counterparts. Independently, Zelazowski and Palacios reported that MT reacts to bind more than six $Ag^{+}$ ions to each domain,[100-102] which raises questions as to whether $Ag_4$-MT forms a compact metal-coordinated structure because no domain is "full", a degree of disorder is retained. Although MTs

bound with $Zn^{2+}$ and $Cd^{2+}$ adopt tetrahedral coordination spheres, where the metal ion is coordinated by four cysteine residues,[1, 28, 103] coordination of $Ag^{+}$ ions by MT are more likely to have digonal or trigonal geometries;[1, 104] consequently, as the numbers of $Ag^{+}$ ions bound to MT increases, the structure of the $Ag_i$-MT complex may be less ordered than are the structures of $Cd_i$- or $Zn_i$ -MT complexes.[105]

Results from collision-induced dissociation (CID) studies provide interesting clues concerning the binding of metal ions to MT. **Figure 2.3** contains CID spectrum for 5+ apo-MT, $Cd_4$-MT, $Zn_4$-MT, $Ag_4$-MT and $Ag_6$-MT. For apo-MT, the most abundant fragment ions are derived from backbone dissociation within the β-domain, and similar fragment ions are observed for all of the $(metal)_4$-MT complexes. The most abundant CID fragment ions correspond to y-type fragment ions, where charge is retained by the C-terminus,[106] and all of these ions, with exception of y24 fragment ions contain four metal ions. Note, however that the b-type fragment ions, where charge is retained by the N-terminus,[106] do not contain metal ions. The CID spectra for 5+ ions of $Cd_4$-MT, $Zn_4$-MT, $Ag_4$-MT and $Ag_6$-MT (see **Figure 2.3B**) are very similar and suggest that $Cd^{2+}$, $Zn^{2+}$, and $Ag^{+}$ are most strongly bound by ligands (thiolates) that fall between Cys14 and Cys60. Note that CID of $Cd_4$-MT, $Ag_4$-MT and $Ag_6$-MT produces y24 fragment ions (corresponding to cleavage at Pro39), which suggest interactions with thiolate ligands near the C-terminus may be weaker than those with the Cys located near the middle of the amino acid chain. Stillman suggested that at physiological pH, $Zn^{2+}$ is bound to the N-terminal Cys5 and Cys7 and forms bead-like structure(s) rather than a $M_4Cys_{11}$ cluster,[107-109] but hereto the CID fragmentation suggest that Cys5 and Cys7 are

at most weakly interacting with the $Zn^{2+}$ in $Zn_4$-MT. The CID results do not preclude the possibility that metal ions initially coordinated by Cys located near the N- (Cys5 and/or Cys7) and C-terminus (Cys located between positions 42 and 61) migrate to new binding sites prior to dissociation. Similar metal ions migration may also occur for $Ag_6$-MT. Even though there are reports that $Ag_6$-MT may have a fully metalated β domain, the CID results of $Ag_6$-MT illustrate that most of the fragmentations are metal containing y-type fragment ions and metal free b-type fragment ions.[102, 110-112]

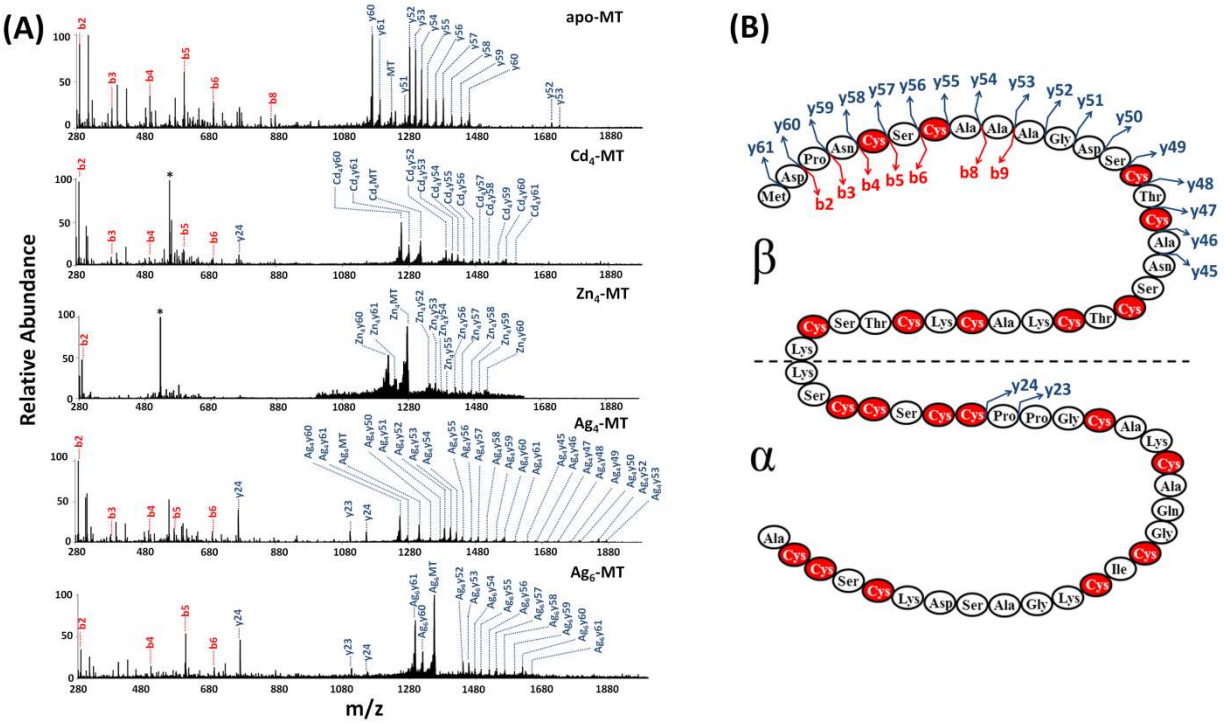


**Figure 2.3.** (A) CID spectra showing the fragmentation product ions from CID of apo-, $Cd_4$-, $Zn_4$-, $Ag_4$- and $Ag_6$-MT. For $Zn_4$-MT, the signal intensity is magnified by 5 times from 1000 to 1570 (m/z). (B) Summary of identified fragment ions from A. α and β indicate the two MT domains. No metal ion dissociation was detected. Note that starred peaks are the products of b5-acetly group and a5-$CH_3SH$. Reprinted with permission from [123].

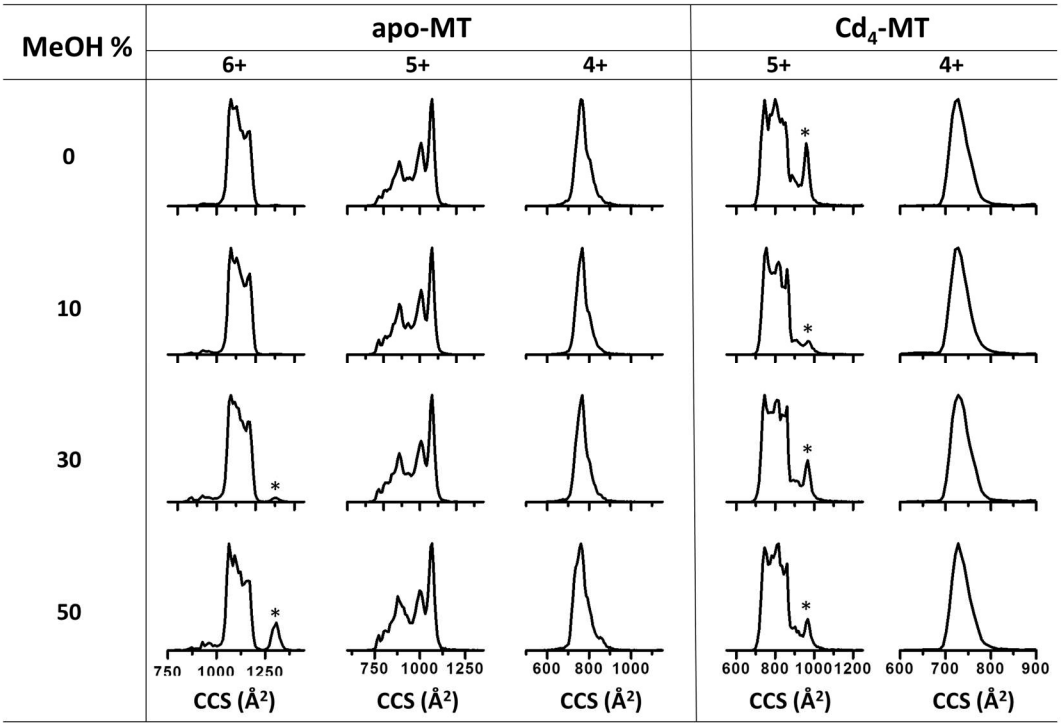


**Figure 2.4.** Ion mobility profiles of apo- and $Cd_4$-MT with different charge states (6+, 5+ and 4+ for apo-MT; 5+ and 4+ for $Cd_4$-MT) and sprayed from different concentrations of methanol (0 - 50% V/V). Note that starred peaks are the products of high background noise and not differences in MT conformational preference. Reprinted with permission from [123].

While nESI-MS and nESI-MS-MS are able to distinguish different metalated species on the basis of mass-to-charge ratios, the mass spectra do not provide secondary/tertiary structural information. Combining ion mobility with nESI-MS, e.g., nESI-IM-MS, affords direct measurements of the conformational diversity of the ion population as well as ion size (shape), information that can be related to structure/conformation.[63, 79, 82, 98] Apo-MT has been described as an intrinsically disordered protein, and indeed the CCS profiles for 6+ and 5+ ions are composed of multiple peaks (**Figure 2.4**), consistent with a heterogeneous population of states, as

opposed to a population of interconverting states. Note also that CCS profiles obtained from methanolic solutions, generally thought to be denaturing conditions, are very similar, suggesting that the addition of methanol does not significantly alter the structure/conformational diversity of MT.[113]

*Collision-Induced Unfolding of $Cd_4$-MT, $Zn_4$-MT, $Ag_4$-MT and $Ag_6$-MT*

CCS profiles for the 5+ ions of $Cd_4$-MT, $Zn_4$-MT, $Ag_4$-MT and $Ag_6$-MT as well as how the CCS profiles change upon collisional activation, viz. collision-induced unfolding (CIU) are shown in panels A and B of **Figure 2.5**. $Cd_4$-MT and $Ag_4$-MT were selected because they are formed in high abundance relative to the $(metal)_i$-MT, where $i$ = 1-3, which suggests that these ions are more stable and/or less reactive toward further metal addition reactions.[56] Although $Zn_4$-MT does not behave similarly to $Cd_4$-MT or $Ag_4$-MT in terms of stability/reactivity toward metalation, it does provide interesting comparisons to the $Cd_4$-MT and $Ag_4$-MT complexes. The relative abundance of the $Ag_6$-MT complex is also not enhanced relative to that of the other $Ag_i$-MT (where $i$ = 5,6 and 8-10; see **Figure 2.6**), but it has been suggested that $Ag_6$-MT "might provide an intact cluster".[110-112] These data allow for comparisons of CIU for mono- and divalent-metal ions, which differ in terms of coordination, diagonal versus tetrahedral, respectively, and it has been reported that fully metalated MTs are known to have different backbone folds.[104, 114]

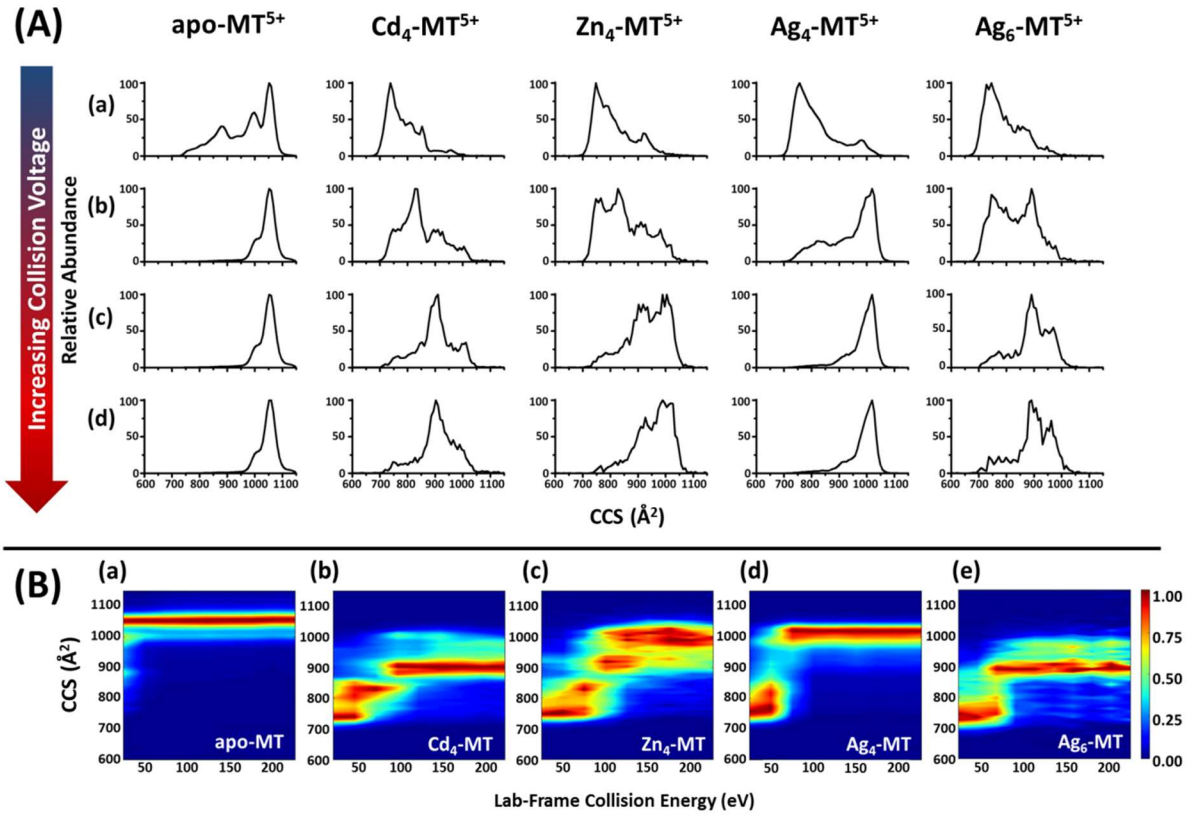


**Figure 2.5.** (A) CCS profiles for the $5^+$ ions of apo-MT, $Cd_4$-MT, $Zn_4$-MT, $Ag_4$-MT and $Ag_6$-MT acquired using different collisional activation conditions. Laboratory frame collision energies are: (a) 25 eV, (b) 75 eV, (c) 125 eV, and (d) 175 eV. (B) CIU heat maps for (a) apo-, (b) $Cd_4$-, (c) $Zn_4$-, (d) $Ag_4$- and (e) $Ag_6$-MT. The collision voltage was changed in increments of 5 V across the full range from 5 V to 45 V. Reprinted with permission from [123].

Prior to CA the CCS profiles for apo-MT ions span the range from ~760-1100 $Å^2$ (**Figure 2.5A(a)**) but the CCS profile for the activated apo-MT ions shift to ~950-1100 $Å^2$ (**Figure 2.5A(b-d)**). Similar shifts in CCS profiles are observed for each of the metalated ions. Prior to CA the peak maximum of the CCS profile for $Cd_4$-MT is centered at approximately 750 $Å^2$, but at the highest CA energies the CCS for $Cd_4$-MT ranges from ~700-1000 $Å^2$ with a peak maximum centered at ~900 $Å^2$. Although the fine

structure in the CCS profiles for $Cd_4$-MT, $Zn_4$-MT, $Ag_4$-MT and $Ag_6$-MT are somewhat different, the overall shapes of the CCS profiles at the various CA energies are quite similar.

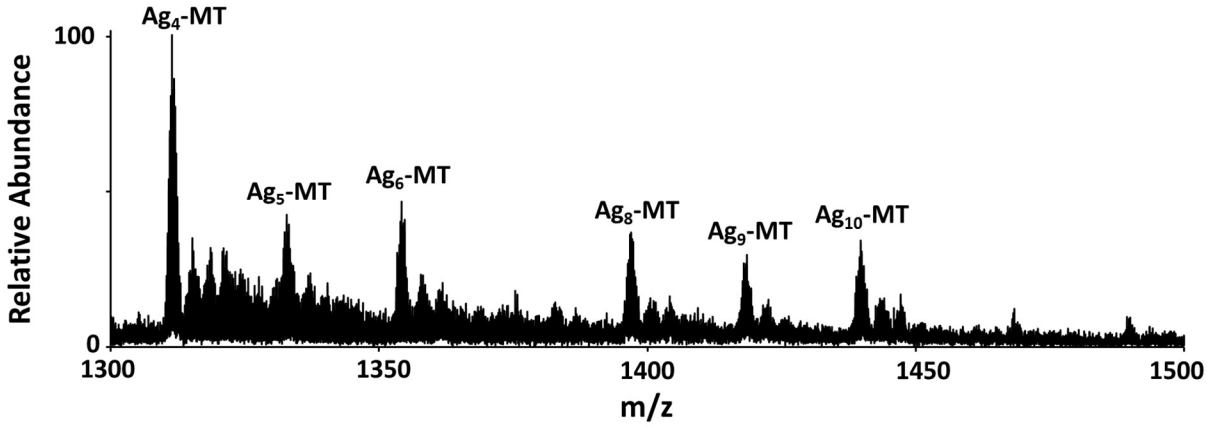


**Figure 2.6.** Mass Spectra (5+) of apo-MT mixing with six equivalents sliver acetate. Reprinted with permission from [123].

The following discussion will be directed toward the CIU heat maps because these data better illustrate the general trends observed in the unfolding reactions. These data better illustrate how small changes in the CA energies induce structural changes of the apo- and metal-MT complex. Apo-MT ions unfold at relatively low (10-25 eV) CA energies to yield an ion population having CCS of approximately 1050 $Å^2$, which was previously assigned to a fully extended conformer.[70] The CIU behavior of $Cd_4$-MT and $Ag_6$-MT ions are similar in terms of the initial and final CCS, but they unfold through different intermediate ion states. $Cd_4$-MT initially unfolds (10-50 eV) to form families of conformers having CCS between 775-850 $Å^2$. At collision energies below <50 eV $Ag_6$-MT unfolds to form conformers having CCS that range from ~725-775 $Å^2$, but these

ions undergoes a one-step unfolding transition at ~ 75 eV to form the final state having a CCS of ~900 Å$^2$. At CA energies above 90 eV the most abundant states have CCS of ~900 Å$^2$ and lower abundance states with CCS extending beyond 1000 Å$^2$. The CIU behavior of $Cd_4$-MT and $Zn_4$-MT are similar in terms of the early unfolding reactions, but $Zn_4$-MT is most similar to $Ag_4$-MT in terms of initial and final unfolded states. $Zn_4$-MT unfolding occurs in four steps, the first three steps yield conformers having CCS that are similar to those for $Cd_4$-MT, and the final unfolded states have CCS that range from 975-1025 Å$^2$. $Ag_4$-MT unfolds at low collision energies similar to that for both $Cd_4$-MT and $Zn_4$-MT, but at collision energies greater than ~50 eV it unfolds to form conformers that are most similar to fully extended apo-MT (CCS ~1000 Å$^2$).

*CIU of $Cd_i$-MT and $Zn_i$-MT ($i$ = 1-3)*

We previously using MD simulations showed that step-wise addition of $Cd^{2+}$ ions to MT promotes folding in the region around the metal ion, whereas other regions that are not involved in metal ion binding remain dynamic.[15] The simulations suggested that species with $i$ = 2-3 were more ordered than are apo- or $Cd_1$-MT ions, but the majority of the backbone remains unstructured and dynamic. CIU provides an experimental means to test the results of the MD simulations and to compare the CIU of $Cd_i$-MT and $Zn_i$-MT ($i$ = 1-3) to $Cd_4$-MT and $Zn_4$-MT. Unfortunately, these same ions ($Ag_i$-MT ($i$ = 1-3)) are only observed at very low abundances (see **Figure 2.7**) and we have been unable to obtain reproducible CIU data using either pre-mixed solutions or the mixing-tee, **Figure 2.8** contains CIU heat maps for $Cd_i$-MT and $Zn_i$-MT ($i$ = 1-3).

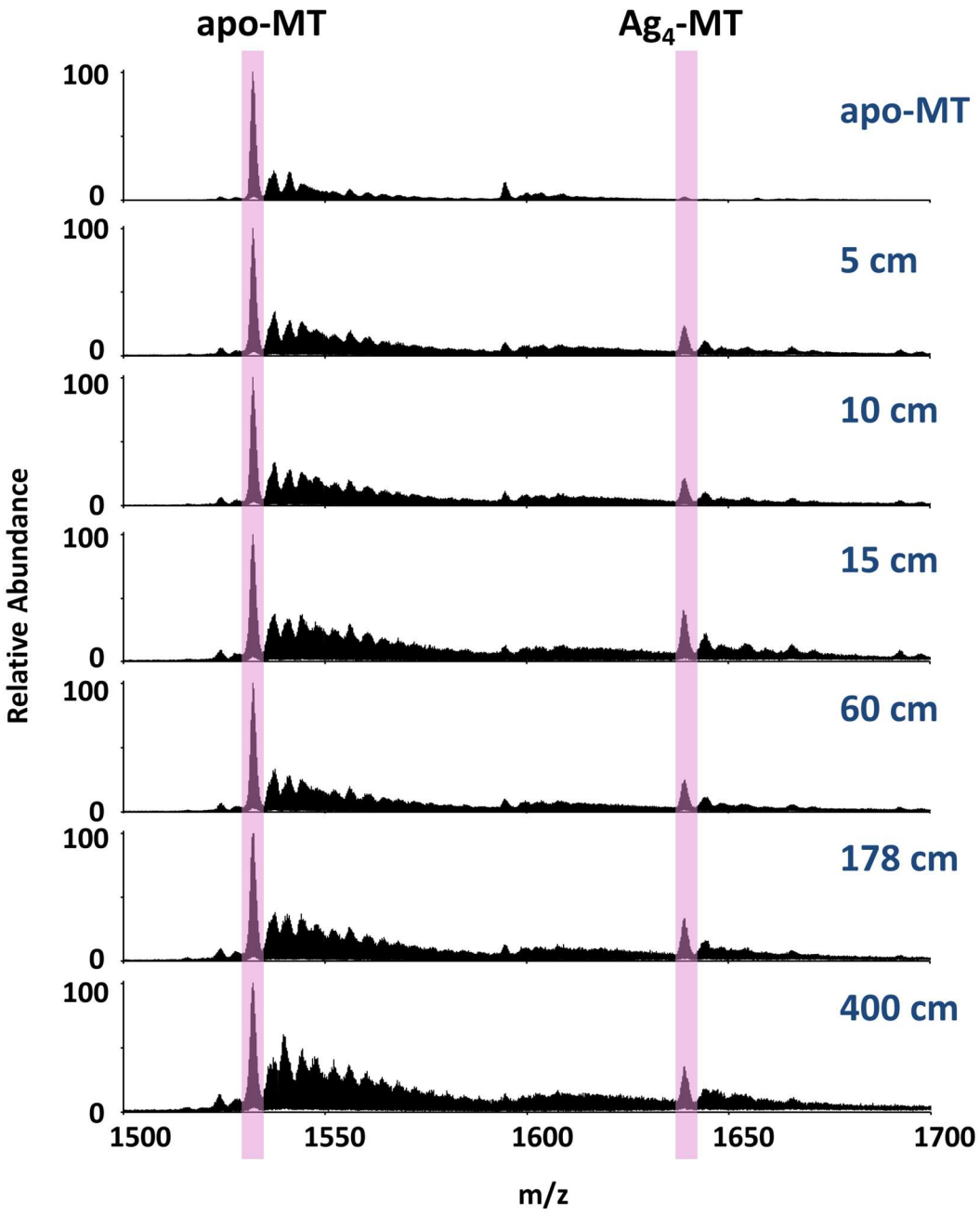


**Figure 2.7.** Mass Spectra (4+) showing using mixing tee and different capillary length to mix apo-MT with four equivalents sliver acetate. The top mass spectrum is of apo-MT acquired without the use of a mixing tee. The capillary length used after is 5 cm, 10 cm, 15 cm, 60 cm, 178 cm and 400 cm (from top to bottom). No partially metalated intermediate is trapped other than $Ag_4$-MT. Reprinted with permission from [123].

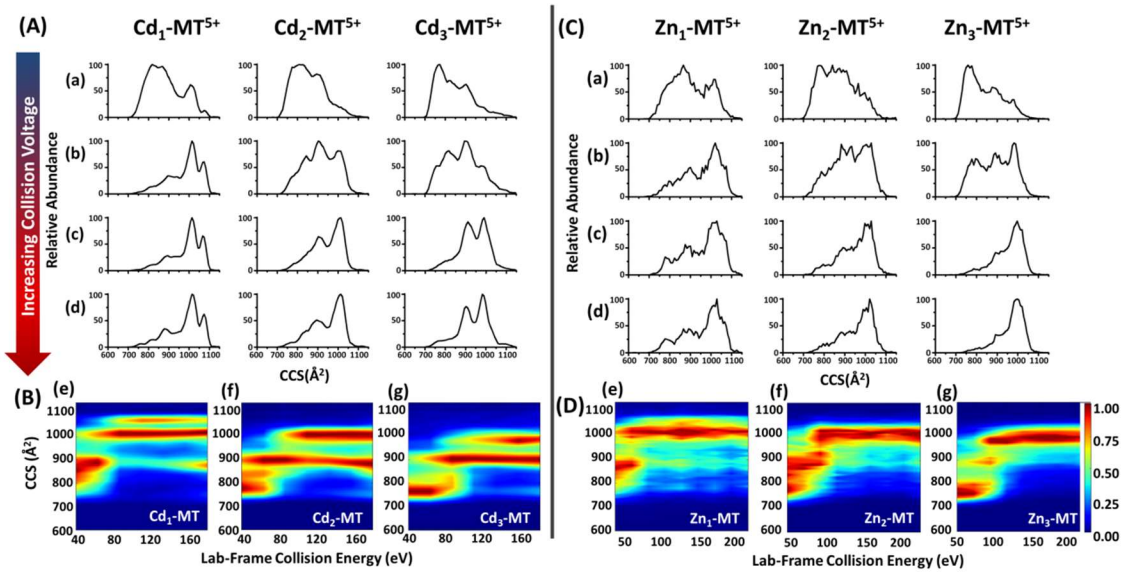


**Figure 2.8.** (A) CCS profiles for the $5^+$ ions of $Cd_1$-, $Cd_2$- and $Cd_3$-MT acquired using different collisional activation conditions. Laboratory frame collision energies are: (a) 25 eV, (b) 75 eV, (c) 125 eV, and (d) 175 eV. (B) CIU heat maps for (e) $Cd_1$-, (f) $Cd_2$- and (g) $Cd_3$-MT. (C) CCS profiles for the $5^+$ ions of $Zn_1$-, $Zn_2$- and $Zn_3$-MT acquired using different collisional activation conditions. Laboratory frame collision energies are: (a) 25 eV, (b) 75 eV, (c) 125 eV, and (d) 175 eV. (D) CIU heat maps for (e) $Zn_1$-, (f) $Zn_2$- and (g) $Zn_3$-MT. Reprinted with permission from [123].

The pre-CA CCS profile for $Cd_1$-MT reveal a high abundance of compact conformers (~725-920 Å$^2$) and a smaller population of ions with CCS ~1000 Å$^2$, but these conformers unfold at relatively low collision energies ($E_{lab}$ < 60 eV) to form conformers with CCS of ~1000-1075 Å$^2$. Interestingly, at collision energies > 80 eV, some of the $Cd_1$-MT ion population adopts a CCS approximating that observed for the fully unfolded apo-MT ions (~1050 Å$^2$); however, the most abundant population has CCS centered at ~ 1000 Å$^2$. $Cd_2$-MT and $Cd_3$-MT also populate compact conformers (~725-800 Å$^2$), but display a higher abundance of ions with a CCS ~750 Å$^2$ and a much lower abundance of the larger ~1000 Å$^2$ conformers. At the highest collision energies these ions unfold to conformers with CCSs of ~900 and then ~1000 Å$^2$. Further unfolding from the 900 Å$^2$ conformers to the more extended ~1000 Å$^2$ conformers occurs at higher collision energy for $Cd_2$-MT and an even higher collision energy for $Cd_3$-MT. Note that the extended conformers with CCS of ~1000 Å$^2$ were not observed for $Cd_4$-MT at any collision energy. Collectively, these results illustrate incremental stabilization (folding) upon binding of $Cd^{2+}$ ions, and on the basis of our prior work we propose that this structural ordering is the result of metalation of the α-domain---the final ordering occurs upon addition of the fourth $Cd^{2+}$ ion.[56]

The CIU heat map of $Zn_1$-MT is remarkably similar to that observed for $Cd_1$-MT, specifically conformers with CCS of ~750-920 Å$^2$ unfold at relatively low collision energies through an intermediate (CCS ~875 Å$^2$) to much more extended conformers (~1000 Å$^2$). $Zn_2$-MT and $Zn_3$-MT ions show greater preferences for the more compact conformers (CCS ~750 Å$^2$) at lower collision energies. As the CA energies are increased

these ions unfold to form a small population of ions having CCS of ~900 $Å^2$, but the dominant products of CIU are ions having CCS of ~1000 $Å^2$, which is very similar to the CCS for the final product observed for $Zn_4$-MT. In fact, the CIU heat maps for $Zn_3$-MT and $Zn_4$-MT are quite similar, but the energies at which unfolding occurs are lower for $Zn_3$-MT than that for $Zn_4$-MT. Overall, $Cd^{2+}$ and $Zn^{2+}$ have different ability to stabilize (fold) MTs.

The initial unfolding of $Zn_4$-MT involves conformers that have CCS that are very similar to $Cd_4$-MT, but the CA energies needed for unfolding are somewhat different. For example, a portion of the $Zn_4$-MT ions are unfolded at ~50 eV, but a significant fraction of the ion population remains folded. Complete unfolding to conformers having CCS of ~900 $Å^2$ requires ~100 eV. The final unfolded conformers of $Zn_4$-MT ions have CCS (~1000 $Å^2$) that are assigned to the fully expended β-domain for $Cd_4$-MT.

**Conclusions**

Chen *et al.*[70] reported IM-MS results and MD simulations that provide strong evidence that all four $Cd^{2+}$ ions of $Cd_4$-MT are located in the α-domain, and the CIU data reported here generally agree with their results. We propose that the early transitions in the CIU of $Cd_4$-MT involve conformational changes involving the metal-free β-domain. The CCS of ~775 $Å^2$ for the calculated compact conformer of $Cd_4$-MT, where all four $Cd^{2+}$ ions are in the α-domain and β-domain is also compact, is in good agreement with the experimental CCS of ~750 $Å^2$. Mild CIU shifts the CCS to 805–875 $Å^2$ owing formation of partially unfolded β-domain, which also agrees quite well with the MD

simulations. Additional increases in the collision energies produces a family of conformers that have CCS of ~900 $Å^2$, and small population of ions have CCS that extend to >950 $Å^2$. The MD simulations suggest that conformers having a native-like α-domain and an extended β-domain should have a CCS greater than 950 $Å^2$. Thus, it appears that the β-domain of $Cd_4$-MT is not fully extended, but rather adopts some partially unfolded conformations. Presumably, these conformers retain some interactions between the thiolates of the β-domain and the $Cd^{2+}$ ions of the α-domain, and the more extended conformers having CCS of ~1000 $Å^2$ are formed upon breaking these interactions. The CIU heat map for $Ag_6$-MT is most similar to that of $Cd_4$-MT, thus we propose that $Ag_6$-MT forms a "metal cluster" within the α-domain similar to that of $Cd_4$-MT. It also appears that thiolate ligands located β-domain inhibit unfolding that yields an extended β -domain in a manner similar to $Cd_4$-MT. It should be noted, however, that Nielson, Li, and Palacios *et al.* have proposed that the $Ag_6Cys_9$ cluster is formed in the β-domain.[102, 110-112]

Although MD simulations have not been performed on $Zn_4$-MT, $Ag_4$-MT or $Ag_6$-MT, it is interesting to use the simulations for $Cd_4$-MT as models for interpreting the results for these complexes. The differences for $Cd_4$-MT and $Zn_4$-MT are for the final unfolded states, which are attributed to the relative binding energies of the β-domain thiolate groups and those located in the α-domain. The absences of similar intermediate states for the $Ag_4$-MT complex suggest that similar interactions are not present, or they are much weaker. Regardless, the population of conformers formed at the highest collision energies for both $Zn_4$-MT and $Ag_4$-MT have CCS that extent to ~ 1000 $Å^2$. The

observed differences for $Ag_4$-MT from $Cd_4$-MT and $Zn_4$-MT are likely a result of the coordination geometries, divalent metals exhibit saturation favor tetrahedral coordinated structures, whereas monovalent metals are likely to form a digonal or trigonal coordination, which have been shown to give rise to different saturated complexes upon addition of twelve or higher numbers of metal ions.[104, 114] Differences in coordination geometries would also influence the energetics of CIU of $Ag_4$-MT relative to both $Cd_4$-MT and $Zn_4$-MT. $Ag_4$-MT ions unfold at quite low collision energies (~10 eV) to form conformers having CCS of 800 $Å^2$, but a fraction of these ions are stable up to ~50 eV at which point they unfold to form conformers having CCS of 1020 $Å^2$, which is assigned to a fully extended conformer. The initial CCS for $Ag_6$-MT are similar to that for $Ag_4$-MT (~750 $Å^2$), but this conformer unfolds to yield a family of conformers that is most similar to that of the most abundant unfolded conformer observed for $Cd_4$-MT, i.e., CCS ~ 900 $Å^2$.

Overall, ion mobility combined with CIU/CID provides additional information as to structural details for each species. As noted above, the mass spectra nor the CID spectra reveal information about conformational preferences of the metal-MT complex; however, the $Cd_4$-MT and $Ag_6$-MT only form low abundances CID spectra provides a very interesting but subtle feature of the metal-complex---the smallest y-fragmentation contained in the CID spectrum is y45, which contains multiple metal ions, and the only metal-free y-fragment ions are y23/y24. These results are evidence that the metal binding affinities for Cys located in the β-domain from Met1 to Ala17 and in the a-domain from Pro39 to Ala62 are smaller than the Cys located in the middle of the

protein, specifically from Asn18 to Cys38. The Cys percentage from Met1 to Ala17 is 23.5%, 33.6% from Pro39 to Ala62 and 42.9% between Asn18 to Cys38. The high percentage of cysteine in the middle of MT may favor inter-domain interactions during CIU/CID process and stabilize bound metal ions. Previous research of our group shows Cys33 played an important role in the metal displacement process,[71] and it is interesting that Cys33 falls in the region of high percentage cysteine binding. Stillman suggested a non-cooperative metal ion binding mechanism, viz. "the metals bind initially to the protein in a non-specific manner followed by a redistribution of the metal ions to the more thermodynamically favorable position'' rather than a domain preference binding pattern.[89, 115] If that is the case, the cysteine rich region from Asn18 to Cys38 may be involved in first stage metal ion recognition and binding before rearrangement. Such a mechanism is consistent with the CIU results, i.e., for all the complexes studies here the last regions of the molecule to take on extended conformations are the terminal regions. In particular, of fully extended conformers at collision energies that approach the dissociation threshold.

The combination of CID and CIU reveals incremental folding and stabilization of MT structure upon addition of each $Cd^{2+}/Zn^{2+}$ ion. This research demonstrates an alternative approach to understanding the physiologically predominant partially metalated species of MT. Lastly, while this is the first report describing differences in structure and coordination of these partially metalated species, the insights obtained about the complexes are very encouraging and clearly illustrate future potential for combining these approaches with molecular dynamics simulations.

# CHAPTER III

# $AG^+$ ION BINDING TO HUMAN METALLOTHIONEIN-2A IS COOPERATIVE AND DOMAIN SPECIFIC

## Introduction

Metallothioneins (MTs) constitute a family of cysteine-rich small proteins that bind a wide range of metal ions.[1-2] While the exact biological function(s) of MTs are not fully understood, they have been implicated in diseases such as Alzheimer's, Parkinson's and cancer, which suggests that MTs have functions other than "sponges" for metal homeostasis, heavy metal detoxification and autoxidation.[1, 3, 116-118] Although apo-MTs lack well-defined tertiary structure, the structure(s) and folding stabilities of metalated forms are largely determined by metal-thiolate bonds.[1, 28] Detailed structural characterization of MTs has proved challenging owing to difficulties associated with growing high-quality crystals required for X-ray crystallography, and it has been equally difficult to locate metal bound cysteine residues using conventional protein NMR spectroscopy.[1-2] While it is possible to substitute NMR silent metal ions with NMR active nuclei*, i.e.*, Zn(II) by $^{111}$Cd(II) or $^{113}$Cd(II), or Cu(I) by $^{109}$Ag(I), it is unclear that such replacements are isostructural.[1] Studies of structure/function relationships of MTs are further complicated by the fact that the physiologically dominant forms of MTs are the apo and partially metalated forms;[85, 119-121] but *their* low abundances and conformational heterogeneity have prohibited *in vitro* studies of partially metalated MTs using traditional structural approaches, *viz.* x-ray cryptography or NMR spectroscopy.[1]

Fenselau[55] and Stillman[122] were the first to exploit electrospray ionization-mass spectrometry (ESI-MS) for studies of partially- and fully-metalated MTs. More recently, nano-electrospray ionization combined with ion mobility-mass spectrometry (nESI-IM-MS) was used to investigate conformational preferences of apo- and partially-metalated MT.[48, 56, 70-71, 123] These early studies showed that under suitable instrumental conditions, it is possible to maintain noncovalent interactions, such as the metal-ligand interactions formed in MTs.[70, 123-124] Collision-induced unfolding (CIU), an IM-MS method that is used to monitor unfolding (changes in the collision cross section) following collisional activation provides additional information on stabilities of gas phase ions,[72] has also been used for studies of metalloproteins and protein complexes.[76-82] Combining nESI-IM-MS with "bottom-up" and "top-down" proteomic strategies in concert with chemical labeling yielded new insights on reactivity and metal binding sites of $Cd_4$-MT.[56] In addition, the combination of IM-MS and molecular dynamic simulations revealed the high-level of conformational diversity for both apo- and partially metalated MT.[70] nESI-IM-MS has also been used to study reactions of $Cd_7$-MT and N-ethylmaleimide (NEM) as well as kinetic stability of $Cd_i$-MT ($i$=1 to 7). This approach also revealed evidence for greater kinetic stability of the α-domain of MT as well as potential role for Cys33 in domain interaction associated with $Cd^{2+}$ binding.[71] More recently, CIU was used to probe the gas-phase stabilities of partially metalated products with different metal species.[123]

These earlier studies on MTs were focused on reactions of divalent metal ions ($Cd^{2+}$ and $Zn^{2+}$); however, monovalent ions such as $Ag^{+}$ are also of physiological

importance.[1, 102, 125-126] Here, direct metalation and collision-induced unfolding (CIU) are used in an effort to better understand this important class of proteins reacting with $Ag^+$, as well as difference between $Ag_i$-MT and $Cd_i$-MT. These results show that the products of metalation and stabilities of the gas-phase ions $Ag_i$-MT complexes are significantly different from those $Cd_i$-MT complexes. Top-down and bottom-up mass proteomic MS data of the NEM labeled $Ag_4$-MT provides strong evidence that all four $Ag^+$ ions on $Ag_4$-MT are strong bound to β-domain, which is significantly different from $Cd_4$-MT complex.[127-128] These differences may play important roles in regulating physiological function(s) for metallothioneins in metal homeostasis and detoxification as well as diseases development.

**Experimental Section**

Silver acetate, cadmium acetate, ammonium acetate, zinc acetate, diethylenetriaminepentaacetic acid (DTPA), dithiothreitol (DTT), tris (2-carboxyethyl) phosphine hydrochloride (TCEP) and N-ethylmaleimide (NEM) were purchased from Sigma-Aldrich (St. Louis, MO). Sequencing grade modified trypsin was purchased from Thermo Fisher Scientific (Waltham, MA). Deionized water (18.2 MΩ) was obtained from a Milli-Q water apparatus (Millipore, Billerica, MA). Micro Bio-Spin 6 columns were purchased from Bio-Rad Laboratories, Inc. (Hercules, CA).

Recombinant human $Zn_7$-MT2A (GS **M**DPNCSCAAG DSCTCAGSCK CKECKCTSCK KSCCSCCPVG CAKCAQGCIC KGASDKCSCC A) was express and purified. Plasmid for MT was constructed with an N-terminally encoded 6xHis+MBP

tag (pET28b) and transformed into *E. coli* cells (DE3, Agilent). Colonies were grown in LB media supplemented with kanamycin (50 mg/ml) and zinc acetate (200 μM) at 37 °C until $OD_{600}$ of 0.6. IPTG (0.5 mM) was used to induce cells with 1 mM zinc acetate and incubated overnight at 16 °C. Cells were harvested and centrifuged to remove cellular debris and loaded on HisTrap HP column (GE Healthcare) pre-equilibrated with 300 mM NaCl, 20 mM Tris, 20 mM imidazole and 1 mM DTT at pH=7.4 (NHA). Bound protein was eluted with buffer NHB (300 mM NaCl, 20 mM Tris, 500 mM imidazole and 1 mM DTT at pH=7.4) and immediately loaded to desalting column (HiPrep 26/10, GE Healthcare) and eluted with NHA buffer. Infused 6×His tag and MBP protein was cleaved using TEV protease overnight at 24 °C. A Superdex HiLoad 16/600 75 pg size-exclusion column (GE Healthcare) was used to separate TEV and cleaved tags from hMT using 50 mM NaCl, 20 mM Tris and 1 mM DTT at pH=7.4 and purified protein was flash frozen and stored at -80 °C.

$Zn_7$-MT was demetalated by 100x DTPA (pH=7.4) and buffer exchanged with Micro Bio-Spin™ 6 Columns (BIO-RAD) to solution of 50 mM ammonium acetate (pH=6.8), 10% MeOH and 1 mM TCEP before using.

Protein storage and preparation process was performed as previously reported.[123] 17.5 μM apo-MT was reconstituted in 50 mM ammonium acetate, 10 % methanol and 1 mM TCEP. The concentration of apo-MT was estimated by $Cd^{2+}$ titration experiments (results are not shown). The $Ag^{+}$ metalation experiment was performed by sequential addition of 1.75 μL 1 mM (one equivalent) silver acetate to 100 μL MT solution until the

metalation degree of products showed saturation. Each time after $Ag^+$ addition, the solution was incubated at room temperature for 1 h and then analyzed by nESI-IM-MS.

All experiments were performed on a Waters Synapt-G2 HDMS instrument (Manchester, UK). Instrumental conditions were tuned to minimize collisional heating as previously described.[48]

nESI-CIU-MS experiments were carried out as described previously.[98, 123] Different collision energies were applied by changing the voltage (increments of 5 V) drop between the exit of the quadrupole and the entrance to the TWIG-trap. The activation energy was reported as lab-frame collision energy.[123-124] Ion mobility profiles under different activation energy were compiled into CIU heat maps using CIUSuite as described by Ruotolo *et al.*[83] CIU50 data were extracted with CIUSuite2 to compare the unfolding energy.[84] Averages and standard deviations were calculated using three acquisitions. The standard deviations are within 3%.

Ag/Cd mixed metal synthesis experiment was performed by addition of ~3.5 equivalent of 1 mM $Ag^+$ to apo-MT and incubating for 1 h at room temperature. Afterwards, 3.5 equivalent of 1 mM $Cd^{2+}$ was added and incubated for 1 h at room temperature. Mass spectra and CIU heat maps of the product ions was obtained. Similar experiment was performed after switching the order of adding $Ag^+$ and $Cd^{2+}$.

An Ag/Cd mixture solution was prepared by mixing 1 mM silver acetate and 1 mM cadmium acetate solution by 1:1 ratio. Apo-MT was mixed with 7 eq of Ag/Cd mixture, and incubated at room temperature for 1 h before analysis.

$Ag_4$-MT was obtained by metalation of apo-MT (adding 7 μL 1 mM $Ag^+$ to a 17.5 μM apo-MT solution). 4 μL 10 mM NEM was added to $Ag_4$-MT and incubated for 1 h at room temperature to completely react with metal-free cysteinyl groups. The alkylated metalated products ($Ag_4NEM_{14}$-MT) were mass-selected for direct sequencing by tandem mass spectrometry (top-down approach).

In-solution digestion of $Ag_4NEM_{14}$-MT was performed by trypsin at a weight ratio of 1:50 (trypsin to protein) at 37 ºC overnight (bottom-up approach). The resulting digest was analyzed by ESI-MS, and the metal-bound peptides ($Ag_4NEM_3$-β domain) were further analyzed by MS-CID-IM-MS. [56, 96]

**Results and Discussion**

Previous studies have illustrated the utility of nESI-MS for MT studies, as well as the added information afforded by combining it with IMS.[1, 48, 56, 70-71] nESI-MS allows detection and separation of each partially metalated MT species, while IMS can probe the shape and size of each individual partially metalated MT.[123] Here, a comprehensive mass spectrometry-based strategy employing metalation, covalent chemical labeling with NEM, top-down and bottom-up proteomic MS and collision-induced unfolding (CIU) is used to better understand the structure and stabilities of products formed by reactions of $Ag^+$ with MT-2A (denoted as MT). Rotationally-averaged collision cross section (CCS) profiles obtained by ion mobility for the 5+ apo-MT ions are multicomponent, a signature for a conformationally heterogeneous, whereas those for 4+ MT ions are narrow indicative of an ion population that contains less conformational

diversity.[129-130] Owing to differences in the conformational diversities of the ion population, the following sections are focused exclusively on the metalation reactions of the $MT^{5+}$ ions. It should be noted, however, the rates of reactions and the numbers of metals ions added to MT are similar for both charge states.

*Synthesis of human $Ag_i$-MT complexes*

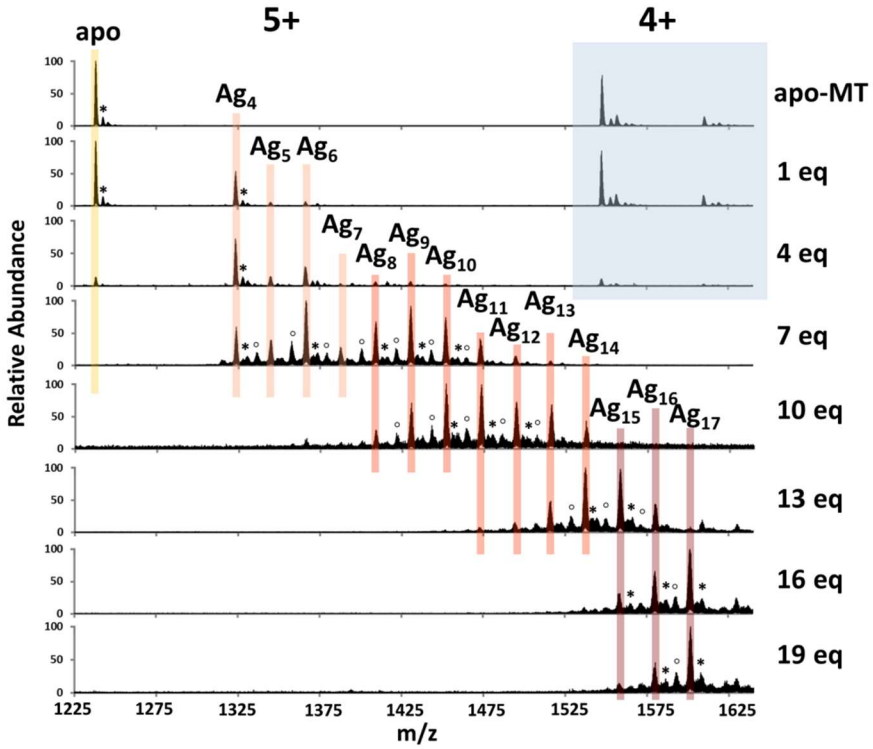


**Figure 3.1.** ESI-MS spectra taken following sequential addition of $Ag^+$ to apo-MT solution. Peaks with asterisks (*) and circles (°) are for ions that shifted by ~23 and ~60 Da, corresponding to sodium and acetate adducts, respectively.

**Figure 3.1** contains mass spectra acquired $Ag^+$ ion titration of human MT. Although the spectral congestion that arises from formation of adduct ions (*e.g.,* $Na^+$, acetate ions and oxidized MT) and the metalated ($Ag_i$-$MT^{5+}$) product ions complicate accurate kinetic measurements, the combined use of IMS and high mass resolution is sufficient to allow for high confidence level assignment of the product ions.[96, 131-132] During the entire titration, MT can bind up to seventeen $Ag^+$ ions. With increasing concentration of $Ag^+$ in MT solution, the abundances of metalated product ions increased. Upon addition of solutions containing $Ag^+$ ions, low abundance signals corresponding to $Ag_i$-MT (i=1-3) and much higher abundance ions corresponding to $Ag_4$-MT are detected. The low abundances of $Ag_i$-MT (i = 1-3) is not surprising owing to the high concentrations of thiol ligands (20 SH group per MT molecule) as well as a high degree of cooperativity for formation of the $Ag_4$-MT product ion. Similar cooperative binding results were obtained for $Cd^{2+}$ titration in our previous research.[56]

*$Ag^+$ displacement by reactions with N-ethylmaleimide (NEM)*

Previous studies on $Cd_7$-$MT^{5+}$ reported that displacement of $Cd^{2+}$ occurred by a two-component, cooperative mechanism, *viz.* rapid displacement of three $Cd^{2+}$ ions followed by slow loss of the remaining four $Cd^{2+}$ ions.[71] Additional experimental results revealed that displacement of $Cd^{2+}$ by NEM was domain specific; the three $Cd^{2+}$ ions that are displaced first are from the β-domain whereas subsequent $Cd^{2+}$ displacement is from the α-domain.[71] Similar experiments were carried out for $Ag_i$-MT ($i$ = 9 - 14) (see **Figure 3.2**). Addition of NEM to a solution containing $Ag_i$-MT ($i$ = 5 - 17) produced primarily the $Ag_4NEM_{14}$-MT complex. The results for displacement of $Ag^+$ by NEM

provide additional evidences of the uniqueness of $Ag_4NEM_{14}$-MT complex, specifically, the $Ag^+$ ions of the $Ag_i$-MT ($i$ = 5 - 17) complexes are considerably more labile than are those of the $Ag_4$-MT in solution phase.

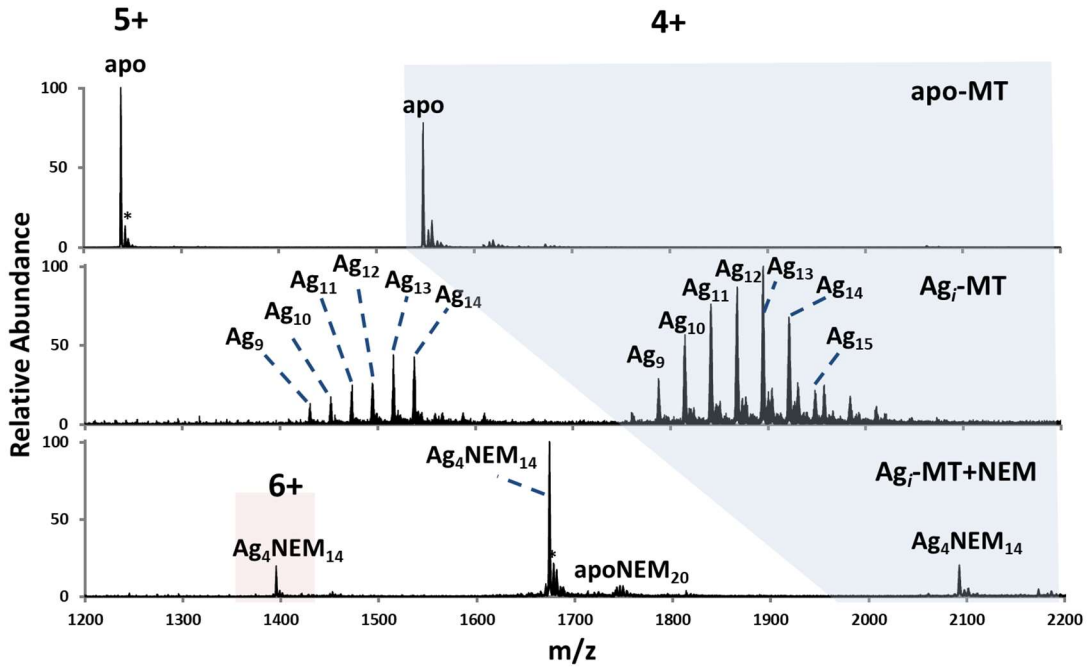


**Figure 3.2.** MS spectra of apo-MT, $Ag_9$- to $Ag_{14}$-MT and $Ag_4NEM_{14}$-MT. Apo-MT was mixed with ~12 eq of $Ag^+$ and incubated in room temperature for 1 h before analysis. After that, the formed $Ag_i$-MT ($i$=9-14) was mixed with 20 eq NEM and incubated in room temperature overnight before MS analysis. The asterisks (*) denote the $Na^+$ adducts.

*Synthesis and stabilities of mixed metal ($Ag^+/Cd^{2+}$) MT: Preferred binding domains for $Ag^+$ and $Cd^{2+}$*

The high abundance of $Ag_4$-MT product ions formed by titration of MT with $Ag^+$ ions are strikingly similar to that for titration of MT by $Cd^{2+}$ ions,[70] *viz.* $Ag_4$-MT appears to be formed cooperatively. This raises a question, do $Ag^+$ and $Cd^{2+}$ ions bind to the same or different domain? [102, 110-112] In an effort to answer this question, cross metalation experiments were performed. These experiments were carried out by addition of $Ag^+$ or $Cd^{2+}$ to aliquots of solutions containing MT to form $Ag_4$-MT (**Figure 3.3A**) and $Cd_4$-MT (**Figure 3.3C**), respectively. Following incubation period (1 hour) each solution was then reacted by addition of $Cd^{2+}$ (**Figure 3.3D**) or addition of $Ag^+$ (**Figure 3.3E**). The final products of these reactions produced mixed metal complexes of $Ag_4Cd_4$-MT or $Cd_4Ag_4$-MT and low abundances of $Ag_5Cd_4$-MT or $Cd_4Ag_5$-MT, respectively. The $Ag_4Cd_4$-MT product was also formed by addition of solutions containing equal concentrations of $Ag^+$ and $Cd^{2+}$ ions to a solution of apo-MT (**Figure 3.3E**). Similar metalated products are obtained regardless of the order of metal addition. No metal replacement is observed. The results from these experiments are interpreted as evidence that $Ag^+$ and $Cd^{2+}$ bind to specific domains (see below).

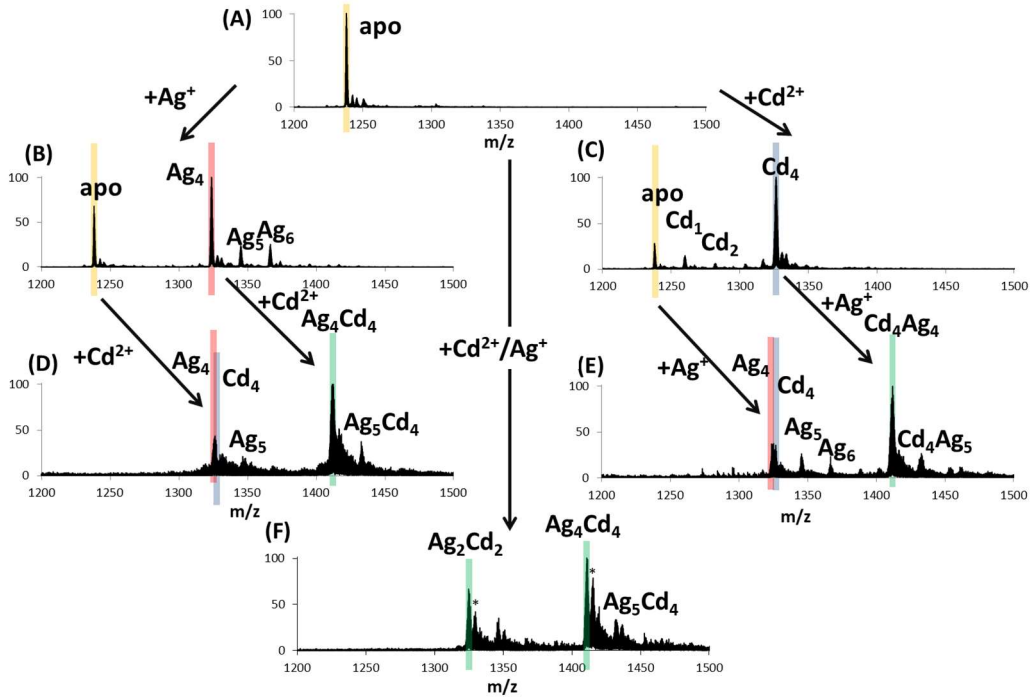


**Figure 3.3.** Mass spectra of MT obtained following addition $Cd^{2+}/Ag^{+}$ ions; (A) apo-MT; (B) after addition of four equivalence $Ag^{+}$; (C) after addition of four equivalence $Cd^{2+}$; (D) addition of four equivalence $Cd^{2+}$ to solution of $Ag_i$-MT; (E) addition of four equivalence $Ag^{+}$ to solution of $Cd_i$-MT; (F) apo-MT reacted with $Ag^{+}/Cd^{2+}$ mixture. Peaks with an asterisk are for $Na^{+}$ adducts.

*Top-down and bottom-up proteomics following covalent labeling of $Ag_4$-MT with NEM: Where are the $Ag^+$ ions bound?*

Top-down proteomics sequencing strategies were combined with NEM labeling to further characterize $Ag_4$-MT. Addition of excess NEM to a solution containing $Ag_4$-MT (prepared as described above) yielded $Ag_4NEM_{14}$-MT. This product suggests that among the 20 cysteine residues in MT, 14 are labeled by NEM and the remaining 6 are coordinated to $Ag^+$ ions. CIU heat maps for $Ag_4NEM_{14}$-MT are shown in **Figure 3.4A**. The shifts in the CCS obtained by CIU are used to track unfolding transition of the $Ag_4NEM_{14}$-MT ions. The CCS of $Ag_4NEM_{14}$-MT is shifted from ~860 $Å^2$ to ~880 $Å^2$ with collisional activation, but at higher collision energies (CE) the CCS remains constant indicating that the $Ag_4NEM_{14}$-MT complex resists unfolding.

The $[Ag_4NEM_{14}\text{-MT}]^{5+}$ ions were also analyzed by MS-CID-IM-MS, which mass-selected $[Ag_4NEM_{14}\text{-MT}]^{5+}$ ions are activated by energetic collisions with a neutral gas atom (Ar) and the product ions formed are then analyzed by ion mobility (on the basis of size-to-charge) and mass spectrometry (on the basis of mass-to-charge) as illustrated in **Figure 3.4B**. Using this approach the CID fragment ions are dispersed along charge-state trendlines, which reduces spectral congestion and simplifies identification of the fragment ions.[56, 60, 96, 132-133] The mass spectra shown in **Figure 3.4C** were obtained by extracting the ion signals bracketed by the dashed lines (marked with charge states) in **Figure 3.4B**. The fragment ions in each spectrum shown in **Figure 3.4C** are then used to assign the locations of the $Ag^+$ ions and NEM labels, as summarized in **Figure 3.4D**.

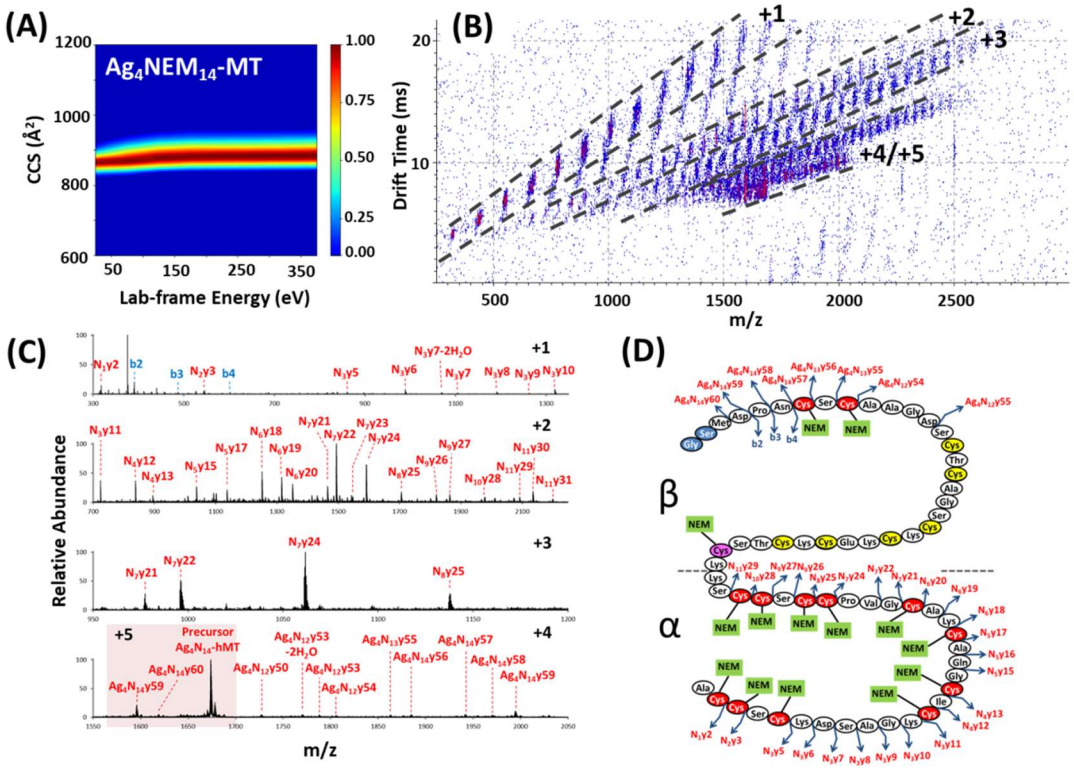


**Figure 3.4.** (A) CIU of $Ag_4NEM_{14}$-MT. Due to the limited fragmentation coverage from Ser12 to Ser32, 13 (colored in red) out of the 14 NEM labeled cysteines can be located with top-down approach. Cys29 (colored in pink) is proved to be NEM labeled later with the bottom-up approach. (B) 2D MS-CID-IM-MS spectrum of $Ag_4NEM_{14}$-MT. The trendlines are shown for ions of different charge states as labeled (+1 to +5). (C) Extracted mass spectra for each trendline; for simplicity NEM is abbreviated as "N". (D) Summary of identified fragment ions and corresponding model from panel C. The labels α and β indicate the location of the domains. The N-terminal GlySer-tag, a product of tag cleavage using TEV protease, is not included in the amino acid position assignments.

The most abundant CID fragment ions correspond to y-type fragment ions, *viz.* fragment ions formed by cleavage of the amide bond with charge retention by the C-terminus.[106] Assignments for the CID fragment ions of the $Ag_4NEM_{14}$-MT species are in **Figure 3.4D**. A series of metal-free, α-domain CID fragments ranging from y2 to y29 also contain 1 to 11 NEM labeled residues serve as evidence that none of cysteine residues in the α-domain are involved in $Ag^+$ binding (see **Figure 3.4D**). In addition, Cys5 and Cys7 are also labeled by NEM, which is considered as evidence that these sites are not involved in binding $Ag^+$ or that the metal binding is weak relative to other binding sites. Among the 7 cysteine residues between Cys13 to Cys29, 6 are involved in binding $Ag^+$ ions and one is labeled by NEM. The limited fragment ion coverage from Ser12 to Ser32 does not allow identification among Cys13 to Cys29; however, similar results for the β domain discussed below help to resolve this issue.

IM-MS data of tryptic digested $Ag_4NEM_{14}$-MT was used to assign the $Ag^+$ binding sites of the β-domain. Tryptic digestion $Ag_4NEM_{14}$-MT produced a number of peptides corresponding to cleavages of α domain (see **Figure 3.5** and **Table 3.1)** as well as tryptic fragments corresponding to the intact β domain, *viz.* m/z 1329.62 ($3^+$) (GlySer-Met1-Lys30) containing four $Ag^+$ ions and three NEM labels. The CIU heat map (**Figure 3.6**) suggests that the $Ag_4NEM_3$-β $domain^{3+}$ is quite stable, *viz.* the complex does not unfold even at the highest CE, and the MS-CID-IM-MS data (**Figure 3.6B and C**) is strong evidence that Cys5, Cys7 and Cys29 are bound to NEM and the four $Ag^+$ ions of $Ag_4NEM_3$-β domain are bound to Cys13, Cys15, Cys19, Cys21, Cys24 and Cys26. Note fragments from y3 to y9 contain one NEM and no $Ag^+$ ion, which suggests

that among Cys24, Cys26 and Cys29, only Cys29 is labeled by NEM. Cys24 and Cys26 are coordinated with $Ag^+$ ions, but the binding between these two cysteines and $Ag^+$ ions are relatively weak upon collisional activation. Lastly, missed tryptic cleavages at Lys20, Lys22, and Lys25 suggests that these residues are buried within a relatively stable $Ag_4Cys_6$ cluster, which is consistent with the CIU heat map (**Figure 3.6A**) for a high degree of stability for the $Ag_4Cys_6$ cluster.

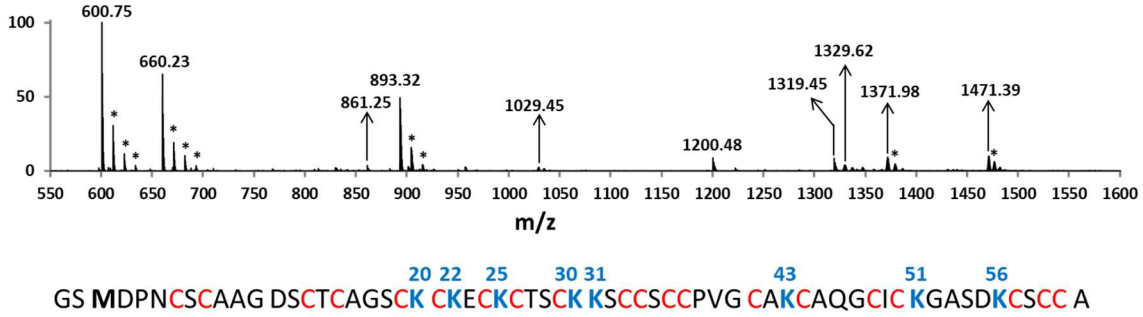


**Figure 3.5.** MS spectra of $Ag_4NEM_{14}$-MT after tryptic digestion. The identified fragmentation and corresponding sequence are listed in Table 3.1.

| m/z | z | Position | Modification | | Sequence |
|---|---|---|---|---|---|
| | | | Ag | NEM | |
| 1471.39 | 4 | GS-1-43 | 4 | 8 | GS-MDPNCSCAAGDSCTCAGSCKCKECKCTSCKKSCCSCCPVGCAK |
| 1371.98 | 3 | GS-1-31 | 4 | 3 | GS-MDPNCSCAAGDSCTCAGSCKCKECKCTSCKK |
| 1029.49 | 4 | | | | |
| 1329.62 | 3 | GS-1-30 | 4 | 3 | GS-MDPNCSCAAGDSCTCAGSCKCKECKCTSCK |
| 1319.45 | 1 | 52-61 | 0 | 3 | GASDKCSCCA |
| 660.23 | 2 | | | | |
| 1251.46 | 2 | 44-61 | 0 | 6 | CAQGCICKGASDKCSCCA |
| 1200.48 | 1 | 44-51 | 0 | 3 | CAQGCICK |
| 600.75 | 2 | | | | |
| 893.32 | 2 | 32-43 | 0 | 5 | SCCSCCPVGCAK |

**Table 3.1**. Identified fragmentation ions of bottom-up approach of $Ag_4NEM_{14}$-MT. The signal at m/z 1329.62 ($3^+$) is assigned as the intact β domain (GlySerMet1-Lys30) containing four $Ag^+$ and three NEM bound. It was further analyzed by MS-CID-IM-MS.

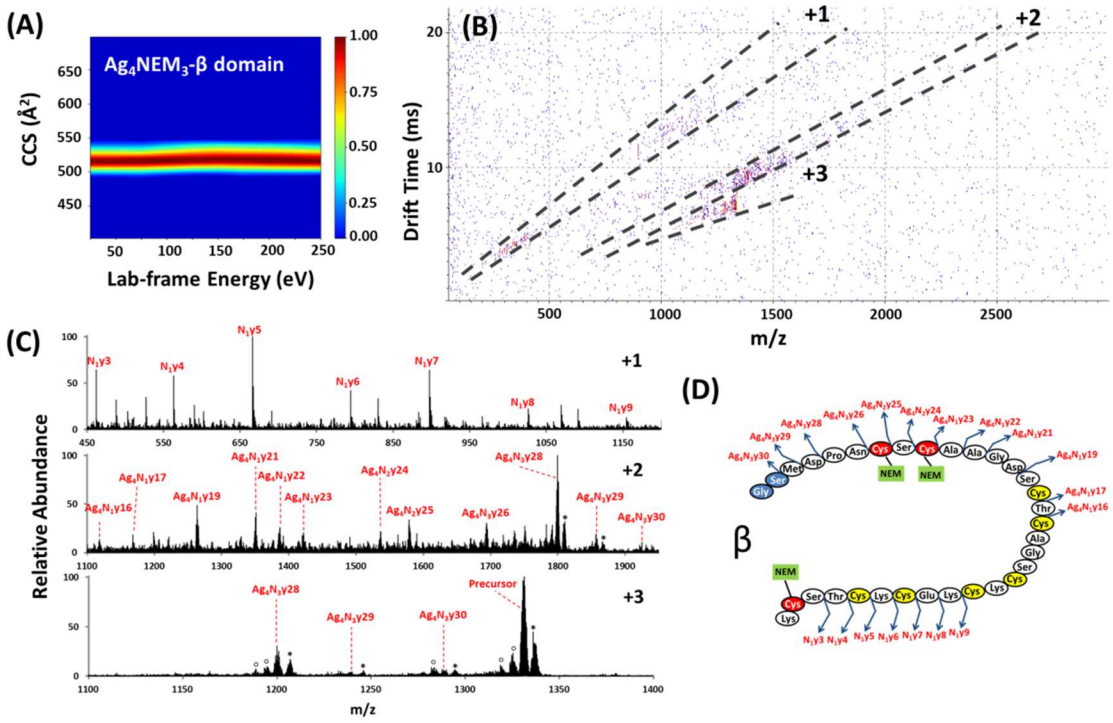


**Figure 3.6.** (A) CIU heat map of $Ag_4NEM_3$-β domain. (B) 2D MS-CID-IM-MS spectrum of $Ag_4NEM_3$-β domain. The trendlines are shown for ions of different charge states as labeled (+1 to +3). (C) Extracted mass spectra for each trendline. NEM is abbreviated as "N" for simplicity. (D) Summary of identified fragment ions and corresponding model from C. The asterisks (*) denote the $Na^+$ adducts and the circles (◦) denote the products formed by loss of $H_2O$.

*Collision-induced unfolding (CIU) of $Ag^+/Cd^{2+}$-MT and $Ag_i$-MT: Stabilities of metalated MT*

While previous studies have shown that sequential addition of metal ions to MTs yields incremental stabilization and unique folding intermediates,[123] the CIU results adds new insights for the effects of metalation and the stabilities of MT. CIU was also used to investigate the stabilites of the mixed metal complexes, *i.e.,* $Ag_4Cd_4$-MT, $Ag_5Cd_4$-MT, and $Cd_4Ag_4$-MT, $Cd_4Ag_5$-MT (**Figure 3.7**). Prior to collisional activation, the CCS profile for $Ag_4Cd_4$-MT ions is centered at ~750 $Å^2$; CCS profiles at different CE are contained in **Figure 3.8**. Parts of those ions unfold at ~75 eV to around 900 $Å^2$, while portions remain folded upon collisional activation. Similar results are observed for $Cd_4Ag_4$-MT except that $Cd_4Ag_4$-MT unfolds at lower activation energy than $Ag_4Cd_4$-MT. The CCS profile for $Ag_5Cd_4$-MT ions is centered at ~ 750 $Å^2$, but small portions of $Ag_5Cd_4$-MT unfold at ~100 eV to around 900 $Å^2$, while the majority stays folded upon collisional activation. Similar results are observed for $Cd_4Ag_5$-MT except that $Cd_4Ag_5$-MT unfolds at lower activation energy than does $Ag_5Cd_4$-MT. Intriguingly, addition of $Cd^{2+}$ followed by addition of $Ag^+$ and addition of a mixture of $Ag^+/Cd^{2+}$ to apo-MT yield almost identical CIU heat maps, whereas addition of $Ag^+$ followed by addition of $Cd^{2+}$ yields products that retain higher abundance of the compact, folded conformers at almost all activation energy.

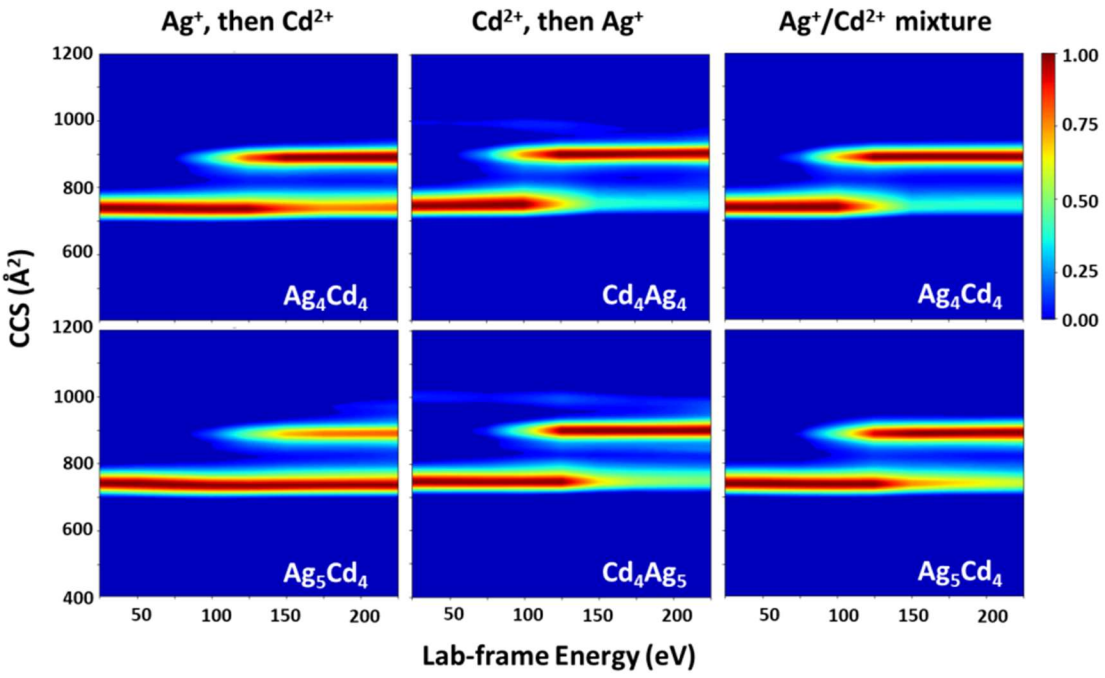


**Figure 3.7.** Collision-induced unfolding (CIU) heat maps for $Ag_4Cd_4$-MT, $Ag_5Cd_4$-MT, and $Cd_4Ag_4$-MT, $Cd_4Ag_5$-MT. The legends at the top of each panel provide the sequence of addition of each metal ion.

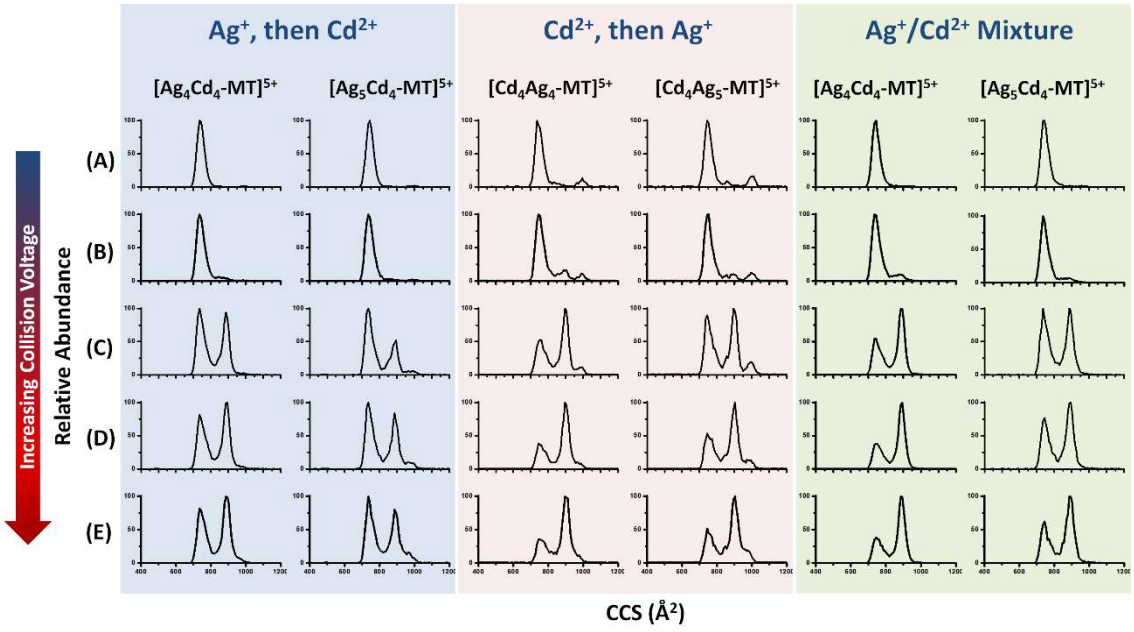


**Figure 3.8.** CCS profiles for 5+ ions of $Ag_4Cd_4$-, $Ag_5Cd_4$-, $Cd_4Ag_4$- and $Cd_4Ag_5$-MT acquired using different collisional activation conditions. Lab-frame collision energies are (A) 25, (B) 75, (C) 125, (D) 175 and (E) 225 eV.

Note that the CIUs of $Cd_4Ag_4$- and $Ag_4Cd_4$-MT show some dependence on the order of metal addition. This effect may be attributed to the influence of Cys33, which was previously shown to be highly solvent exposed and a weak binding site of $Cd^{2+}$ ions that can be displaced upon addition of NEM.[71, 134] It may have weak interaction with $Ag^+$ in the formation of $Ag_4$-MT. With the addition of $Cd^{2+}$, the interaction between Cys33 and $Ag^+$ can be partially maintained. However, if $Cd^{2+}$ is added before $Ag^+$, the $Cd_4Cys_{11}$ cluster formed in α domain may inhibit interactions between $Ag^+$ and Cys33. As a result, MT metalated by $Ag^+$, then by $Cd^{2+}$ produces higher abundance of compact conformer than MT metalated by $Cd^{2+}$ first or by $Ag^+/Cd^{2+}$ mixture.

Results from CIU also allows for comparisons of the stabilities of the various $Ag_i$-MT ($i$ = 4 - 17) complexes (**Figure 3.9)**.[72, 123] CCS profiles for the $Ag_4$-MT ions are relatively broad and span the range from ~ 650 to 800 $Å^2$, and a low abundance signals are observed as high as 950 $Å^2$ (see **Figure 3.10**). Similar to that observed for apo-MT, the width of the CCS profile is a signature for a conformationally disordered ion population.[123] As CE increased, the CCS of the ions increase to a maximum value of ~1000 $Å^2$. For example, at CE ~45 eV the abundances of ions with CCS of 750 $Å^2$ decreases and those in the range from ~850 $Å^2$ steadily increases, and at CE of approximately 60 eV the abundances of ions with CCS ~950 $Å^2$ has increased, and at CE of ~75 eV conformers with CCS of ~1000 $Å^2$ reach a maximum. Although the CCSs for $Ag_5$-MT to $Ag_7$-MT show some differences, an intermediate state is observed across a narrow range of CE for $Ag_5$-MT, and a similar state is observed for $Ag_6$- and $Ag_7$-MT,

but this state appears to be more stable that observed for $Ag_5$-MT. In fact, a state with a similar CCS (~ 875 $Å^2$) appears to be the final state for $Ag_8$-, $Ag_9$-, $Ag_{10}$- and $Ag_{11}$-MT.

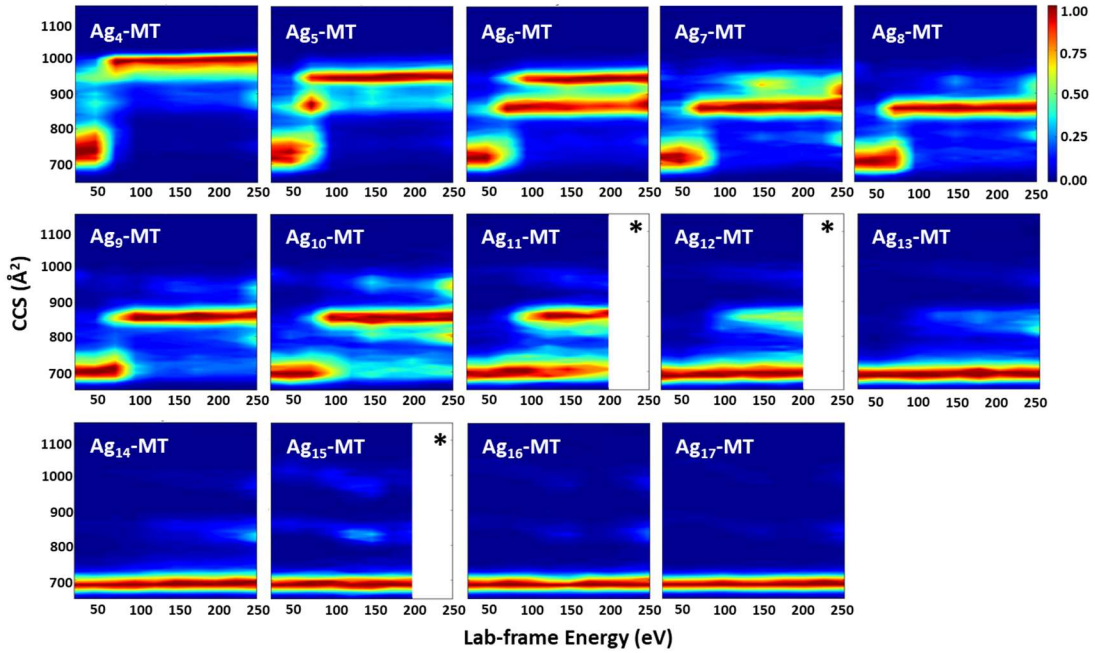


**Figure 3.9.** CIU heat maps for $Ag_4$-MT to $Ag_{17}$-MT. Asterisks (*) indicate that the CIU heat maps are truncated due to collision-induced dissociation. CID forms fragmentations from N-terminus; no $Ag^+$ dissociation is detected.

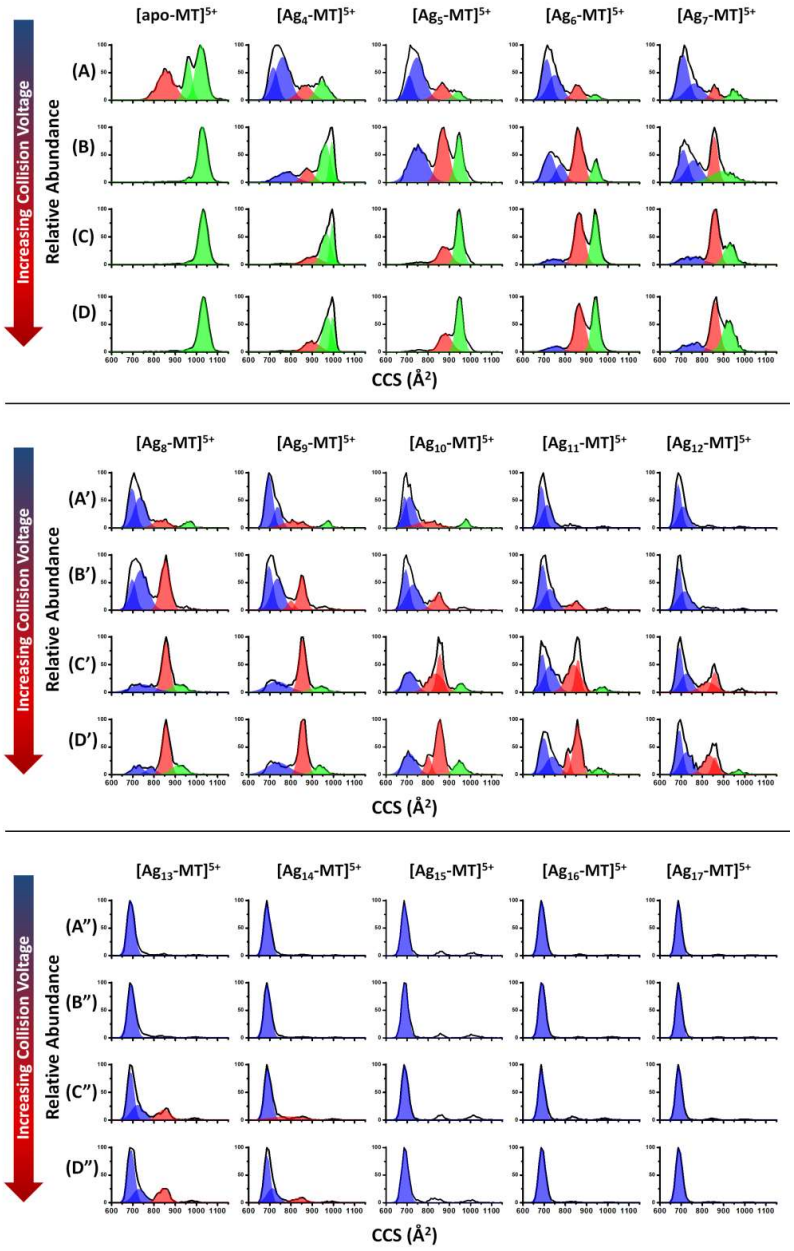


**Figure 3.10.** CCS profiles for 5+ ions of apo- and $Ag_i$-MT (i=4-17) acquired at different collisional activation conditions. Lab-frame collision energies are (A)(A')(A") 25, (B)(B')(B") 75, (C)(C')(C") 125, and (D)(D')(D") 175 eV. Each IMS is mathematically deconvoluted with minimums peaks to ensure $R^2$>0.99. Multiple peaks under each CCS profile is a signature for structural heterogeneity. Based on peak position, fitted peaks are divided into three groups: relatively compacted conformers (~ 650-800 $Å^2$) labeled by blue, intermediate conformers (~800-900 $Å^2$) labeled by red and extended conformers (larger than 900 $Å^2$) labeled green.

The CIU heat maps for $Ag_4$-MT through $Ag_7$-MT show considerable differences, whereas those for $Ag_8$-MT through $Ag_{11}$-MT are quite similar, as summarized in **Figure 3.11.** At low CE the CCS center on ~ 700 $Å^2$ and a maximum value ~850 $Å^2$ at the higher CE from $Ag_8$-MT to $Ag_{11}$-MT; however, the threshold CE required to produce ions having the higher CCS increases as the numbers of bound $Ag^+$ ions increases from a CE value of ~55 eV for $Ag_4$-MT to ~110 eV for $Ag_{11}$-MT. For $Ag_{12}$-MT through $Ag_{17}$-MT the CCS remain constant; for all of these ions that no change in CCS occurs as the collision energy is increased. However, at the high energies (200 eV) some of these ions begin to dissociate, without loss of $Ag^+$ ions.

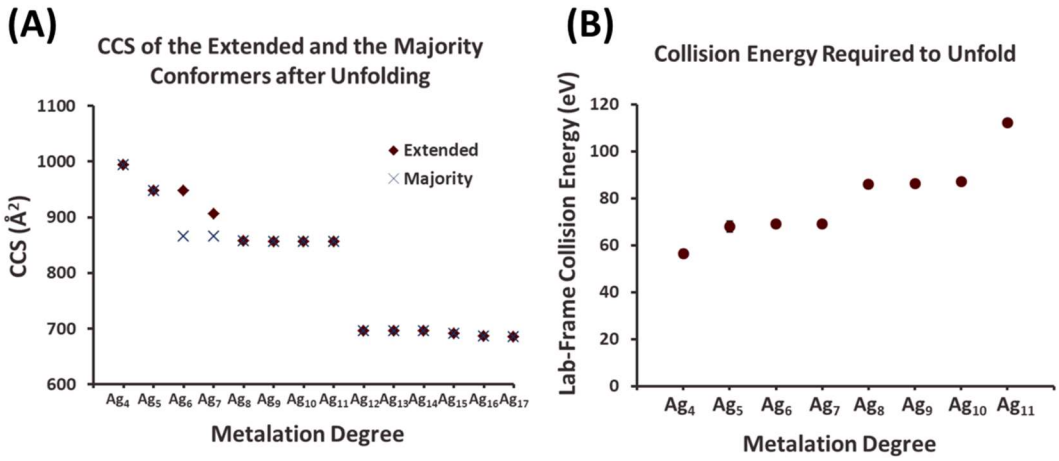


**Figure 3.11.** (A) CCS of the extended and the major conformers after unfolding. (B) Lab-frame collision energy correspond to CIU50 for each $Ag^+$ metalated product.

There is a sharp drop in the CCSs for $Ag_{12}$-MT through $Ag_{17}$-MT, see **Figure 3.11A**. Nielson, Li and Zelazowski *et al.* have shown that MT requires at least 12 $Ag^+$ ions to fully metalate both domains, which is also supported by the results reported here.[100, 110-111] $Ag_{12}$-MT is resistant to unfolding because both domains are fully metalated. $Ag^+$ can adopt two different binding geometries with thiolates: trigonal and diagonal.[1, 104] For trigonal binding geometries, each $Ag^+$ ion interacts with three cysteines; whereas, in diagonal binding geometries, each $Ag^+$ ion interacts with two cysteines. Consequently, more $Ag^+$ ions can be accommodated if $Ag^+$ ion adopts diagonal geometry comparing with trigonal geometry. $Ag_{12}$-MT cannot be unfolded by CIU, which suggests it is a fully metalated product and $Ag^+$ ions probably adopt trigonal geometry. All 20 cysteines are involved in binding with $Ag^+$ ions. Because of trigonal geometry, 12 $Ag^+$ are the minimal amount that is required to fully metalated MT. Following addition of more $Ag^+$ ions, the binding geometries of the excess $Ag^+$ ions can change from trigonal to diagonal and terminal cysteines turn to bridging cysteines. The binding geometry changes increase MT tolerance to $Ag^+$ ions, resulting in the formation of $Ag_{13}$-MT to $Ag_{17}$-MT.

Another possible mechanism for the formation of $Ag_{12}$- to $Ag_{17}$-MT is the influence of Ag-Ag interaction.[135-136] That is, formation of Ag nanoclusters have been previously reported for nucleic acids/silver complexes,[137-139] and similar products may be formed by partially and/or fully metalated MTs. Studies are underway to explore whether Ag nanoclusters are indeed formed.

For comparison, ESI-MS spectra and CIU heat maps for $Ag_i$-rMT (rabbit MT) are provided in here (**Figure 3.12** and **3.13**, respectively). The CCSs for $Ag_i$-rMT are somewhat larger than those for $Ag_i$-MT, but CIU heat maps show similar changes to those of $Ag_i$-MT. Blindauer states that the folding of MTs is dominated by metal binding and the formation of metal-cysteine clusters,[1] therefore, the structure should be mainly influenced by metal ions and cysteine residuals involved in metal binding. In our experiment, CIU heat maps during $Ag^+$ titration are quite similar for both types of MTs, which represents similar stabilities of $Ag_i$-rMT and $Ag_i$-MT ($i$=4 to 17). Similar CIU process of partially metalated MTs with difference in non-cysteine residuals is consistent with Blindauer's statement.

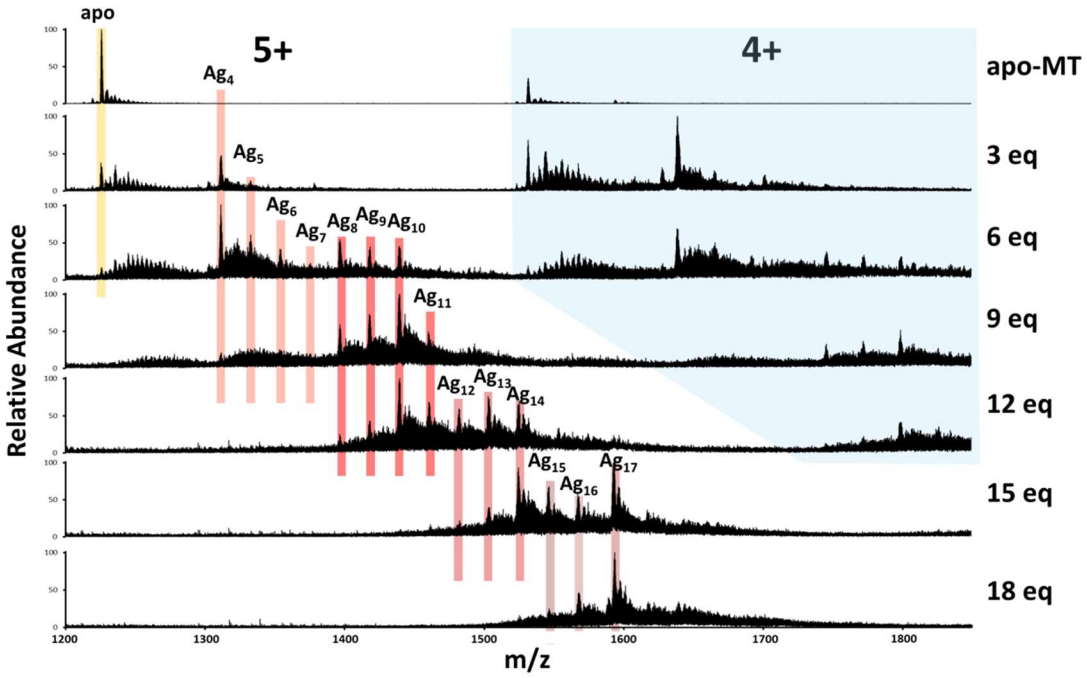


**Figure 3.12.** ESI-MS spectra of sequential addition of $Ag^+$ to apo-rMT solution.

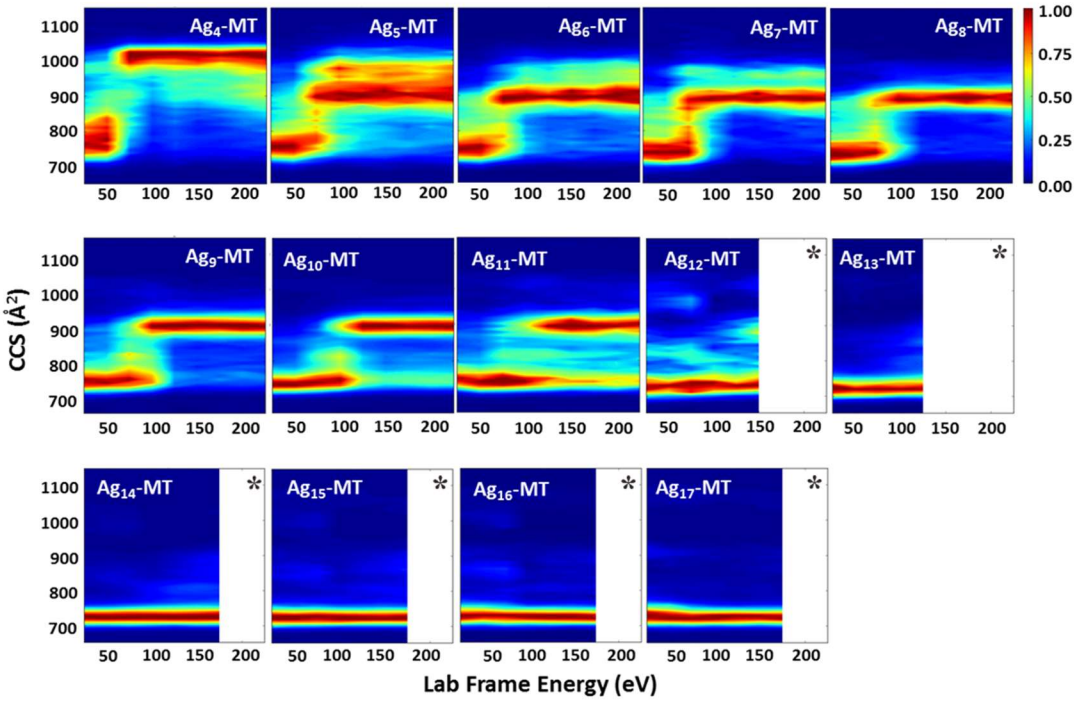


**Figure 3.13.** CIU of $Ag_i$-rMT (i=4-17).

## Conclusions

Since the discovery of mammalian metallothioneis in 1957, it has received tense attention and research.[6] ESI-MS can be used to assign the products formed by reactions of MT with metal ions; however, combining ESI-MS with ion mobility spectrometry provides additional information on the structures and stabilities of the metal-containing products. Here, a comprehensive ESI-IM-MS approach, *viz.* nESI-MS-CID-IM-MS has been combined with covalent labeling of the cysteine residues in an effort to better understand this complex system. The end results of the investigation can be summarized as follows:

The $Ag_4$-MT complex formed by reaction with $Ag^+$ occurs by a cooperative mechanism, and top-down proteomic tandem mass spectrometry data for the NEM labeled complex, $Ag_4NEM_{14}$-MT, clearly shows that the four $Ag^+$ ions are bound to cysteine side chains located in the β-domain, *viz.* in the region of the protein between Cys13 through Cys29. Similar studies of the $Ag_4NEM_3$-β-domain complex, formed by tryptic digestion of the $Ag_4NEM_{14}$-MT complex, shows that Cys29 also carries an NEM label, thus $Ag^+$ binding sides can be unequivocally assigned to Cys13-Cys26. It is interesting to note that the favored metal ion binding domains of $Ag_4$-MT and $Cd_4$-MT are very different as illustrated in **Figure 3.14**.

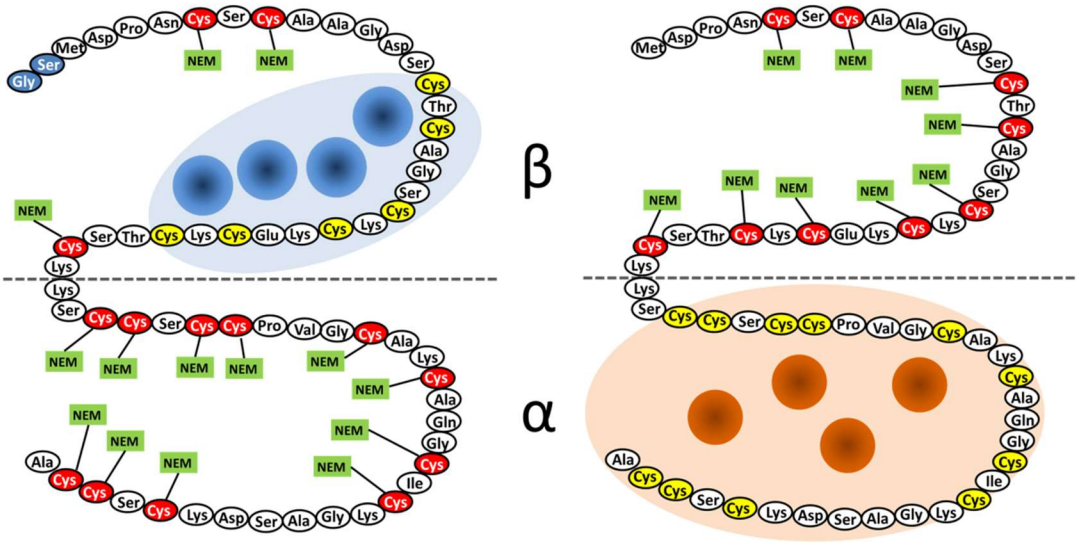


**Figure 3.14.** Summary of binding sites identification. $Ag^{+}$ ions (blue) of $Ag_4$-MT are located in the β-domain whereas $Cd^{2+}$ ions (orange) of $Cd_4$-MT are located in the α-domain. The binding sites for $Cd_4$-MT are summarized from previous publication.[56]

$Ag^{+}$ ions in $Ag_i$-MT (i=5 to 17) can be displaced by NEM to form $Ag_4NEM_{14}$-MT. Such metal displacement was reported previously.[71, 127] In those cases, the dissociation equilibrium of metal-thiolate bond provides thiolate sites that are weakly associated with metal ions; those thiolate sites are easier to be attacked by NEM.[71, 127] The $Ag^{+}$ ions that can be replaced by NEM are more labile in solution phase.

The metal binding affinities for Cys located in the β-domain (from Met1 to Ser18) and in the α-domain (from Pro38 to Ala61) appear to be smaller than the Cys located in the middle of the protein (ignoring GlySer tag).[123] The Cys percentage from Met1 to Ser18 is 22.2%, 29.2% from Pro38 to Ala61 and 47.4% between the middle region from Cys19 to Cys37. We previously showed that Cys33 played an important role in the formation of $Cd_4Cys_{11}$ cluster in α domain.[71] Cys33 is in the region of high cysteine percentage as well. The binding sites identified for $Ag_4$-MT also falls in this

region, which further suggests that the mid-region of MT, specifically from Cys19 to Cys37, play key roles in early stage metalation.

CIU heat maps indicate that binding with different metal ions varies the structure of MT, altering the number and location of metal-free cysteines, and further influencing the metal binding affinity of MT. However, as shown in MT reacting with mixed metal ions ($Ag^{+}$ and $Cd^{2+}$), when binding to different domains, the bound metal ions in one domain may have limited influence on the binding behavior in the other domain. The metal selectivity in different domains may be important to MTs' physiologically function in metal homeostasis and detoxification.

# CHAPTER IV

# FUTURE DIRECTIONS

Our current work presented here provides a better understanding of partially metalated metallothioneins in metalation, gas-phase stability and binding sites identification. However, new questions have been raised in the same time. Some attempts focusing on real-time mass spectrometry, $Cu^{+}$ binding as well as possible differences in solution phase structures of $MT^{4+}$ and $MT^{5+}$ have been summarized below, which may inspire future MT study.

## Real-time mass spectrometry with a micromixing tee and the application to kinetic studies of $Cd^{2+}$ binding to methallothionein-2A

*Background*

Trapping and studying intermediates during reactions is of significance to understand the mechanism and biological functions of a certain reaction,[140-142] which requires analytical methods that can response within short time. Optical methods such as UV-vis or fluorescence are suitable for short time scale analyses, but they can only detect one or two species at a time, making them difficult to be applied to multistep reactions with a large number of species involved.[140, 143] Circular dichroism (CD) spectra can provide information related to secondary structure with high sensitivity, such as the formation of metal-cysteine bonds; [144-145] however, it is different to obtain quantitate kinetic data with CD spectra.

Real-time mass spectrometry, or time-resolved electrospray ionization, was initially designed to study rapid chemical and biochemical reactions occurring in the millisecond to second time-scale without a chromophore.[146] One of the most classic capillary based systems consists of a static mixing tee.[91, 147-148] The length of capillaries after mixing is variable, allowing the changing of reaction time. The mixing tee apparatus has advantages including straight-forward assignment and low cost. Other mixing systems includes apparatus with an adjustable reaction chamber to measure various reaction times in a single experiment[149] or combined with a microfluidic chip[150]. We chose for our experiments the static mixing tee with variable lengths of capillary to probe abundance change of partially metalated species during short reaction time. Mixing tee has the potential to trap intermediates under pre-stable states; which is applied to study the CIU of partially metalated MTs.

The assumptions to apply mass spectrometry in quantification research are summarized by Stillman *et al*.[31, 33] as follows: (i) each species should have similar ionization ability with the ESI source; (ii) the signal abundance of each species is proportional to its concentration in the solution phase; (iii) the concentrations of all the species are proportional to their respective concentration in solution; (iv) for MTs, no metal ion is lost or bound in the ESI process. MT species of same isoform but differ in metalation degree are assumed to share same ionization efficiency according to Palacios *et al*.[151]

*Methods*

For reaction time calibration of the mixing tee, 10 μM Bradykinin (BK) ($Arg^1$-$Pro^2$-$Pro^3$-$Gly^4$-$Phe^5$-$Ser^6$-$Pro^7$-$Phe^8$-$Arg^9$) and P3A/P7A Bradykinin mutant peptide (BKM) were prepared in 0.1 % Formic Acid. BK was introduced at 2 μL/min until stable spray established. At the start of acquisition, BKM was added at 1 μL/min, and the flow rate of BK was slowed down to 1 μL/min simultaneous. The two peptides were switched afterward: BKM was introduced until stable spray established. BK was added at the start of acquisition. The time required for the added peptide to be detected was acquired with capillaries ranging from 4.95 cm to 177.50 cm in length and a constant diameter of 75 μm. A plot of capillary length vs time required for the added peptide to be detected was used as a calibration curve. Averages and standard deviations were calculated using 6 acquisitions. 3 for BK added to BKM, 3 for BKM added to BK.

The calibration curve was applied to the kinetic study of MT binding with four equivalent of $Cd^{2+}$. One channel of the mixing tee contained 16 μM apo-MT in 1 mM TCEP, 10% MeOH and 50 mM ammonium acetate; the other contained four equivalents of cadmium acetate in 10% MeOH and 50 mM ammonium acetate. $Cd^{2+}$ solution was introduced first, and then MT was added, as described before.

*Results*

**Figure 4.1A** shows the 2+ charge state mass spectrum when BK was added to BKM. The signal of BKM was observed as dominant at the start of an acquisition. However, at the end of an acquisition， the signal of BK was dominant. The small difference in abundance could come from the different purity of two purchased samples.

Sample plots of the relative abundance of all BK ions vs. time using different capillary lengths were showed in **Figure 4.1B**. BK had a relative abundance of about 5% at the start, and this number rose to above 65% at the end of mixing. Signals have good stabilities at the start and the end of an acquisition. The relative abundance changing of the signal was dramatic within 28 s. Plot of capillary length vs time required for the added peptide to be detected is shown in **Figure 4.1C**. Averages and standard deviations were calculated using 6 acquisitions. The relationship between length and time was directly proportional.

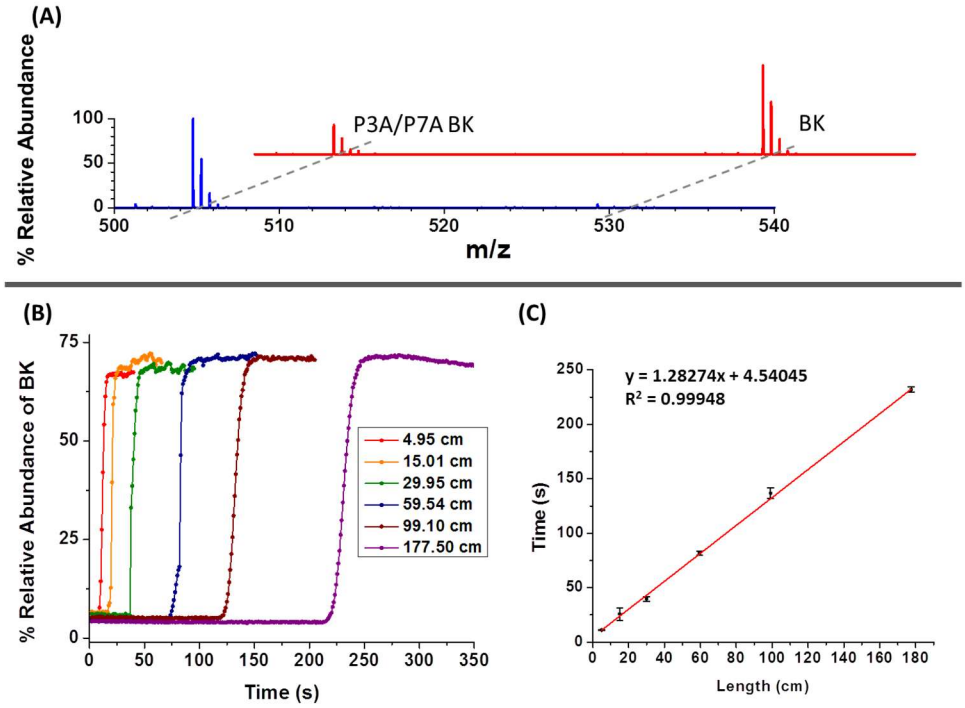


**Figure 4.1.** (A) Mass spectrums show the 2+ charge state for both the P3A/P7A mutant and BK at the start of an acquisition (blue) and at the end of an acquisition (red). (B) Sample plots of the relative abundance of all BK ions vs. time using different capillary lengths. Note that the mutant was allowed to fill the capillary prior to acquisition; the addition of BK began at the start of acquisition. (C) Plot of capillary length vs time required for the added peptide to be detected. Averages and standard deviations were calculated using 6 acquisitions**.**

The kinetic plots for apo- and $Cd_i$-MT (i=1-5) are summarized in **Figure 4.2**. 5+ mass spectra (**Figure 4.2A**) showed the similar trends as the 4+ (**Figure 4.2B**). The signal abundance of 4+ ions was larger, resulting in a higher signal to noise ratio. We attribute the charge state difference between apo-MT and metalated MT to structure folding induced by $Cd^{2+}$ binding. The metal induced folding of MT decreases the solvent accessible surface area, making lower charge state more favorable. The signals for the same number of metal ions bound (*i*) but differing in charge state (4+ and 5+) are summed together to provide a total abundance of the $Cd_i$-MT species (**Figure 4.2C**).

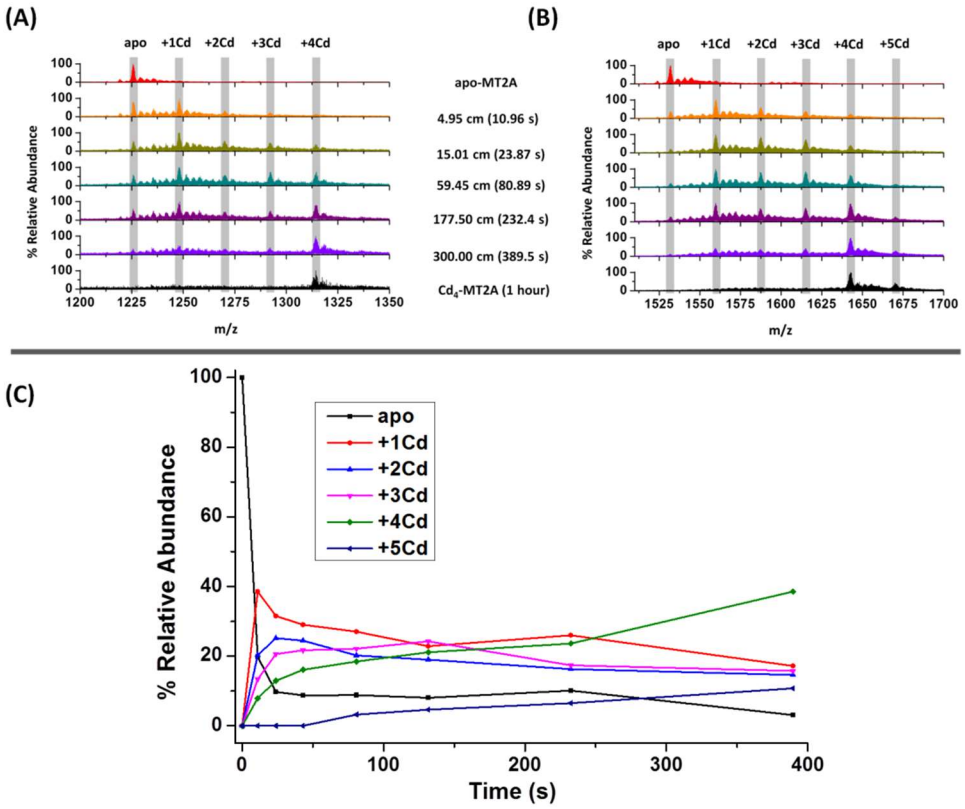


**Figure 4.2.** (A) 5+ and (B) 4+ mass spectrum acquired at different reaction time and after incubation in room temperature for 1 h. (C) kinetic plots for apo-, $Cd_i$-MT (i=1-5) for 4+ and 5+ summations.

*Future Work*

The calibration curve is impressive. It has the potential to be applied to other similar real-time mass spectrometry systems. Currently, the calibration curve was acquired only with peptides smaller than 1100 Da. A similar reacting time calibration should be done with larger proteins such as ubiquitin and myoglobin before it can be confidently applied to larger protein systems.

The kinetic study of MT shows interesting results. The capillary length can be increased until the spectrum matches that after incubating at room temperature for 1 h.

The ratio of protein and metal solution can also be varied to obtain kinetic information for other intermediates such as $Cd_6$-, $Cd_7$-MT.

Multiple mixing tee systems can be established. For example, the outcoming solution of the first mixing tee can be introduced into another mixing tee, and mixed with a model alkylating agent like NEM, more detailed binding information of intermediates could be obtained.

**Combining direct metalation and collision-induced unfolding to track structural changes of metalliothioneins in sequential metalation by copper ions**

*Background*

Alzheimer's disease (AD) is a neurodegenerative disorder characterized by memory loss, cognitive decline and physical deterioration.[152-153] The neuropathology of AD includes the accumulation of extracellular plaques containing amyloid β peptide (Aβ) in the cortical regions of the brain.[154] The aggregation of Aβ is catalyzed by reactions with zinc and copper.[155-156] In fact, in AD Cu is abnormally redistributed to the plaques, leaving the tissue and cells deficient in Cu.[157]

MTs uphold the metal homeostasis in the body, appearing to be a strategy for preventing the formation of Cu-Aβ complexes.[158-159] One specific isoforms of MTs, MT3, is reduced in AD brain[160] and can antagonize the neurotoxic and neurotrophic effects of Aβ complexes.[14, 161] Faller *et al.* studied the metal exchange between $Zn_7$-MT3 and Cu-Aβ complexes, showing that an Aβ-metal-MT3 was not formed, however, "key questions about the metal exchange mechanisms remain unanswered".[162] A decrease in

Cu-Aβ mediated cytotoxicity was also reported for MT2A (donate as MT), and MT2A showed an even stronger capability than MT3 to prevent Aβ related neurotoxicity.[163]

Here, direct metalation and collision-induced unfolding (CIU) are used in an effort to better understand MT reacting with $Cu^{+}$, and the difference between $Cu_i$-MT and $Ag_i$-MT, as well as divalent-ion-metalated products ($Cd_i$-MT and $Zn_i$-MT). These results show that the metalation process and stabilities of the gas-phase ions of $Cu^{+}$ bound MTs complexes are significantly different from those for other metal ions.

*Methods*

nESI-IM-MS was performed on a Waters Synapt-G2 HDMS instrument (Manchester, UK). The metalation experiment was performed by sequential addition of 1 to 12 μL of 1 mM of copper acetate to 100 μL of a 7 μM apo-MT solution. Following each addition of $Cu^{2+}$, the protein was allowed to react with the metal ion for 1 h under ambient conditions before MS measurement. nESI-IM-MS experiments were carried out using instrument conditions that minimize collisional heating as previously described.[48]

For CIU studies, different collision energies were applied by changing the voltage (increments of 5 V) drop between the exit of the quadrupole and the entrance to the TWIG-trap region filled with the collision gas argon. CA data were compiled into CIU heat maps using CIUSuite.[83]

*Results*

Directly metalation provides a general view of MT's metalation process in thermodynamically stable mode. **Figure 4.3** shows the sequential metalation of apo-MT by $Cu^{2+}$. The mass spectrum for apo-MT was acquired before $Cu^{2+}$ addition. Low abundance oxidized peaks were detected. No metalated product was detected for apo-MT. Metalated MT started to form after $Cu^{2+}$ addition. With increasing concentration of $Cu^{2+}$ in MT solution, the metalation degree of products increased. No signal from $Cu_1$- to $Cu_3$-MT was detected; $Cu_4$-MT was the first detected metalated product. Intriguingly, metalation of MT by $Cu^{2+}$ showed a preference for binding even numbers of copper ions per protein molecule, *etc.* $Cu_4$-, $Cu_6$-, $Cu_8$- and $Cu_{10}$-MT. Signal to noise ratio decreased significantly with copper concentration, which might be caused by protein participation and fragmentation. The charge state of copper bound to MT could be a mixture of $Cu^{+}$ and $Cu^{2+}$.

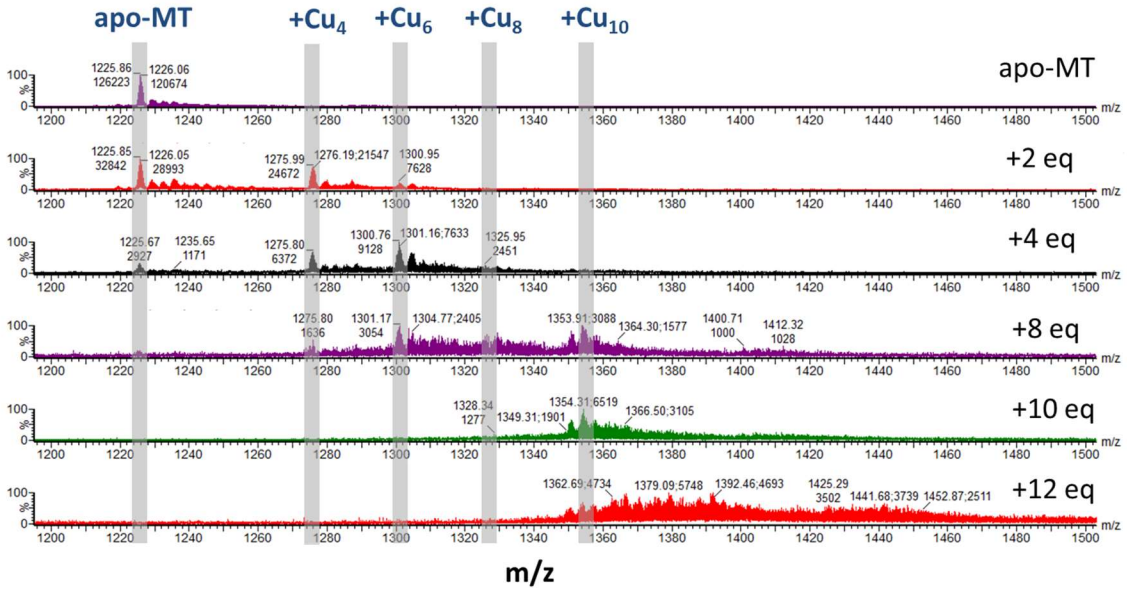


**Figure 4.3.** ESI-MS spectra (5+) of sequential addition of $Cu^{2+}$ to apo-MT solution.

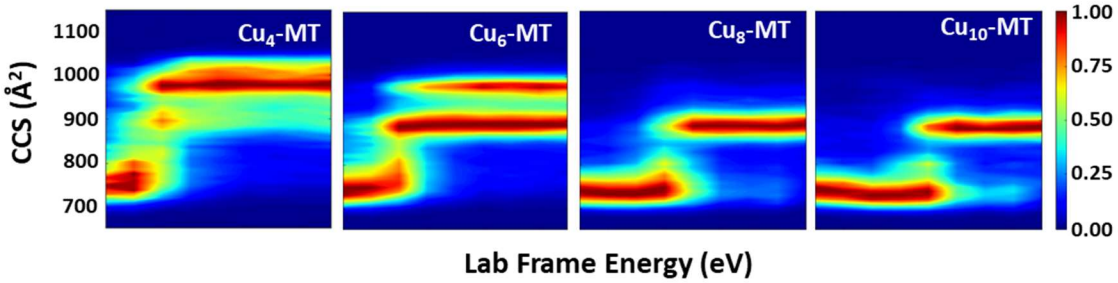


**Figure 4.4.** CIU heat maps for $Cu_4$-,$Cu_6$-, $Cu_8$-and $Cu_{10}$-MT.

CIU heat maps from $Cu_4$-MT to $Cu_{10}$-MT are shown in **Figure 4.4**. With the binding of each $Cu^+$, the energy required for unfolding increases; CCS of the most extended conformer after unfolding decreases. $Cu_4$-MT unfolded from around 750 $Å^2$ to above 1100 $Å^2$; $Cu_6$-MT unfolded to two distinguishable states with higher activation energy, while both $Cu_8$- and $Cu_{10}$-MT unfold to round ~900 $Å^2$ with collisional activation.

Comparing CIU heat maps of $Cu_i$-MT to $Cd_i$-, $Zn_i$- and $Ag_i$-MT provide more information about the structure heterogeneity of MTs. The CIU heat maps for $Cd_i$-, $Zn_i$- and $Ag_i$-MT are reported previous.[123] As summarized in **Figure 4.5**, lab-frame collision energy required to start the unfolding and CCS of the most extended conformer after unfolding not only depend on the metalation degree, but also the species of metal ion that binds to MT.

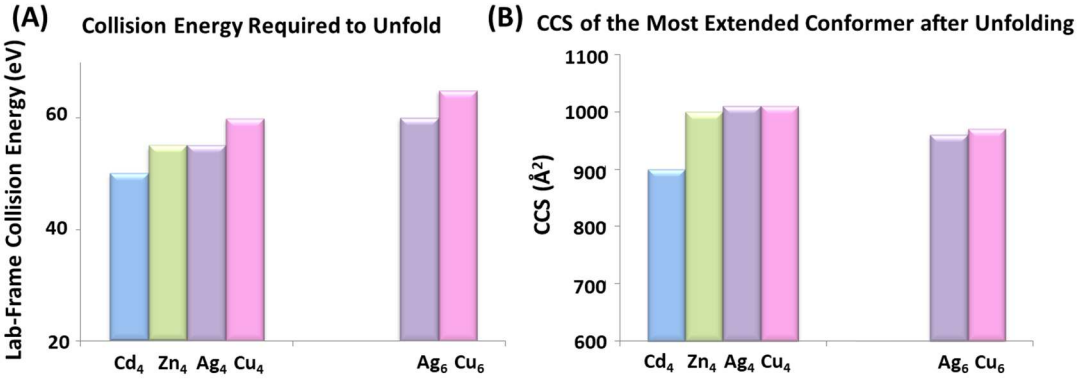


**Figure 4.5.** (A) Lab-frame collision energy when $Cd_4$-, $Zn_4$-, $Ag_4$- and $Cu_4$-MT, $Ag_6$- and $Cu_6$-MT starts to unfold. (B) CCS of the most extended conformer after unfolding for $Cd_4$-, $Zn_4$-, $Ag_4$- and $Cu_4$-MT, $Ag_6$- and $Cu_6$-MT.

Both $Zn_4$- and $Ag_4$-MT start to unfold at comparable lab-frame collision energy (~50 eV). $Cd_4$-MT starts to unfold at lowest activation energy, while $Cu_4$-MT requires highest activation energy. The order of unfolding energy is consistent with the order of the dissociation energy of each metal-sulfur bond. The dissociation energy of Cu-S bound is 274.5 ± 14.6 kJ/mol, higher than all the other metal-sulfur bound (Cd-S 208.5 ± 20.9 kJ/mol, Zn-S 224.8 ± 12.6 kJ/mol, Ag-S 216.7 ± 14.6 kJ/mol).[164] The strength of Cu-S bound attributes to higher collision energy required for unfolding. $Ag_6$-MT unfolds at higher energy than $Ag_4$-MT; $Cu_6$-MT unfolds at higher energy than $Cu_4$-MT. With more metal ions bound, increasing numbers of cysteines are involved binding with metal ions, making the metalated products harder to unfold.

The CCS of the most extended conformer after unfolding also varies with metal species. $Cd_4$-MT has the most compacted CCS after fully unfolding. As we reported previously, this CCS correspond to a compacted α domain and a fully unfolded β domain.[56, 123] $Zn_4$-MT, $Ag_4$-MT and $Cu_4$-MT have similar CCS after unfolding. None of

them may adopt a fully metalated domain.[123] The binding mechanism for $Zn^{2+}$ is still amphibolous. Stillman raised a mechanism that $Zn^{2+}$ is bound to the N-terminal Cys5 and Cys7 to form bead-like structure(s) rather than a $M_4Cys_{11}$ cluster;[107-109] meanwhile, some reports suggest that MT binds more than 12 monovalent ions like $Ag^+$ and $Cu^+$, and the first six metal ions would bind to β domain.[101-102, 111] The CIU maps show that $Ag_6$- and $Cu_6$-MT have comparable CCS after unfolding, which may indicate they adopt similar structures.

*Future Work*

$Cu^{2+}$ binding to MT provides the most interesting results so far. The first question need to be answered is why $Cu^{2+}$ binds in pairs, as well as what is the charge state of the bound Cu pairs. Are they $Cu^+$ with $Cu^+$, or $Cu^0$ with $Cu^{2+}$, or $Cu^{2+}$ with $Cu^{2+}$? Is there any oxidation-reduction reaction that influences the binding mechanism? As shown previous study, MT binds to $Cd^{2+}$ and $Ag^+$ cooperatively and domain specifically.[56, 123] Does $Cu^{2+}$ also bind specifically to a certain domain? If so, which domain is it? A combination of chemical labeling, proteomics and even computer simulation need to be considered to better understand the process of copper binding to MT.

**Do different charges of metallothioneins in mass spectroscopy originate from different solution phase structures?**

*Background*

Many scientists in the field of mass spectrometry did not believe that covalent bonds can be maintained when biomolecules transfer into gas phase.[165] Even after the introduction of soft ionization methods such as matrix-assisted laser desorption (MALDI)[166] and electrospray ionization (ESI)[167], there is still debate on whether the results of gas-phase experiments obtained by MS is faithful to reflect solution-phase characteristics.[168]

The retention of native like structure for protein and protein complexes presented by ESI-MS has been reported.[169-173] However, some globular proteins such as cytochrome *c* and ubiquitin undergo side-chain collapse, unfolding and refolding into new gas phase structures.[174-175] Metallothioneins (MTs) are considered as one type of intrinsically unfolded proteins.[4, 176] The apo form of MT lacks tertiary structures; after reacting with metal ions, metal-cysteine clusters start to form, and then relatively stable structures of MT start to build.[1, 4] In other words, the structures and folding of metalated MTs are dominated by the formation of metal–thiolate bonds. The overall stability constants of the metal-cysteine complexes are very high.[177-179] Can MTs maintain solution phase structure when transfers into gas phase with ESI-MS? We have noticed the IM spectra of MT in different charge states shares limited similarity.[70] Different instrumental conditions are applied to understand the relationship between different IM spectra and effective ion temperature ($T_{eff}$).[48] However, even under "cool condition", 4+

and 5+ of MT present distinguishing IM spectra.[48, 70] $MT^{5+}$ is more pronounced for conformational diversity and disorder, while $MT^{4+}$ keeps compacted. Although for higher charge state, the larger Columbic repulsion between the charge charring amino acids can lead to broader conformers with larger CCS, it is also possible that $MT^{5+}$ comes from solution phase conformers with higher structural disorder and larger solvent accessible surface area (SASA), while $MT^{4+}$ comes from solution phase conformers with lower structural disorder and smaller SASA.

Here, CIU of apo-, $Cd_4$-, $Zn_4$- and $Ag_4$-MT (4+ and 5+) are obtained for understanding the stability of apo- and partially metalated metalothionein-2A in gas phase. NEM titration are performed for apo-MT and $Cd_4$-MT. Different charge states (6+, 5+ and 4+ for apo-MT; 5+ and 4+ for $Cd_4$-MT) are compared to illustrate if cysteine residues are exposed differently in solution phase.

*Methods*

nESI-IM-MS was performed on a Waters Synapt-G2 HDMS instrument (Manchester, UK). Four equivalents of cadmium acetate, zinc acetate and silver acetate were added for studies on partial metalation. The solution was incubated for 1 h at RT and then analyzed by nESI-IM-MS. For nESI-CA-IM-MS, target ions were selected in the quadrupole and collisionally-activated (CA) prior to IM. CA data were compiled into CIU curves, CCS vs. collision voltage maps. CIU and difference plots were compiled using CIUSuite 2.[84]

The NEM titration experiment was performed by sequential addition of 4 to 12 equivalents of 4 mM NEM solution to 100 µL 16 µM apo-MT or 100 µL 16 µM $Cd_4$-MT solution. Following each addition of NEM, the solution was incubated for 1 h at RT before MS measurement. nESI-IM-MS experiments were carried out using instrument conditions that minimize collisional heating as previously described.[48, 123]

*Results*

As shown in Chapter II **Figure 2.2**, metalation alters charge state distribution. The predominant charge state is metal dependent. The 5+ charge state is predominant for apo-MT under cool experimental conditions, however, after binding with four equivalents of $Cd^{2+}$ or $Zn^{2+}$, 4+ becomes the predominant charge state; $Ag_4$-MT, on the other hand, shows a preference for 5+ ions, which can be explained by a change in solvent accessible surface area (SASA).

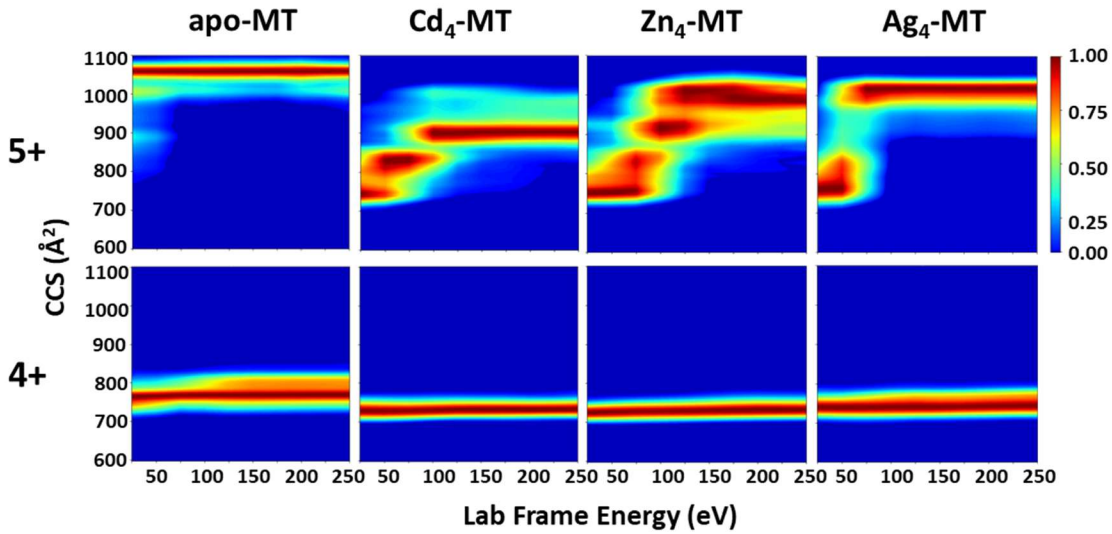


**Figure 4.6.** CIU heat maps ($5^+$ and $4^+$, top to bottom) for apo-, $Cd_4$-, $Zn_4$- and $Ag_4$-MT.

CIU profiles of apo-, $Cd_4$-, $Zn_4$- and $Ag_4$-MT (4+ and 5+) are shown in **Figure 4.6**. The 5+ ions show incremental unfolding with increasing activation voltage. Several unfolding stages are observed, which is more obvious for the metalated species. $Cd_4$-$MT^{5+}$ shows three, $Zn_4$-$MT^{5+}$ shows four while $Ag_4$-$MT^{4+}$ shows two unfolding stages. Intriguingly, the 4+ ions almost keep the same CCS regardless of activation voltage and don't unfold before fragmentation. Overall, the CIU profiles obtained for apo-$MT^{4+}$ and $Metal_4$-$MT^{4+}$ (Metal = Cd, Zn and Ag) are significantly smaller than that for apo-$MT^{5+}$ and $Metal_4$-$MT^{5+}$.

Since there is a strong correlation between observed charge states and SASA, ESI charge-state distributions have been directly related to solution-phase conformation.[129, 180] Do $MT^{4+}$ and $MT^{5+}$ originate from conformers that have different SASA in solution phase? NEM titration experiment has been performed attempting to gradually label the solvent exposed cysteines. ESI-MS spectra (6+, 5+ and 4+) of sequential addition of NEM to apo-MT solution is shown in **Figure 4.7 (A)**. Relative abundance of MTs binding with different numbers of NEM as well as average number of NEM bounded per MT molecule during NEM titration are summarized in **Figure 4.7 (B)** and **(C)** for better illustration. For all three charge states studied, with increasing NEM concentration in solution, the overall distribution of NEM bound MT shifts to the right, showing more cysteine residuals are labeled. However, the average number of NEM bounded per MT molecule during NEM titration doesn't differ much from 6+ to 4+. The average number of NEM bounded per MT molecule is proportional to the equivalence of

NEM added in solution, which indicates that all 20 cysteine residuals of MT are to some degree solvent exposed.

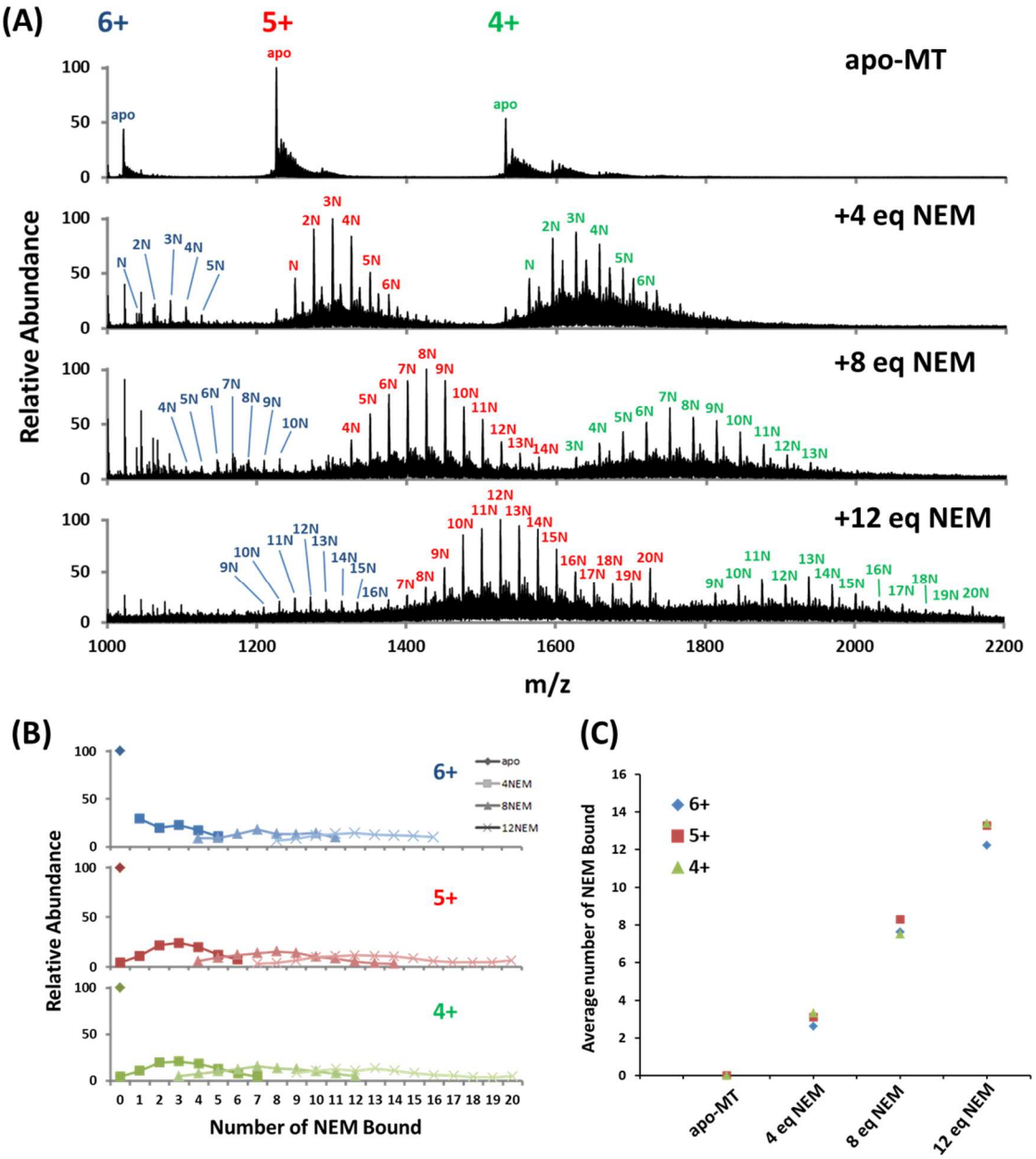


**Figure 4.7.** (A) MS spectra of apo-MT and apo-MT reacting with NEM, (B) relative abundance of MTs binding with different numbers of NEM and (C) average number of NEM bounded per MT molecule during NEM titration. For simplicity NEM is abbreviated as "N".

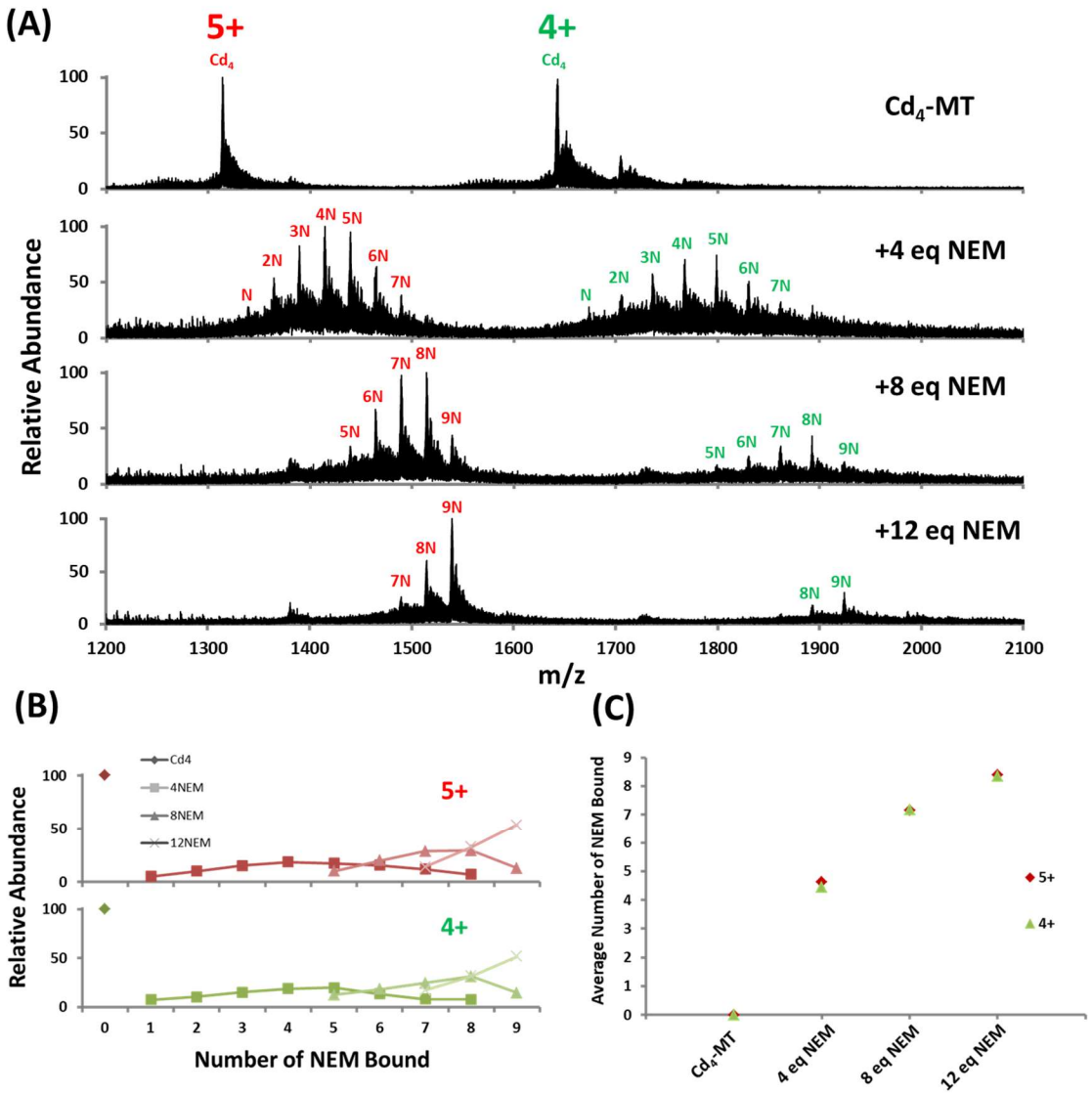


**Figure 4.8.** (A) MS spectra of $Cd_4$-MT and $Cd_4$-MT reacting with NEM, (B) relative abundance of MTs binding with different numbers of NEM and (C) average number of NEM bounded per MT molecule during NEM titration. For simplicity NEM is abbreviated as "N".

Similar NEM titration experiment was performed for $Cd_4$-MT (**Figure 4.8**). Our previous results show that the α domain of MT is fully metalated in $Cd_4$-MT, forming a $Cd_4Cys_{11}$ cluster.[56] This stable cluster structure induces folding of MT, further decreasing SASA and making lower charge states more favorable.[123] As a result, 6+ ions are no longer detected. However, 5+ and 4+ behave almost the same during NEM titration. The key different of $Cd_4$-MT from apo-MT when reacting with NEM is that the average number of NEM bounded per MT molecule is no longer linearly increasing with NEM concentration in solution. NEM can label all 9 cysteine residuals in the metal-free β domain, however, the labeling process slows down with 8 and 12 eq NEM added. Those cysteines that are harder to be labeled in β domain may be located close to α domain, *viz.*, Cys29, Cys 26 or Cys 24. The relatively bulky $Cd_4Cys_{11}$ cluster formed in α domain can limit the attacking direction of NEM and decrease the reaction rate of NEM labeling.

*Future Work*

The CIU profiles of apo- and metalated MT show a strong dependence on charge state. The difference CIU of each charge state may reflect different solution phase structures, or simply reflect different gas phase structures forming in ESI process. However, different charges of apo-MT or $Cd_4$-MT behave similarly during NEM titration. NEM is a small size, relatively strong alkyl agent; other weaker or bulky alkyl agents may be able to distinguish the different solvent exposed cysteines in solution phase. Meanwhile, binding NEM may induce MT to unfold and refold in solution phase,

which can also alter the detected charge states in gas phase. X/D exchange will be another method to study the SASA of MT in solution phase.

# CHAPTER V

# CONCLUSIONS

MTs have attracted attention and been extensively studied since their discovery in 1950s. Although a tremendous amount of knowledge has been accumulated, some questions concerning the fundamental understanding of MTs are still unanswered, especially related to partially metalated intermediates.

In our research here, CIU/CID of partially metalated MT with different metal species ($Cd^{2+}$, $Zn^{2+}$ and $Ag^{+}$) has been studied, which provide a global view of metal-dependent gas phase stabilities of partially metalated MTs. Our results show that despite their similar ion mobility profiles, $Cd_4$-MT, $Zn_4$-MT, $Ag_4$-MT and $Ag_6$-MT differ dramatically in their gas-phase stabilities. Furthermore, the sequential addition of each $Cd^{2+}$ and $Zn^{2+}$ ion results in the incremental stabilization of unique unfolding intermediates. The introduction of a micromixing tee allows the trapping of transient intermediates in a pre-equilibrium condition, which can be applied to intermediates study of other systems.

It has been noticed that monovalent metal ions, such as $Ag^{+}$, behaved dramatically different than divalent metal ions ($Cd^{2+}$ and $Zn^{2+}$) during the metalation process. We combined nano ESI-MS and nano-ESI-IM-MS with collision-induced unfolding (CIU), chemical labeling using N-ethylmaleimide (NEM) and both bottom-up and top-down proteomics in an effort to better understand the metal binding sites of the partially metalated forms of human MT, *viz.* $Ag_4$-MT. The results for $Ag_4$-MT are then compared to similar results obtained previously for $Cd_4$-MT. The results show that $Ag_4$-

MT is a cooperative product, and data from top-down and bottom-up proteomic mass spectrometry analysis combined with NEM labeling revealed that all four $Ag^+$ ions of $Ag_4$-MT are bound to the β-domain. While both $Ag^+$ and $Cd^{2+}$ react with MT to yield cooperative products, *i.e.*, $Ag_4$-MT and $Cd_4$-MT, $Ag^+$ ions of $Ag_4$-MT are located in the β-domain whereas $Cd^{2+}$ ions of $Cd_4$-MT are located in the α-domain.

To our best knowledge, our report is the first report focusing on the unfolding process of partially metalated MTs and unambiguously identifying the binding sites of $Ag_4$-MT. The results of our research provide a global view of metal-induced conformational transition of MT binding with different metal species or different metalation degree, which leads to new insights regarding the metalation activity and structure-function relationship of MT.

## REFERENCES


1. Blindauer, C. A.; Leszczyszyn, O. I., Metallothioneins: unparalleled diversity in structures and functions for metal ion homeostasis and more. *Nat Prod Rep* **2010,** *27* (5), 720-741.

2. Capdevila, M.; Bofill, R.; Palacios, O.; Atrian, S., State-of-the-art of metallothioneins at the beginning of the 21st century. *Coordin Chem Rev* **2012,** *256* (1-2), 46-62.

3. Coyle, P.; Philcox, J. C.; Carey, L. C.; Rofe, A. M., Metallothionein: The multipurpose protein. *Cell Mol Life Sci* **2002,** *59* (4), 627-647.

4. Romero-Isart, N.; Vasak, M., Advances in the structure and chemistry of metallothioneins. *J Inorg Biochem* **2002,** *88* (3-4), 388-396.

5. Simpkins, C. O., Metallothionein in human disease. *Cell Mol Biol* **2000,** *46* (2), 465-488.

6. Margoshes, M.; Vallee, B. L., A Cadmium Protein from Equine Kidney Cortex. *J Am Chem Soc* **1957,** *79* (17), 4813-4814.

7. Palmiter, R. D., The elusive function of metallothioneins. *P Natl Acad Sci USA* **1998,** *95* (15), 8428-8430.

8. Suzuki, K. T.; Someya, A.; Komada, Y.; Ogra, Y., Roles of metallothionein in copper homeostasis: responses to Cu-deficient diets in mice. *J Inorg Biochem* **2002,** *88* (2), 173-182.

9. Maret, W., The function of zinc metallothionein: A link between cellular zinc and redox state. *J Nutr* **2000,** *130* (5), 1455s-1458s.

10. Squibb, K. S.; Cousins, R. J.; Silbon, B. L.; Levin, S., Liver and Intestinal Metallothionein - Function in Acute Cadmium Toxicity. *Exp Mol Pathol* **1976,** *25* (2), 163-171.

11. Thornalley, P. J.; Vasak, M., Possible Role for Metallothionein in Protection against Radiation-Induced Oxidative Stress - Kinetics and Mechanism of Its Reaction with Superoxide and Hydroxyl Radicals. *Biochim Biophys Acta* **1985,** *827* (1), 36-44.

12. Huang, Z. X., Neuronal growth-inhibitory factor (metallothionein-3): a unique metalloprotein. *Febs J* **2010,** *277* (14), 2911-2911.

13. Faller, P., Neuronal growth-inhibitory factor (metallothionein-3): reactivity and structure of metal-thiolate clusters*. *Febs J* **2010,** *277* (14), 2921-2930.

14. Meloni, G.; Sonois, V.; Delaine, T.; Guilloreau, L.; Gillet, A.; Teissie, J.; Faller, P.; Vasak, M., Metal swap between Zn(7)-metallothionein-3 and amyloid-beta-Cu protects against amyloid-beta toxicity. *Nat Chem Biol* **2008,** *4* (6), 366-372.

15. Tsuji, S.; Kobayashi, H.; Uchida, Y.; Ihara, Y.; Miyatake, T., Molecular-Cloning of Human Growth Inhibitory Factor Cdna and Its down-Regulation in Alzheimers-Disease. *Embo J* **1992,** *11* (13), 4843-4850.

16. Aschner, M.; Cherian, M. G.; Klaassen, C. D.; Palmiter, R. D.; Erickson, J. C.; Bush, A. I., Metallothioneins in brain - The role in physiology and pathology. *Toxicol Appl Pharm* **1997,** *142* (2), 229-242.

17. Tio, L.; Villarreal, L.; Atrian, S.; Capdevila, M., Functional differentiation in the mammalian metallothionein gene family - Metal binding features of mouse MT4 and comparison with its paralog MT1. *J Biol Chem* **2004,** *279* (23), 24403-24413.

18. Meloni, G.; Zovo, K.; Kazantseva, J.; Palumaa, P.; Vasak, M., Organization and assembly of metal-thiolate clusters in epithelium-specific metallothionein-4. *J Biol Chem* **2006,** *281* (21), 14588-14595.

19. Quaife, C. J.; Findley, S. D.; Erickson, J. C.; Froelick, G. J.; Kelly, E. J.; Zambrowicz, B. P.; Palmiter, R. D., Induction of a New Metallothionein Isoform (Mt-Iv) Occurs during Differentiation of Stratified Squamous Epithelia. *Biochemistry-Us* **1994,** *33* (23), 7250-7259.

20. Oh, S. H.; Deagen, J. T.; Whanger, P. D.; Weswig, P. H., Biological function of metallothionein. V. Its induction in rats by various stresses. *American Journal of Physiology - Endocrinology And Metabolism* **1978,** *234* (3), E282.

21. Krizkova, S.; Fabrik, I.; Adam, V.; Hrabeta, J.; Eckschlager, T.; Kizek, R., Metallothionein--a promising tool for cancer diagnostics. *Bratislavské lekárske listy* **2008,** *110* (2), 93-97.

22. Pedersen, M. O.; Larsen, A.; Stoltenberg, M.; Penkowa, M., The role of metallothionein in oncogenesis and cancer prognosis. *Prog Histochem Cyto* **2009,** *44* (1), 29-64.

23. Creamer, T. P., *Unfolded proteins: from denatured to intrinsically disordered*. Nova Publishers: 2008.

24. Sutherland, D. E. K.; Stillman, M. J., The "magic numbers" of metallothionein. *Metallomics* **2011,** *3* (5), 444-463.

25. Isani, G.; Carpenè, E., Metallothioneins, unconventional proteins from unconventional animals: a long journey from nematodes to mammals. *Biomolecules* **2014,** *4* (2), 435-457.

26. Stillman, M. J., Metallothioneins. *Coordin Chem Rev* **1995,** *144*, 461-511.

27. Sakulsak, N., Metallothionein: An Overview on its Metal Homeostatic Regulation in Mammals. *Int J Morphol* **2012,** *30* (3), 1007-1012.

28. Arseniev, A.; Schultze, P.; Worgotter, E.; Braun, W.; Wagner, G.; Vasak, M.; Kagi, J. H. R.; Wuthrich, K., 3-Dimensional Structure of Rabbit Liver [Cd7]Metallothionein-2a in Aqueous-Solution Determined by Nuclear Magnetic-Resonance. *J Mol Biol* **1988,** *201* (3), 637-657.

29. Nielsen, A. E.; Bohr, A.; Penkowa, M., The balance between life and death of cells: roles of metallothioneins. *Biomarker insights* **2006,** *1*, 117727190600100016.

30. Beltramini, M.; Lerch, K., Spectroscopic Studies on Neurospora Copper Metallothionein. *Biochemistry-Us* **1983,** *22* (9), 2043-2048.

31. Ngu, T. T.; Stillman, M. J., Metal-binding mechanisms in metallothioneins. *Dalton T* **2009,** (28), 5425-5433.

32. Vasak, M.; Kagi, J. H. R.; Hill, H. A. O., Zinc(Ii), Cadmium(Ii), and Mercury(Ii) Thiolate Transitions in Metallothionein. *Biochemistry-Us* **1981,** *20* (10), 2852-2856.

33. Ngu, T. T.; Stillman, M. J., Metalation of Metallothioneins. *Iubmb Life* **2009,** *61* (4), 438-446.

34. Stillman, M. J.; Presta, A.; Gui, Z.; Jiang, D.-T., Spectroscopic studies of copper, silver and gold-metallothioneins. *Metal-Based Drugs* **1994,** *1* (5-6), 375-394.

35. Presta, A.; Stillman, M. J., Chiral Copper(I) Thiolate Clusters in Metallothionein and Glutathione. *Chirality* **1994,** *6* (7), 521-530.

36. Pande, J.; Pande, C.; Gilg, D.; Vasak, M.; Callender, R.; Kagi, J. H. R., Raman, Infrared, and Circular-Dichroism Spectroscopic Studies on Metallothionein - a Predominantly Turn-Containing Protein. *Biochemistry-Us* **1986,** *25* (19), 5526-5532.

37. Torreggiani, A.; Tinti, A., Raman spectroscopy a promising technique for investigations of metallothioneins. *Metallomics* **2010,** *2* (4), 246-260.

38. Prinz, R.; Weser, U., Naturally Occurring Cu-Thioneine in Saccharomyces-Cerevisiae. *H-S Z Physiol Chem* **1975,** *356* (6), 767-776.

39. Calderone, V.; Dolderer, B.; Hartmann, H. J.; Echner, H.; Luchinat, C.; Del Bianco, C.; Mangani, S.; Weser, U., The crystal structure of yeast copper thionein: The solution of a long-lasting enigma. *Proc. Natl. Acad. Sci. U. S. A.* **2005,** *102* (1), 51-56.

40. Boulanger, Y.; Armitage, I. M., Cd-113 Nmr-Study of the Metal Cluster Structure of Human-Liver Metallothionein. *J Inorg Biochem* **1982,** *17* (2), 147-153.

41. Boulanger, Y.; Armitage, I. M.; Miklossy, K. A.; Winge, D. R., Cd-113 Nmr-Study of a Metallothionein Fragment - Evidence for a 2-Domain Structure. *J Biol Chem* **1982,** *257* (22), 13717-13719.

42. Braun, W.; Vasak, M.; Robbins, A. H.; Stout, C. D.; Wagner, G.; Kagi, J. H. R.; Wuthrich, K., Comparison of the Nmr Solution Structure and the X-Ray Crystal-Structure of Rat Metallothionein-2. *Proc. Natl. Acad. Sci. U. S. A.* **1992,** *89* (21), 10124-10128.

43. Yang, Y.; Maret, W.; Vallee, B. L., Differential fluorescence labeling of cysteinyl clusters uncovers high tissue levels of thionein. *Proceedings of the National Academy of Sciences* **2001,** *98* (10), 5556-5559.

44. Ruttkay-Nedecky, B.; Nejdl, L.; Gumulec, J.; Zitka, O.; Masarik, M.; Eckschlager, T.; Stiborova, M.; Adam, V.; Kizek, R., The Role of Metallothionein in Oxidative Stress. *Int J Mol Sci* **2013,** *14* (3), 6044-6066.

45. Jacob, C.; Maret, W.; Vallee, B. L., Control of zinc transfer between thionein, metallothionein, and zinc proteins. *Proc. Natl. Acad. Sci. U. S. A.* **1998,** *95* (7), 3489-3494.

46. El-Aneed, A.; Cohen, A.; Banoub, J., Mass Spectrometry, Review of the Basics: Electrospray, MALDI, and Commonly Used Mass Analyzers. *Appl Spectrosc Rev* **2009,** *44* (3), 210-230.

47. Yamashita, M.; Fenn, J. B., Electrospray Ion-Source - Another Variation on the Free-Jet Theme. *J Phys Chem-Us* **1984,** *88* (20), 4451-4459.

48. Chen, S. H.; Russell, D. H., How Closely Related Are Conformations of Protein Ions Sampled by IM-MS to Native Solution Structures? *J Am Soc Mass Spectr* **2015,** *26* (9), 1433-1443.

49. Aldini, G.; Dalle-Donne, I.; Vistoli, G.; Facino, R. M.; Carini, M., Covalent modification of actin by 4-hydroxy-trans-2-nonenal (HNE): LC-ESI-MS/MS evidence for Cys374 Michael adduction. *J Mass Spectrom* **2005,** *40* (7), 946-954.

50. Farwanah, H.; Pierstorff, B.; Schmelzer, C. E. H.; Raith, K.; Neubert, R. H. H.; Kolter, T.; Sandhoff, K., Separation and mass spectrometric characterization of

covalently bound skin ceramides using LC/APCI-MS and nano-ESI-MS/MS. *J Chromatogr B* **2007,** *852* (1-2), 562-570.

51. Veenstra, T. D., Electrospray ionization mass spectrometry: A promising new technique in the study of protein/DNA noncovalent complexes. *Biochem Bioph Res Co* **1999,** *257* (1), 1-5.

52. Veenstra, T. D., Electrospray ionization mass spectrometry in the study of biomolecular non-covalent interactions. *Biophys Chem* **1999,** *79* (2), 63-79.

53. Hofstadler, S. A.; Sannes-Lowery, K. A., Applications of ESI-MS in drug discovery: interrogation of noncovalent complexes. *Nat Rev Drug Discov* **2006,** *5* (7), 585-595.

54. Solomon, E. I.; Gorelsky, S. I.; Dey, A., Metal–thiolate bonds in bioinorganic chemistry. *Journal of computational chemistry* **2006,** *27* (12), 1415-1428.

55. Yu, X. L.; Wojciechowski, M.; Fenselau, C., Assessment of Metals in Reconstituted Metallothioneins by Electrospray Mass-Spectrometry. *Anal Chem* **1993,** *65* (10), 1355-1359.

56. Chen, S. H.; Russell, W. K.; Russell, D. H., Combining Chemical Labeling, Bottom-Up and Top-Down Ion-Mobility Mass Spectrometry To Identify Metal-Binding Sites of Partially Metalated Metallothionein. *Anal Chem* **2013,** *85* (6), 3229-3237.

57. Gehrig, P. M.; You, C. H.; Dallinger, R.; Gruber, C.; Brouwer, M.; Kagi, J. H. R.; Hunziker, P. E., Electrospray ionization mass spectrometry of zinc, cadmium, and copper metallothioneins: Evidence for metal-binding cooperativity. *Protein Sci* **2000,** *9* (2), 395-402.

58. Chan, J.; Huang, Z.; Watt, I.; Kille, P.; Stillman, M. J., Characterization of the conformational changes in recombinant human metallothioneins using ESI-MS and molecular modeling. *Canadian Journal of Chemistry* **2007,** *85* (10), 898-912.

59. Perez-Rafael, S.; Atrian, S.; Capdevila, M.; Palacios, O., Differential ESI-MS behaviour of highly similar metallothioneins. *Talanta* **2011,** *83* (3), 1057-1061.

60. McLean, J. A.; Ruotolo, B. T.; Gillig, K. J.; Russell, D. H., Ion mobility-mass spectrometry: a new paradigm for proteomics. *Int J Mass Spectrom* **2005,** *240* (3), 301-315.

61. Kanu, A. B.; Dwivedi, P.; Tam, M.; Matz, L.; Hill, H. H., Ion mobility-mass spectrometry. *J Mass Spectrom* **2008,** *43* (1), 1-22.

62. Ruotolo, B. T.; Benesch, J. L. P.; Sandercock, A. M.; Hyung, S. J.; Robinson, C. V., Ion mobility-mass spectrometry analysis of large protein complexes. *Nat Protoc* **2008,** *3* (7), 1139-1152.

63. Patrick, J. W.; Gamez, R. C.; Russell, D. H., Elucidation of Conformer Preferences for a Hydrophobic Antimicrobial Peptide by Vesicle Capture-Freeze-Drying: A Preparatory Method Coupled to Ion Mobility-Mass Spectrometry. *Anal Chem* **2015,** *87* (1), 578-583.

64. Leaf-nosed bat. In *Encyclopædia Britannica*, Encyclopædia Britannica Online: 2009.

65. Lanucara, F.; Holman, S. W.; Gray, C. J.; Eyers, C. E., The power of ion mobility-mass spectrometry for structural characterization and the study of conformational dynamics. *Nat Chem* **2014,** *6* (4), 281-294.

66. Mallis, C. S.; Saha, M. L.; Stang, P. J.; Russell, D. H., Topological Characterization of Coordination-Driven Self-assembly Complexes: Applications of Ion Mobility-Mass Spectrometry. *J Am Soc Mass Spectr* **2019,** *30* (9), 1654-1662.

67. Conant, C. R.; Fuller, D. R.; Zhang, Z. C.; Woodall, D. W.; Russell, D. H.; Clemmer, D. E., Substance P in the Gas Phase: Conformational Changes and Dissociations Induced by Collisional Activation in a Drift Tube. *J Am Soc Mass Spectr* **2019,** *30* (6), 932-945.

68. Woodall, D. W.; El-Baba, T. J.; Fuller, D. R.; Liu, W.; Brown, C. J.; Laganowsky, A.; Russell, D. H.; Clemmer, D. E., Variable-Temperature ESI-IMS-MS Analysis of Myohemerythrin Reveals Ligand Losses, Unfolding, and a Non-Native Disulfide Bond. *Anal Chem* **2019,** *91* (10), 6808-6814.

69. Konijnenberg, A.; Butterer, A.; Sobott, F., Native ion mobility-mass spectrometry and related methods in structural biology. *Bba-Proteins Proteom* **2013,** *1834* (6), 1239-1256.

70. Chen, S. H.; Chen, L. X.; Russell, D. H., Metal-Induced Conformational Changes of Human Metallothionein-2A: A Combined Theoretical and Experimental Study of Metal-Free and Partially Metalated Intermediates. *J Am Chem Soc* **2014,** *136* (26), 9499-9508.

71. Chen, S. H.; Russell, D. H., Reaction of Human Cd(7)metallothionein and N-Ethylmaleimide: Kinetic and Structural Insights from Electrospray Ionization Mass Spectrometry. *Biochemistry-Us* **2015,** *54* (39), 6021-6028.

72. Dixit, S. M.; Polasky, D. A.; Ruotolo, B. T., Collision induced unfolding of isolated proteins in the gas phase: past, present, and future. *Curr Opin Chem Biol* **2018,** *42*, 93-100.

73. Shelimov, K. B.; Clemmer, D. E.; Hudgins, R. R.; Jarrold, M. F., Protein Structure in Vacuo: Gas-Phase Conformations of BPTI and Cytochrome c. *J Am Chem Soc* **1997,** *119* (9), 2240-2248.

74. Shelimov, K. B.; Jarrold, M. F., Conformations, unfolding, and refolding of apomyoglobin in vacuum: An activation barrier for gas-phase protein folding. *J Am Chem Soc* **1997,** *119* (13), 2987-2994.

75. Allison, T. M.; Reading, E.; Liko, I.; Baldwin, A. J.; Laganowsky, A.; Robinson, C. V., Quantifying the stabilizing effects of protein-ligand interactions in the gas phase. *Nat Commun* **2015,** *6*.

76. Han, L. J.; Hyung, S. J.; Mayers, J. J. S.; Ruotolo, B. T., Bound Anions Differentially Stabilize Multiprotein Complexes in the Absence of Bulk Solvent. *J Am Chem Soc* **2011,** *133* (29), 11358-11367.

77. Tian, Y. W.; Han, L. J.; Buckner, A. C.; Ruotolo, B. T., Collision Induced Unfolding of Intact Antibodies: Rapid Characterization of Disulfide Bonding Patterns, Glycosylation, and Structures. *Anal Chem* **2015,** *87* (22), 11509-11515.

78. Watanabe, Y.; Vasiljevic, S.; Allen, J. D.; Seabright, G. E.; Duyvesteyn, H. M. E.; Doores, K. J.; Crispin, M.; Struwe, W. B., Signature of Antibody Domain Exchange by Native Mass Spectrometry and Collision-Induced Unfolding. *Anal Chem* **2018,** *90* (12), 7325-7331.

79. Hopper, J. T. S.; Oldham, N. J., Collision Induced Unfolding of Protein Ions in the Gas Phase Studied by Ion Mobility-Mass Spectrometry: The Effect of Ligand Binding on Conformational Stability. *J Am Soc Mass Spectr* **2009,** *20* (10), 1851-1858.

80. Tian, Y. W.; Ruotolo, B. T., Collision induced unfolding detects subtle differences in intact antibody glycoforms and associated fragments. *Int J Mass Spectrom* **2018,** *425*, 1-9.

81. Tian, Y. W.; Ruotolo, B. T., The growing role of structural mass spectrometry in the discovery and development of therapeutic antibodies. *Analyst* **2018,** *143* (11), 2459-2468.

82. Laganowsky, A.; Reading, E.; Allison, T. M.; Ulmschneider, M. B.; Degiacomi, M. T.; Baldwin, A. J.; Robinson, C. V., Membrane proteins bind lipids selectively to modulate their structure and function. *Nature* **2014,** *510* (7503), 172-175.

83. Eschweiler, J. D.; Rabuck-Gibbons, J. N.; Tian, Y. W.; Ruotolo, B. T., CIUSuite: A Quantitative Analysis Package for Collision Induced Unfolding Measurements of Gas-Phase Protein Ions. *Anal Chem* **2015,** *87* (22), 11516-11522.

84. Polasky, D. A.; Dixit, S. M.; Fantin, S. M.; Ruotolo, B. T., CIUSuite 2: Next-Generation Software for the Analysis of Gas-Phase Protein Unfolding Data. *Anal Chem* **2019,** *91* (4), 3147-3155.

85. Yang, Y.; Maret, W.; Vallee, B. L., Differential fluorescence labeling of cysteinyl clusters uncovers high tissue levels of thionein. *Proc. Natl. Acad. Sci. U. S. A.* **2001,** *98* (10), 5556-5559.

86. Petering, D. H.; Zhu, J. Y.; Krezoski, S.; Meeusen, J.; Kiekenbush, C.; Krull, S.; Specher, T.; Dughish, M., Apo-metallothionein emerging as a major player in the cellular activities of metallothionein. *Exp Biol Med* **2006,** *231* (9), 1528-1534.

87. Irvine, G. W.; Stillman, M. J., Residue Modification and Mass Spectrometry for the Investigation of Structural and Metalation Properties of Metallothionein and Cysteine-Rich Proteins. *Int J Mol Sci* **2017,** *18* (5).

88. Pinter, T. B. J.; Stillman, M. J., Kinetics of Zinc and Cadmium Exchanges between Metallothionein and Carbonic Anhydrase. *Biochemistry-Us* **2015,** *54* (40), 6284-6293.

89. Pinter, T. B. J.; Irvine, G. W.; Stillman, M. J., Domain Selection in Metallothionein 1A: Affinity-Controlled Mechanisms of Zinc Binding and Cadmium Exchange. *Biochemistry-Us* **2015,** *54* (32), 5006-5016.

90. Irvine, G. W.; Santolini, M.; Stillman, M. J., Selective cysteine modification of metal-free human metallothionein 1a and its isolated domain fragments: Solution structural properties revealed via ESI-MS. *Protein Sci* **2017,** *26* (5), 960-971.

91. Ngu, T. T.; Easton, A.; Stillman, M. J., Kinetic Analysis of Arsenic-Metalation of Human Metallothionein: Significance of the Two-Domain Structure. *J Am Chem Soc* **2008,** *130* (50), 17016-17028.

92. Verbeck, G.; Ruotolo, B.; Sawyer, H.; Gillig, K.; Russell, D., A fundamental introduction to ion mobility mass spectrometry applied to the analysis of biomolecules. *Journal of biomolecular techniques: JBT* **2002,** *13* (2), 56.

93. Marcoux, J.; Robinson, C. V., Twenty Years of Gas Phase Structural Biology. *Structure* **2013,** *21* (9), 1541-1550.

94. Sharon, M.; Robinson, C. V., The role of mass Spectrometry in structure elucidation of dynamic protein complexes. *Annu Rev Biochem* **2007,** *76*, 167-193.

95. Bailey, A. O.; Panchenko, T.; Sathyan, K. M.; Petkowski, J. J.; Pai, P. J.; Bai, D. L.; Russell, D. H.; Macara, I. G.; Shabanowitz, J.; Hunt, D. F.; Black, B. E.; Foltz, D. R., Posttranslational modification of CENP-A influences the conformation of centromeric chromatin. *Proc. Natl. Acad. Sci. U. S. A.* **2013,** *110* (29), 11827-11832.

96. Zinnel, N. F.; Pai, P. J.; Russell, D. H., Ion Mobility-Mass Spectrometry (IM-MS) for Top-Down Proteomics: Increased Dynamic Range Affords Increased Sequence Coverage. *Anal Chem* **2012,** *84* (7), 3390-3397.

97. El-Baba, T. J.; Woodall, D. W.; Raab, S. A.; Fuller, D. R.; Laganowsky, A.; Russell, D. H.; Clemnier, D. E., Melting Proteins: Evidence for Multiple Stable Structures upon Thermal Denaturation of Native Ubiquitin from Ion Mobility Spectrometry-Mass Spectrometry Measurements. *J Am Chem Soc* **2017,** *139* (18), 6306-6309.

98. Wagner, N. D.; Kim, D.; Russell, D. H., Increasing Ubiquitin Ion Resistance to Unfolding in the Gas Phase Using Chloride Adduction: Preserving More "Native-Like" Conformations Despite Collisional Activation. *Anal. Chem.* **2016,** *88* (11), 5934-5940.

99. Messerle, B. A.; Schaffer, A.; Vasak, M.; Kagi, J. H. R.; Wuthrich, K., Comparison of the Solution Conformations of Human [Zn7]-Metallothionein-2 and

[Cd7]-Metallothionein-2 Using Nuclear-Magnetic-Resonance Spectroscopy. *J Mol Biol* **1992,** *225* (2), 433-443.

100. Zelazowski, A. J.; Gasyna, Z.; Stillman, M. J., Silver Binding to Rabbit Liver Metallothionein - Circular-Dichroism and Emission Study of Silver-Thiolate Cluster Formation with Apometallothionein and the Alpha-Fragments and Beta-Fragments. *J Biol Chem* **1989,** *264* (29), 17091-17099.

101. Salgado, M. T.; Bacher, K. L.; Stillman, M. J., Probing structural changes in the alpha and beta domains of copper- and silver-substituted metallothionein by emission spectroscopy and electrospray ionization mass spectrometry. *J Biol Inorg Chem* **2007,** *12* (3), 294-312.

102. Palacios, O.; Polec-Pawlak, K.; Lobinski, R.; Capdevila, M.; Gonzalez-Duarte, P., Is Ag(I) an adequate probe for Cu(I) in structural copper-metallothionein studies? The binding features of Ag(I) to mammalian metallothionein 1. *J Biol Inorg Chem* **2003,** *8* (8), 831-842.

103. Messerle, B. A.; Schaffer, A.; Vasak, M.; Kagi, J. H. R.; Wuthrich, K., 3-Dimensional Structure of Human [(Cd7)-Cd-113]Metallothionein-2 in Solution Determined by Nuclear-Magnetic-Resonance Spectroscopy. *J Mol Biol* **1990,** *214* (3), 765-779.

104. Peterson, C. W.; Narula, S. S.; Armitage, I. M., 3D solution structure of copper and silver-substituted yeast metallothioneins. *Febs Lett* **1996,** *379* (1), 85-93.

105. Guo, Y. Z.; Ling, Y.; Thomson, B. A.; Siu, K. W. M., Combined ion-mobility and mass-spectrometry investigations of metallothionein complexes using a tandem

mass spectrometer with a segmented second quadrupole. *J Am Soc Mass Spectr* **2005,** *16* (11), 1787-1794.

106. Roepstorff, P.; Fohlman, J., Proposal for a Common Nomenclature for Sequence Ions in Mass-Spectra of Peptides. *Biomed Mass Spectrom* **1984,** *11* (11), 601-601.

107. Sutherland, D. E. K.; Summers, K. L.; Stillman, M. J., Noncooperative Metalation of Metallothionein 1a and Its Isolated Domains with Zinc. *Biochemistry-Us* **2012,** *51* (33), 6690-6700.

108. Irvine, G. W.; Pinter, T. B. J.; Stillman, M. J., Defining the metal binding pathways of human metallothionein 1a: balancing zinc availability and cadmium seclusion. *Metallomics* **2016,** *8* (1), 71-81.

109. Jayawardena, D. P.; Heinemann, I. U.; Stillman, M. J., Zinc binds non-cooperatively to human liver metallothionein 2a at physiological pH. *Biochem Bioph Res Co* **2017,** *493* (1), 650-653.

110. Nielson, K. B.; Winge, D. R., Independence of the Domains of Metallothionein in Metal-Binding. *J Biol Chem* **1985,** *260* (15), 8698-8701.

111. Li, H.; Otvos, J. D., Cd-111 NMR studies of the domain specificity of Ag+ and Cu+ binding to metallothionein. *Biochemistry-Us* **1996,** *35* (44), 13929-13936.

112. Li, H.; Otvos, J. D., Biphasic kinetics of Zn2+ removal from Zn metallothionein by nitrilotriacetate are associated with differential reactivity of the two metal clusters. *J Inorg Biochem* **1998,** *70* (3-4), 187-194.

113. Ejnik, J.; Robinson, J.; Zhu, J. Y.; Forsterling, H.; Shaw, C. F.; Petering, D. H., Folding pathway of apo-metallothionein induced by $Zn^{2+}$, $Cd^{2+}$ and $Co^{2+}$. *J Inorg Biochem* **2002,** *88* (2), 144-152.

114. Nielson, K. B.; Atkin, C. L.; Winge, D. R., Distinct Metal-Binding Configurations in Metallothionein. *J Biol Chem* **1985,** *260* (9), 5342-5350.

115. Duncan, K. E. R.; Stillman, M. J., Metal-dependent protein folding: Metallation of metallothionein. *J Inorg Biochem* **2006,** *100* (12), 2101-2107.

116. Vallee, B. L., The Function of Metallothionein. *Neurochem Int* **1995,** *27* (1), 23-33.

117. Davis, S. R.; Cousins, R. J., Metallothionein expression in animals: A physiological perspective on function. *J Nutr* **2000,** *130* (5), 1085-1088.

118. Kang, Y. J., Metallothionein redox cycle and function. *Exp Biol Med* **2006,** *231* (9), 1459-1467.

119. Giles, N. M.; Watts, A. B.; Giles, G. I.; Fry, F. H.; Littlechild, J. A.; Jacob, C., Metal and redox modulation of cysteine protein function. *Chem Biol* **2003,** *10* (8), 677-693.

120. Bell, S. G.; Vallee, B. L., The Metallothionein/Thionein System: An Oxidoreductive Metabolic Zinc Link. *Chembiochem* **2009,** *10* (1), 55-62.

121. Petering, D. H.; Mahim, A., Proteomic High Affinity Zn2+ Trafficking: Where Does Metallothionein Fit in? *Int J Mol Sci* **2017,** *18* (6).

122. Scheller, J. S.; Irvine, G. W.; Stillman, M. J., Unravelling the mechanistic details of metal binding to mammalian metallothioneins from stoichiometric, kinetic, and binding affinity data. *Dalton T* **2018,** *47* (11), 3613-3637.

123. Dong, S. Y.; Wagner, N. D.; Russell, D. H., Collision-Induced Unfolding of Partially Metalated Metallothionein-2A: Tracking Unfolding Reactions of Gas-Phase Ions. *Anal Chem* **2018,** *90* (20), 11856-11862.

124. Wagner, N. D.; Russell, D. H., Defining Noncovalent Ubiquitin Homodimer Interfacial Interactions through Comparisons with Covalently Linked Diubiquitin. *J Am Chem Soc* **2016,** *138* (51), 16588-16591.

125. Osobova, M.; Urban, V.; Jedelsky, P. L.; Borovicka, J.; Gryndler, M.; Ruml, T.; Kotrba, P., Three metallothionein isoforms and sequestration of intracellular silver in the hyperaccumulator Amanita strobiliformis. *New Phytol* **2011,** *190* (4), 916-926.

126. Hogstrand, C.; Galvez, F.; Wood, C. M., Toxicity, silver accumulation and metallothionein induction in freshwater rainbow trout during exposure to different silver salts. *Environmental Toxicology and Chemistry: An International Journal* **1996,** *15* (7), 1102-1108.

127. Shaw, C. F.; He, L. B.; Munoz, A.; Savas, M. M.; Chi, S.; Fink, C. L.; Gan, T.; Petering, D. H., Kinetics of reversible N-ethylmaleimide alkylation of metallothionein and the subsequent metal release. *J Biol Inorg Chem* **1997,** *2* (1), 65-73.

128. Krezel, A.; Maret, W., Different redox states of metallothionein/thionein in biological tissue. *Biochem J* **2007,** *402*, 551-558.

129. Testa, L.; Brocca, S.; Grandori, R., Charge-Surface Correlation in Electrospray Ionization of Folded and Unfolded Proteins. *Anal Chem* **2011,** *83* (17), 6459-6463.

130. Grabenauer, M.; Wyttenbach, T.; Sanghera, N.; Slade, S. E.; Pinheiro, T. J. T.; Scrivens, J. H.; Bowers, M. T., Conformational Stability of Syrian Hamster Prion Protein PrP(90-231). *J Am Chem Soc* **2010,** *132* (26), 8816-8818.

131. Pai, P. J.; Cologna, S. M.; Russell, W. K.; Vigh, G.; Russell, D. H., Efficient Electrophoretic Method to Remove Neutral Additives from Protein Solutions Followed by Mass Spectrometry Analysis. *Anal Chem* **2011,** *83* (7), 2814-2818.

132. Zinnel, N. F.; Russell, D. H., Size-to-Charge Dispersion of Collision-Induced Dissociation Product Ions for Enhancement of Structural Information and Product Ion Identification. *Anal Chem* **2014,** *86* (10), 4791-4798.

133. Sowell, R. A.; Koeniger, S. L.; Valentine, S. J.; Moon, M. H.; Clemmer, D. E., Nanoflow LCAMS-MS and LCAMS-CID/MS of protein mixtures. *J Am Soc Mass Spectr* **2004,** *15* (9), 1341-1353.

134. Robbins, A. H.; Mcree, D. E.; Williamson, M.; Collett, S. A.; Xuong, N. H.; Furey, W. F.; Wang, B. C.; Stout, C. D., Refined Crystal-Structure of Cd, Zn Metallothionein at 2.0 a Resolution. *J Mol Biol* **1991,** *221* (4), 1269-1293.

135. Hu, S. Q.; Ye, B. Y.; Yi, X. Y.; Cao, Z. Z.; Wu, D. H.; Shen, C. C.; Wang, J. X., Dumbbell-shaped metallothionein-templated silver nanoclusters with applications in cell imaging and Hg2+ sensing. *Talanta* **2016,** *155*, 272-277.

136. Cui, Y. Y.; Wang, Y. L.; Zhao, L. N., Cysteine-Ag Cluster Hydrogel Confirmed by Experimental and Numerical Studies. *Small* **2015,** *11* (38), 5118-5125.

137. Choi, S.; Yu, J. H., Recent development in deciphering the structure of luminescent silver nanodots. *Apl Mater* **2017,** *5* (5).

138. Sych, T. S.; Reveguk, Z. V.; Pomogaev, V. A.; Buglak, A. A.; Reveguk, A. A.; Ramazanov, R. R.; Romanov, N. M.; Chikhirzhina, E. V.; Polyanichko, A. M.; Kononov, A. I., Fluorescent Silver Clusters on Protein Templates: Understanding Their Structure. *J Phys Chem C* **2018,** *122* (51), 29549-29558.

139. Huard, D. J. E.; Demissie, A.; Kim, D.; Lewis, D.; Dickson, R. M.; Petty, J. T.; Lieberman, R. L., Atomic Structure of a Fluorescent Ag8 Cluster Templated by a Multistranded DNA Scaffold. *J Am Chem Soc* **2018**.

140. Ali, M.; Stein, N.; Mao, Y. X.; Shahid, S.; Schmidt, M.; Bennett, B.; Pacheco, A. A., Trapping of a Putative Intermediate in the Cytochrome c Nitrite Reductase (ccNiR)-Catalyzed Reduction of Nitrite: Implications for the ccNiR Reaction Mechanism. *J Am Chem Soc* **2019,** *141* (34), 13358-13371.

141. Volbeda, A.; Cabodevilla, J. S.; Darnault, C.; Gigarel, O.; Han, T. H. L.; Renoux, O.; Hamelin, O.; Agnier-de-Choudens, S.; Amara, P.; Fontecilla-Camps, J. C., Crystallographic Trapping of Reaction Intermediates in Quinolinic Acid Synthesis by NadA. *Acs Chem Biol* **2018,** *13* (5), 1209-1217.

142. Varela, A. E.; England, K. A.; Cavagnero, S., Kinetic trapping in protein folding. *Protein Engineering, Design and Selection* **2019,** *32* (2), 103-108.

143. Zhang, R. R.; Schroeder, A. B.; Grudzinski, J. J.; Rosenthal, E. L.; Warram, J. M.; Pinchuk, A. N.; Eliceiri, K. W.; Kuo, J. S.; Weichert, J. P., Beyond the margins:

real-time detection of cancer using targeted fluorophores. *Nat Rev Clin Oncol* **2017,** *14* (6), 347-364.

144. Ngu, T. T.; Sturzenbaum, S. R.; Stillman, M. J., Cadmium binding studies to the earthworm Lumbricus rubellus metallothionein by electrospray mass spectrometry and circular dichroism spectroscopy. *Biochem. Biophys. Res. Commun.* **2006,** *351* (1), 229-233.

145. Tarasava, K.; Johannsen, S.; Freisinger, E., Solution Structure of the Circular gamma-Domain Analog from the Wheat Metallothionein E-c-1. *Molecules* **2013,** *18* (11), 14414-14429.

146. Lento, C.; Audette, G. F.; Wilson, D. J., Time-resolved electrospray mass spectrometry—a brief history. *Can. J. Chem.* **2014,** *93* (1), 7-12.

147. Konermann, L.; Collings, B. A.; Douglas, D. J., Cytochrome c folding kinetics studied by time-resolved electrospray ionization mass spectrometry. *Biochemistry-Us* **1997,** *36* (18), 5554-5559.

148. Ngu, T. T.; Stillman, M. J., Arsenic binding to human metallothionein. *J. Am. Chem. Soc.* **2006,** *128* (38), 12473-12483.

149. Wilson, D. J.; Konermann, L., A capillary mixer with adjustable reaction chamber volume for millisecond time-resolved studies by electrospray mass spectrometry. *Anal. Chem.* **2003,** *75* (23), 6408-6414.

150. Resetca, D.; Wilson, D. J., Characterizing rapid, activity-linked conformational transitions in proteins via sub-second hydrogen deuterium exchange mass spectrometry. *FEBS J.* **2013,** *280* (22), 5616-5625.

151. Pérez-Rafael, S.; Atrian, S.; Capdevila, M.; Palacios, Ò., Differential ESI-MS behaviour of highly similar metallothioneins. *Talanta* **2011,** *83* (3), 1057-1061.

152. Tougu, V.; Karafin, A.; Zovo, K.; Chung, R. S.; Howells, C.; West, A. K.; Palumaa, P., Zn(II)- and Cu(II)-induced non-fibrillar aggregates of amyloid-beta (1-42) peptide are transformed to amyloid fibrils, both spontaneously and under the influence of metal chelators. *J. Neurochem.* **2009,** *110* (6), 1784-1795.

153. Selkoe, D. J.; Hardy, J., The amyloid hypothesis of Alzheimer's disease at 25years. *Embo Mol Med* **2016,** *8* (6), 595-608.

154. Ryan, T. M.; Kirby, N.; Mertens, H. D. T.; Roberts, B.; Barnham, K. J.; Cappai, R.; Pham, C. L. L.; Masters, C. L.; Curtain, C. C., Small angle X-ray scattering analysis of Cu2+-induced oligomers of the Alzheimer's amyloid beta peptide. *Metallomics* **2015,** *7* (3), 536-543.

155. Faller, P., Copper and Zinc Binding to Amyloid-beta: Coordination, Dynamics, Aggregation, Reactivity and Metal-Ion Transfer. *ChemBioChem* **2009,** *10* (18), 2837-2845.

156. Gaggelli, E.; Kozlowski, H.; Valensin, D.; Valensin, G., Copper homeostasis and neurodegenerative disorders (Alzheimer's, prion, and Parkinson's diseases and amyotrophic lateral sclerosis). *Chem. Rev.* **2006,** *106* (6), 1995-2044.

157. Roberts, B. R.; Ryan, T. M.; Bush, A. I.; Masters, C. L.; Duce, J. A., The role of metallobiology and amyloid-ss peptides in Alzheimer's disease. *J. Neurochem.* **2012,** *120*, 149-166.

158. Manso, Y.; Carrasco, J.; Comes, G.; Meloni, G.; Adlard, P. A.; Bush, A. I.; Vasak, M.; Hidalgo, J., Characterization of the role of metallothionein-3 in an animal model of Alzheimer's disease. *Cell Mol Life Sci* **2012,** *69* (21), 3683-3700.

159. Uchida, Y.; Takio, K.; Titani, K.; Ihara, Y.; Tomonaga, M., The Growth Inhibitory Factor That Is Deficient in the Alzheimers-Disease Brain Is a 68-Amino Acid Metallothionein-Like Protein. *Neuron* **1991,** *7* (2), 337-347.

160. Yu, W. H.; Lukiw, W. J.; Bergeron, C.; Niznik, H. B.; Fraser, P. E., Metallothionein III is reduced in Alzheimer's disease. *Brain Res.* **2001,** *894* (1), 37-45.

161. Irie, Y.; Keung, W. M., Metallothionein-III antagonizes the neurotoxic and neurotrophic effects of amyloid beta peptides. *Biochem. Biophys. Res. Commun.* **2001,** *282* (2), 416-420.

162. Pedersen, J. T.; Hureau, C.; Hemmingsen, L.; Heegaard, N. H. H.; Ostergaard, J.; Vasak, M.; Faller, P., Rapid Exchange of Metal between Zn-7-Metallothionein-3 and Amyloid-beta Peptide Promotes Amyloid-Related Structural Changes. *Biochemistry* **2012,** *51* (8), 1697-1706.

163. Chung, R. S.; Howells, C.; Eaton, E. D.; Shabala, L.; Zovo, K.; Palumaa, P.; Sillard, R.; Woodhouse, A.; Bennett, W. R.; Ray, S.; Vickers, J. C.; West, A. K., The Native Copper- and Zinc- Binding Protein Metallothionein Blocks Copper-Mediated A beta Aggregation and Toxicity in Rat Cortical Neurons. *Plos One* **2010,** *5* (8).

164. Luo, Y.-R., *Comprehensive handbook of chemical bond energies*. CRC press: 2007.

165. Breuker, K.; McLafferty, F. W., Stepwise evolution of protein native structure with electrospray into the gas phase, 10(-12) to 10(2) S. *Proc. Natl. Acad. Sci. U. S. A.* **2008,** *105* (47), 18145-18152.

166. Karas, M.; Bachmann, D.; Bahr, U.; Hillenkamp, F., Matrix-Assisted Ultraviolet-Laser Desorption of Nonvolatile Compounds. *International Journal of Mass Spectrometry and Ion Processes* **1987,** *78*, 53-68.

167. Fenn, J. B.; Mann, M.; Meng, C. K.; Wong, S. F.; Whitehouse, C. M., Electrospray Ionization for Mass-Spectrometry of Large Biomolecules. *Science* **1989,** *246* (4926), 64-71.

168. Loo, J. A., Studying noncovalent protein complexes by electrospray ionization mass spectrometry. *Mass Spectrom Rev* **1997,** *16* (1), 1-23.

169. Mehmood, S.; Allison, T. M.; Robinson, C. V., Mass Spectrometry of Protein Complexes: From Origins to Applications. *Annu Rev Phys Chem* **2015,** *66*, 453-474.

170. Thompson, N. J.; Rosati, S.; Heck, A. J. R., Performing native mass spectrometry analysis on therapeutic antibodies. *Methods* **2014,** *65* (1), 11-17.

171. Moghadamchargari, Z.; Huddleston, J.; Shirzadeh, M.; Zheng, X. Y.; Clemmer, D. E.; Raushel, F. M.; Russell, D. H.; Laganows, A., Intrinsic GTPase Activity of K-RAS Monitored by Native Mass Spectrometry. *Biochemistry-Us* **2019,** *58* (31), 3396-3405.

172. Laganowsky, A.; Reading, E.; Hopper, J. T. S.; Robinson, C. V., Mass spectrometry of intact membrane protein complexes. *Nat Protoc* **2013,** *8* (4), 639-651.

173. Snijder, J.; Rose, R. J.; Veesler, D.; Johnson, J. E.; Heck, A. J. R., Studying 18 MDa Virus Assemblies with Native Mass Spectrometry. *Angew Chem Int Edit* **2013,** *52* (14), 4020-4023.

174. Breuker, K.; Oh, H. B.; Horn, D. M.; Cerda, B. A.; McLafferty, F. W., Detailed unfolding and folding of gaseous ubiquitin ions characterized by electron capture dissociation. *J Am Chem Soc* **2002,** *124* (22), 6407-6420.

175. Badman, E. R.; Myung, S.; Clemmer, D. E., Evidence for unfolding and refolding of gas-phase cytochrome c ions in a Paul trap. *J Am Soc Mass Spectr* **2005,** *16* (9), 1493-1497.

176. Li, Y.; Maret, W., Human metallothionein metallomics. *J Anal Atom Spectrom* **2008,** *23* (8), 1055-1062.

177. Erk, M.; Raspor, B., Evaluation of cadmium-metallothionein stability constants based on voltammetric measurements. *Anal Chim Acta* **1998,** *360* (1-3), 189-194.

178. Muñoz, A.; Rodríguez, A. R., Electrochemical behavior of metallothioneins and related molecules. Part III: Metallothionein. *Electroanalysis* **1995,** *7* (7), 674-680.

179. Otvos, J. D.; Petering, D. H.; Shaw, C. F., Structure—Reactivity Relationships of Metallothionein, a Unique Metal-Binding Protein. *Comments on Inorganic Chemistry* **1989,** *9* (1), 1-35.

180. Kaltashov, I. A.; Mohimen, A., Estimates of protein surface areas in solution by electrospray ionization mass spectrometry. *Anal Chem* **2005,** *77* (16), 5370-5379.